Diss. ETH No. 16524

Selective Catalytic Reduction (SCR) of Nitrogen Oxides with Ammonia over Fe-ZSM5

Mukundan Devadas

Diss. ETH No. 16524

Selective Catalytic Reduction (SCR) of Nitrogen Oxides with Ammonia over Fe-ZSM5

A dissertation submitted to the
SWISS FEDERAL INSTITUTE OF TECHNOLOGY ZURICH
for the degree of
DOCTOR OF TECHNICAL SCIENCES

presented by
MUKUNDAN DEVADAS
M. Sc. (Chem. Engg), University Erlangen-Nürenberg, Germany
born July 3, 1976
in Chennai, India

Accepted on the recommendation of
Prof. Dr. A. Wokaun, examiner
Prof. Dr. A. Baiker, co-examiner
Dr. O. Kröcher, co-examiner

2006

With love to my parents

Table of Contents

Acknowledgements

In a long odyssey of research it is lot easier when you travel together. This doctoral thesis is the result of four years of work whereby I have been accompanied and supported by many people. I believe that I must thank one and all associated with this project, though only a few of those inspiring force have been mentioned in this section.

I am grateful to **Prof. Dr. Alexander Wokaun** for his precious instructions. His dynamic thoughts, broad and profound knowledge, warm smile and his patient instructions have given me a great help to complete this project. I would like to express my sincere thanks to **Prof. Dr. Alfons Baiker** for accepting to be the co-examiner and for devoting his kind attention in refereeing this thesis.

I remain highly indebt to **Dr. Oliver Kröcher** for his valuable guidance, thought provoking suggestions, constant encouragement, critical reviews and above all his tolerance and perseverance to make this project a success. Also, I would like to express my deep gratitude for his timely advice which provided me the right direction in the course of my project.

Many thanks to **Mr. Martin Elsener** who advised and helped me in various aspects of my research. He is the one that I can always count on to discuss the tiniest details of a problem, and who knows all the laboratory tools inside-out. Special thanks to **Dr. Manfred Koebel** for his valuable advises and effective contribution during the first year of my thesis. I am grateful to **Dr. Agniezska Held** for effective discussion on research and for her kind hospitality during my visit to Poland. Thanks are also due to all colleagues, especially to **Miss. Gaia Piazzesi** and **Mr. Kirill Tikhomirov**, with whom I shared delightful and enjoyable memories in the last four years at PSI. Their presence and their humor created a nice working atmosphere. Thanks to my friends from India for their constant support.

I would like to express my thanks to the following people for their contribution towards my thesis: **Mrs. Friederike Geiger** (BET measurements), **Mr. Alwin Fry** (XRD analysis), **Mr. Ramar Amuthan** (TEM), **Dr. George Mitrikas** (EPR), **Dr. Gerhard Pirngruber** (UV-vis) and **Mr. Dilip G. Poduval** (NMR). Also I wish to thank all left unnamed who contributed in several ways to this thesis. Financial help from **Umicore AG**, Germany is gratefully acknowledged.

I am very grateful to all the Srilankan families in Switzerland for their moral support and affection showered upon me during my thesis time. I would like to thank **Miss. Babitha Rajendran Kailasam** for her support and love. Though her participation to this thesis was in the last 7 months, her role during my thesis writing was a valuable one. Special gratitude to my brother and sister for their encouragement and love.

Last but not the least I would like to thank my beloved parents and almighty for giving me strength and courage throughout my thesis and during my stay in Switzerland.

Summary

Fe-ZSM5 has been found to be an efficient catalyst for the selective catalytic reduction of nitrogen oxides in the exhaust of diesel vehicles by urea (urea-SCR) beside the established V_2O_5/WO_3-TiO_2 catalysts. The performance of Fe-ZSM5 as SCR catalyst is tested under near “real” world conditions in order to reveal the possibilities and limits. Powder Fe-ZSM5 is used for the physico-chemical characterization, in order to explore the structural aspects of the catalyst. Fe-ZSM5 coated on cordierite monolith was investigated in the SCR reaction of NO with ammonia over a broad temperature range, applying simulated diesel exhaust gas conditions.

The catalyst exhibited over 80 % NO_x reduction (DeNOx) from 400 to 650 °C at very good selectivity. The dosage of variable amounts of ammonia in the catalytic tests revealed that the SCR reaction is inhibited by ammonia. At very high temperatures DeNOx is reduced due to the selective catalytic oxidation (SCO) of ammonia to nitrogen and the oxidation to NO. Water-free experiments resulted in generally higher DeNOx values, which are explained by the inhibiting effect of water on the NO oxidation capability of Fe-ZSM5. The catalyst was stable upon thermal ageing and only 5-15 % loss in DeNOx activity was observed after hydrothermal treatment. This loss in DeNOx is in parallel with a loss of ammonia storage capacity of the aged catalyst.

The influence of NO_2 on the SCR reaction of NO with ammonia was studied over Fe-ZSM5. NO_2 in the feed drastically enhanced the DeNOx up to 600 °C, whereas the promoting effect was most pronounced at the low temperature end. The maximum activity was found for $NO_2/NO_x = 50$ %, which is explained by the stoichiometry of the actual SCR reaction over Fe-ZSM5, requiring a NH_3:NO:NO_2 ratio of 2:1:1. Thereby, it is a special feature of Fe-ZSM5 to keep this activity level almost up to $NO_2/NO_x = 100$ %. The addition of NO_2 to the feed gas was always accompanied by the production of N_2O at lower and intermediate temperatures. The absence of N_2O at the high temperature end was reduced to the N_2O decomposition and N_2O-SCR reaction. Water and oxygen

influence the SCR reaction indirectly. Oxygen enhances the oxidation of NO to NO_2 and water suppresses the oxidation of NO to NO_2, which is an essential preceding step for the actual SCR reaction at $NO_2/NO_x < 50$ %.

Fe-ZSM5 was characterized by ICP-AES, BET surface measurements, TEM, NH_3-TPD and ^{27}Al MAS NMR, UV-vis, EPR and DRIFT spectroscopy. The formation of small Fe_2O_3 particles could be identified by UV-vis, EPR and TEM measurements, which were proved to be not active for the SCR reaction. DRIFT investigations under SCR conditions showed adsorbates on Fe^{2+} up to 300 °C. The high SCR activity above 300 °C might be explained by a faster reoxidation of Fe^{2+} to Fe^{3+} sites at high temperatures. The observed inhibition of the SCR reaction by excess ammonia at low and intermediate temperatures can be explained in this context by the reducing properties of ammonia converting Fe^{3+} to Fe^{2+} or by preventing the reoxidation of Fe^{2+}. FTIR investigations of the catalyst under different pre-treatment and operating conditions are suggestive of a common intermediate, from which the main product N_2 is formed with NO and the side-product N_2O by reaction with gas phase NO_2.

Kurzfassung

Fe-ZSM5 hat sich als effizienter Katalysator für die selektive katalytische Reduktion (SCR) von Stickoxiden mit Harnstoff in Dieselabgasen herausgestellt und ist damit eine interessante Alternative zu den bewährten V_2O_5/WO_3-TiO_2-Systemen. Die Eigenschaften von Fe-ZSM5 als SCR-Katalysator wurden unter realitätsnahen Bedingungen getestet, um deren Möglichkeiten und Grenzen aufzudecken. Zur Untersuchung der Katalysatorstruktur wurden pulverförmige Proben von Fe-ZSM5 physikalisch-chemisch charakterisiert. Darüber hinaus wurden Kordieritträger mit Fe-ZSM5-Pulver beschichtet und in einem breiten Temperaturbereich für die selektive katalytische Reduktion von NO mit Ammoniak in einer Modellgasanlage getestet.

Der Katalysator zeigte über 80 % NO_x-Reduktion (DeNOx) von 450 bis 650 °C bei sehr guter Selektivität. Die Dosierung verschiedener Ammoniakmengen zeigte, dass die SCR-Reaktion durch Ammoniak inhibiert wird. Bei sehr hohen Temperaturen wird das DeNOx durch die selektive katalytische Oxidation (SCO) von Ammoniak zu Stickstoff and durch die Oxidation von Ammoniak zu NO reduziert. Wasser-freie Experimente führten zu generell höheren DeNOx-Werten, was durch den inhibierenden Effekt von Wasser auf die NO-Oxidation über Fe-ZSM5 erklärt wird. Der Katalysator war gegen thermische Alterung stabil und verlor nur 5-15 % seiner DeNOx-Aktivität nach hydrothermaler Behandlung. Dieser Verlust in DeNOx-Aktivität geht mit einem Verlust an Ammoniak-Speicherkapazität einher.

Es wurde auch der Einfluss von NO_2 auf die SCR-Reaktion von NO mit Ammoniak über Fe-ZSM5 untersucht. NO_2 im Feed-Gas erhöhte die DeNOx-Werte drastisch, wobei der promotierende Effekt bei tiefen Temperaturen am ausgeprägtesten war. Die maximale Aktivität wurde für $NO_2/NO_x = 50$ % gefunden, was sich aus der Stöchiometrie der tatsächlich ablaufenden SCR-Reaktion auf Fe-ZSM5 erklärt, die ein Verhältnis von NH_3:NO:NO_2 von 2:1:1 verlangt. Dabei weist Fe-ZSM5 die spezielle Eigenschaft auf, diese hohe Aktivität bis annähernd $NO_2/NO_x = 100$ % beizubehalten. Die Zugabe von

NO_2 zum Feed-Gas war stets mit der Produktion von N_2O bei tiefen und mittleren Temperaturen verbunden. Das Fehlen von N_2O bei hohen Temperaturen wurde auf die N_2O-Zersetzungs- und N_2O-SCR-Reaktion zurückgeführt. Wasser und Sauerstoff beeinflussen die SCR-Reaktion indirekt. Sauerstoff fördert die Oxidation von NO zu NO_2 und Wasser unterdrückt die Oxidation von NO zu NO_2, die ein essentieller vorausgehender Schritt für die SCR-Reaktion bei $NO_2/NO_x < 50$ % ist.

Fe-ZSM5 wurde durch ICP-AES, BET-Oberflächenmessungen, TEM, NH_3-TPD sowie ^{27}Al-MAS-NMR-, UV-Vis-, EPR- und DRIFT-Spektroskopie untersucht. Mit Hilfe von UV-Vis- und EPR-Spektroskopie sowie TEM-Messungen konnte die Bildung kleiner Fe_2O_3-Partikel identifiziert werden, die sich als nicht SCR-aktiv erwiesen. DRIFT-Untersuchungen unter SCR-Bedingungen zeigten Adsorbate auf Fe^{2+} bis 300 °C. Die hohe SCR-Aktivität über 300 °C könnte über eine schnellere Reoxidation von Fe^{2+} zu Fe^{3+} bei hohen Temperaturen erklärt werden. Die beobachtete Inhibierung der SCR-Reaktion durch überschüssigen Ammoniak bei tiefen und mittleren Temperaturen kann in diesem Zusammenhang durch die reduzierenden Eigenschaften des Ammoniaks erklärt werden, der Fe^{3+} zu Fe^{2+} konvertiert oder die Reoxidation von Fe^{2+} verhindert. FTIR-Untersuchungen des Katalysators unter verschiedenen Vorbehandlungen und Reaktionsbedingungen deuten auf ein gemeinsames Intermediat hin, von dem das Hauptprodukt N_2 mit NO und das Nebenprodukte N_2O durch die Reaktion mit Gasphasen-NO_2 gebildet wird.

1

Introduction

1.1 Introduction

Nitrogen oxides or NO_x, is the generic term for a group of gases, which mainly consists of NO and NO_2. NO_x is formed in gas phase reactions mostly through oxidation of nitrogen in the combustion air ("thermal NO_x") and through oxidation of nitrogen containing compounds in the fuel or biomass ("fuel NO_x") [1, 2]. Thermal NO_x are formed at very high temperatures (1100 °C) [1]. Thermal NO_x formation is sensitive to flame temperature i.e., on increasing the flame temperature the contribution of thermal NO_x increases. The formation of fuel NO_x is independent of temperature of flame and is insensitive to the nature of nitrogen compound.

Approximately 90 to 95% of the nitrogen oxides generated in combustion processes are in the form of nitric oxide (NO) [2]. These nitrogen oxides are one of the main air pollutants which are responsible for ozone depletion, photochemical smog formation and causing severe respiratory problems to humans [3]. An estimated amount of 30 million tonnes per year of nitrogen oxides are emitted into the atmosphere world wide [3]. As it can be seen in figure 1.1, the primary source of NO_x emissions in the year 2003, in the USA, are motor vehicles with a 55 % share [4], as well as other sources of NO_x emissions are electric utilities and other commercial as well as residential sources that burn fuels.

Therefore, it is a significant challenge for the scientific community to improve the efficiency of NO_x removal (DeNOx) technologies in the transport sector. This task is getting even more important due to the tightening NO_x emission limits throughout the world.

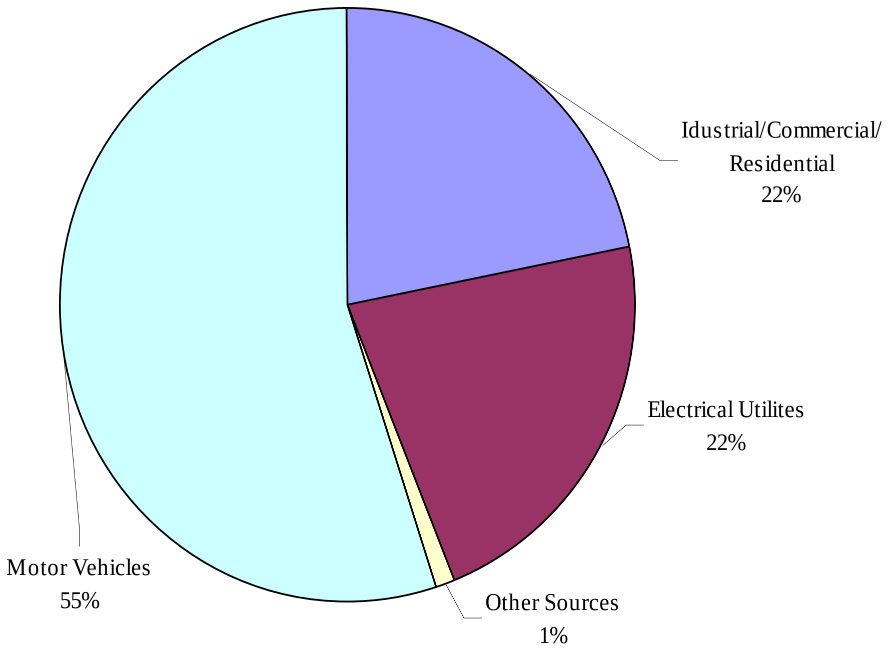

Figure 1.1 Sources of NO_x emissions in the USA (2003).

1.2 European legislation standard

The European legislation standards were designed in order to control the emissions from all type of vehicles, from passenger cars to heavy-duty trucks and motorcycles [5, 6]. The control of particulate emissions and NO_x represents a challenge to the diesel engine manufacturers because they are interlinked i.e., for lower maximum combustion temperatures, less NO_x but more particulates are produced whereas at higher combustion temperatures less particulates and more NO_x are generated. This characteristic dependency is referred as NO_x-particulate trade-off which is plotted for heavy duty diesel engines in figure 1.2.

The Euro II stage started in 1996, the Euro III stage in 2000, the Euro IV stage in 2005 and the future Euro V will start in January 2008. In order to achieve the Euro IV target, it is clear that internal measures (engine development) are not sufficient and that exhaust gas after treatment techniques are necessary. If the combustion process is optimized for lower NO_x emissions a particulate filter may be applied for the reduction of soot emissions. If the engine is tuned for lower a particulates but higher NO_x emissions, an efficient DeNOx system is required.

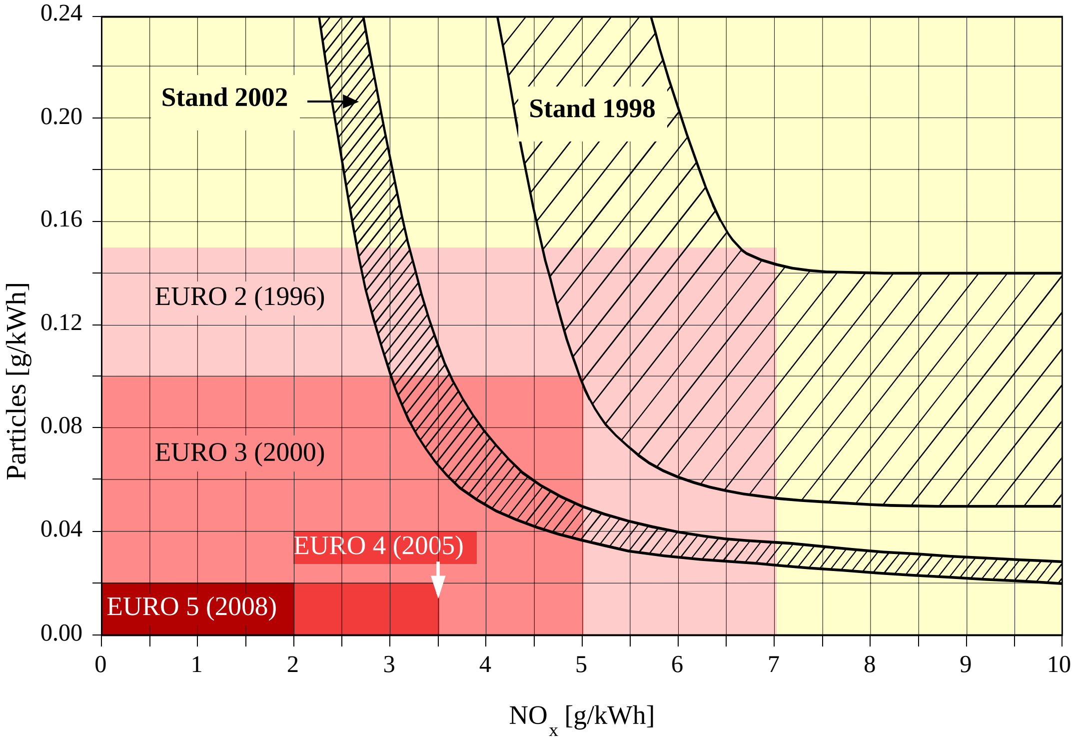

Figure 1.2 Trade-off between particulate matter and NO_x for heavy-duty truck engines and European emission standards.

1.3 Summary of DeNOx techniques

1.3.1 Selective non-catalytic reduction (SNCR)

The main advantage of SNCR is that, this process does not need any catalyst. In the SNCR process, the reducing agent (ammonia or urea) is injected into the flue gas at temperatures between 800 °C-1100 °C [7]. This method does not exhibit a high DeNOx activity (25-70 %) and moreover it consumes high amounts of reducing agents [8].

1.3.2 Non-selective catalytic reduction (NSCR)

This technique is used to remove the NO_x emission from nitric acid plants and gasoline engines [9]. The waste gas of a nitric acid plant contains excess of oxygen. The excess oxygen is consumed by combustion of a fuel reductant, which also reduces catalytically the NO_x to N_2. The Three Way Catalytic technology (TWC) is based on the same chemistry. This technology was primarily used in gasoline engines. Carbon monoxide and unburnt hydrocarbons react with the remaining oxygen to carbon dioxide and water, whereas the NO_x is reduced to nitrogen by carbon monoxide.

To be effective, the engine has to run under stoichiometric conditions i.e., the air-to-fuel ratio is fixed accordingly to the stoichiometry of the ratio between oxygen and fuel to carbon dioxide and water. If the mixture is too rich there is not enough oxygen to remove the carbon monoxide and hydrocarbons, if too lean (i.e. excess of oxygen) the nitrogen oxides cannot be reduced. A drawback of the TWC technology is the partial reduction of NO_x to undesired nitrous oxide or ammonia under certain operating conditions of the engine. The reduction of NO_x in lean exhaust requires a reducing agent which reacts selectively with NO_x in the presence of oxygen.

1.3.3 Selective catalytic reduction (SCR)

The SCR process was first applied in the 1970s in Japan for reduction of the NO_x emissions from the lean exhaust of stationary plants by using ammonia as reducing agent. This process is until today regarded as the most effective method for NO_x reduction in stationary applications [10, 11]. The same process with urea as reducing agent instead of ammonia is presently considered to be also the best technology for the removal of nitrogen oxides from the exhaust of heavy-duty diesel vehicles, e.g. trucks [12]. In automotive applications, urea is advantageous compared to ammonia, because it is a harmless and environmentally storage compound for ammonia, which is released in the hot exhaust gas. In typical diesel exhaust, the nitrogen oxides are mainly composed of NO (> 90%), so that the reaction of NO with NH_3 on the SCR catalyst has to be regarded as and there fore called as “standard SCR”.

1.4 SCR chemistry

The standard SCR follows a 1:1 stoichiometry for ammonia and NO (> 90% of NO_x of an exhaust gas is formed by NO) is maintained along with consumption of oxygen (reaction 1.1) [12].

$$4\ NH_3 + 4\ NO + O_2 \rightarrow 4\ N_2 + 6\ H_2O \tag{1.1}$$

When equimolar amounts of (50 %) NO and NO_2 are present in the feed, SCR process is accelerated and is termed as “fast SCR” reaction (reaction 1.2)

$$4\ NH_3 + 2\ NO + 2\ NO_2 \rightarrow 4\ N_2 + 6\ H_2O \tag{1.2}$$

When pure (100 %) NO_2 is present the feed, the reduction process is termed as “NO_2-SCR” (reaction 1.3).

$$4\ NH_3 + 3\ NO_2 \rightarrow 3.5\ N_2 + 6\ H_2O \tag{1.3}$$

Urea is usually atomized as 32.5 % aqueous solution into the hot exhaust gas (250-450 °C). The first steps are the evaporation of water from the droplets, and the melting of the urea, which cannot be clearly separated (reaction 1.4).

$$H_2N\text{-}CO\text{-}NH_{2\ (aq)} \rightarrow H_2N\text{-}CO\text{-}NH_{2\ (liq)} + H_2O_{\ (gas)} \tag{1.4}$$

Subsequently, urea is thermally decomposed (thermolyzed) into equimolar amounts of ammonia and isoycanic acid (reaction 1.5)

$$H_2N\text{-}CO\text{-}NH_{2\ (liq)} \rightarrow NH_{3\ (gas)} + HNCO_{\ (gas)} \tag{1.5}$$

which easily hydrolyzes according to reaction 1.6.

$$HNCO_{\ (gas)} + H_2O \rightarrow NH_3 + CO_{2\ (gas)} \tag{1.6}$$

1.5 Summary of different types of catalysts used in NH_3-SCR

The main types of catalyst involved in NH_3-SCR systems are noble metals, metal oxides and zeolites. Noble metals are active for NO_x reduction, but they have a major drawback. The oxidation capacity of these catalysts are high and thereby undesired side products like nitrous oxide are formed. These catalysts are active only in narrow temperature window (150-300 °C). Among the various investigated metal oxide mixtures those based on vanadia supported on titania and promoted with tungsten or molybdenum oxide are preferred, not only due to their high activity and selectivity but also because of their resistance towards poisoning by SO_2 (10, 13-14). They are active between 250-500 °C. At higher temperatures, direct ammonia oxidation is significant and decreases the selectivity to N_2 and H_2O. Other drawbacks of the vanadia catalyst are the formation of N_2O at higher temperatures and the risk of emission of volatile vanadium at $T > 650$ °C.

Zeolite based SCR catalysts are used for high temperature (> 500 °C) applications. They function in a broad temperature and more resistant to thermal excursions [15] SCR catalysts are under development which can resist temperatures up to 900 °C. Zeolite based catalysts such as mordenite, faujasite and pentasil [16, 17] are used for NO_x reduction, but the most active type for NH_3-SCR is transition metal exchanged ZSM5.

1.6 Scope of thesis

The main task of this work, is a comprehensive catalytic investigation and characterization of Fe-ZSM5 coated on cordierite monoliths. The performance of Fe-ZSM5 as SCR catalyst is tested under near “real” world conditions in order to reveal the possibilities and limits. The thermal and hydrothermal stability as well as the sulphur resistance of the Fe-ZSM5 are checked. Apart from this, the NH_3 dosing strategy is also analysed in order to improve the activity of the catalyst. Powder Fe-ZSM5 is used for the physico-chemical characterization, in order to explore the structural aspects of the catalyst. By combining the catalytic and characterization investigation the functionality of this catalyst type is explained.

1.7 References

[1] J. G. Henry, G. W. Heinke, “Environmental Science and Engineering”, Prentice-Hall, Englewood Cliffs, New Jersey, 1989.

[2] M. B. Hocking, “Modern Chemical Technology and Emission Control”, Springer, Berlin, 1985.

[3] A. Y. Watson, R. R. Bates, D. Kennedy, “Air Pollution, The Automobile and Public Health”, National Academic Press, Washington, 1988.

[4] “United Stated Environmental Protection Agency (EPA)”, EPA-456/F-98-005 Documents, URL://www.epa.gov.

[5] P. Greening, Top. Catal. 16 (2001) 5.

[6] G. Emmerling and F. I. Zuther, in: A. Leipertz (Ed.), Motorische Verbrennung - aktuelle Probleme und moderne Lösungsätze, Berichte zur Energie- und Verfahrenstechnik, Schriftenreihe Heft 99.1, Erlangen (1999), p. 581.

[7] F. Kasuya, P. Glarborg, J. E. Johnsson, K. D. Johansen, Chem. Eng. Sci. 50 (1995) 1455.

[8] S. C. Wood, Chem. Eng. Prog. 90 (I) (1994) 47.

[9] R. M. Heck, R. J. Farrauto, “Catalytic Air Pollution Control: Commercial Technology”, New York 1995.

[10] P. Forzatti, L. Lietti, Heter. Chem. Rev. 3 (1996) 33.

[11] H. Bosch, F. Janssen, Catal. Today 2 (1998) 369.

[12] M. Koebel, M. Elsener, M. Kleemann, Catal. Today 59 (2000) 335.

[13] G. Ramis, Y. Li, G. Busca, M. Turco, E. Kotur, R. J. Willey, J. Catal. 157 (1995) 523.

[14] M. D. Amiridis, R. V. Duevel, I. E. Wachs, Appl. Catal. B 20 (2001) 111.

[15] S. A. Stevenson, J. C. Vartuli, J. Catal. 208 (2002) 100.

[16] R. Q. Long, R. T. Yang, J. Catal. 207 (2002) 274.

[17] Y. H. Yeom, B. Wen, W. M. H. Sachtler, E. Weitz, J. Phys. Chem. B 108 (2004) 5386.

2

Literature Review

2.1 Zeolites

2.1.1 General aspects

The observation that a certain mineral began to bubble on strong heating led the Swedish mineralogist A. F. Cronstedt in 1756 to give the name “zeolites” to such materials from the Greek word zeo: (to boil) and lithos: (stone) [1, 2]. One finds naturally developed zeolites as deposits in sedimentary rocks, where they are formed under hydrothermal conditions by the effect of hot alkaline salt solutions from volcanic ash and pumice stones. Technical production of zeolites in the 60’s enabled its industrial application and forced the research on these materials in the field of heterogeneous catalysis [3].

2.1.2 Structure of zeolites

Zeolites are crystalline, hydrated aluminosilicates of group 1 and group 2 elements, in particular sodium, potassium, magnesium, calcium, strontium and barium. Structurally the zeolites are “framework” aluminosilicates, which are based on an infinitely extending three-dimensional network of AlO_4 and SiO_4 tetrahedra linked to each other by sharing all of the oxygen. Zeolites may be represented by the empirical formula:

$$M_{2/n}O \cdot Al_2O_3 \cdot xO_2 \cdot yH_2O$$

In this oxide formula, x is generally equal to or greater than 2 since AlO_4 tetrahedra are joined only to SiO_4 tetrahedra, n is the cation valence. The framework contains channels and interconnected voids, which are occupied by the cation and water molecules. The cations are quite mobile and may usually be exchanged to varying degrees. In some synthetic zeolites, aluminium cations may be substituted by gallium ions and silicon ions by germanium or phosphorous ions. The latter necessitates a modification of the structural formula.

The structural formula of a zeolite is best expressed for the crystallographic unit cell as:

$$M_{x/n}[\ (AlO_2)_x\ (SiO_2)_y\ ]\ wH_2O$$

Where M is the cation of valence n, w is the number of water molecules and the ratio y/x have values between 1-1000 depending upon the structure. The sum (x+y) is the total number of tetrahedral in the unit cell. The ratio of AlO_2 to SiO_2 represents the framework composition. The structure of the three dimensional zeolite lattice consists of several construction units. The primary construction units SiO_4 and SiO_2 are in tetrahedral position. From the linkage of the tetrahedrally coordinated primary construction units over common oxygen atom leads to the secondary construction unit SBU (secondary building unit). These consist, for example, of simple rings and prisms of various sizes. By the combination of such basic units the known zeolite frameworks can be constructed. Figure 2.1 represents the three dimensional structure of the zeolite of type ZSM5.

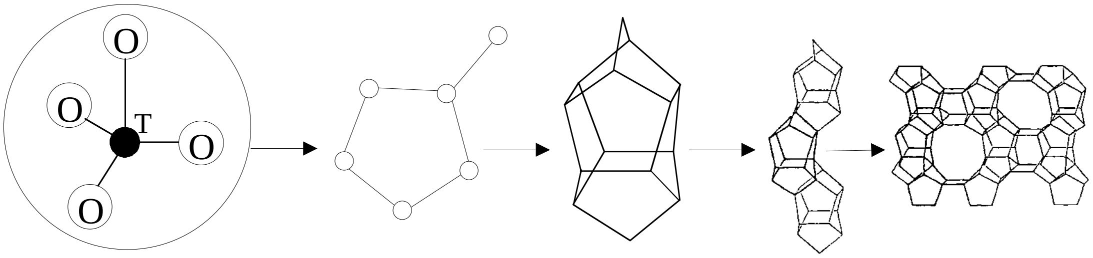

Figure 2.1 Three dimensional structure of zeolite of type ZSM5.

2.1.3 Catalytic activity of zeolites

The use of zeolites in heterogeneous catalysis is justified by the special characteristics of this material, which are closely connected with its void structure and its acidity. The void structures of the zeolites are divided into close, central or broad types. The defined pore sizes of the respective zeolites are between 3 Å and 11 Å and form the principal reason for its selectivity [4]. The acidity of zeolites has a strong influence on the catalytic activity and it is due to the presence of both Brønsted and Lewis acid centers.

The heterogeneous lattice structure (installation of trivalent metal ions into SiO_2 lattice) yields a negative charge, which is compensated by mono or divalent cations. If the negative charge is balanced with protons, SiOH groups (Silanol group) are formed, which can act as Brønsted acid centers. Figure 2.2 shows such a Brønsted acid center in the lattice structure.

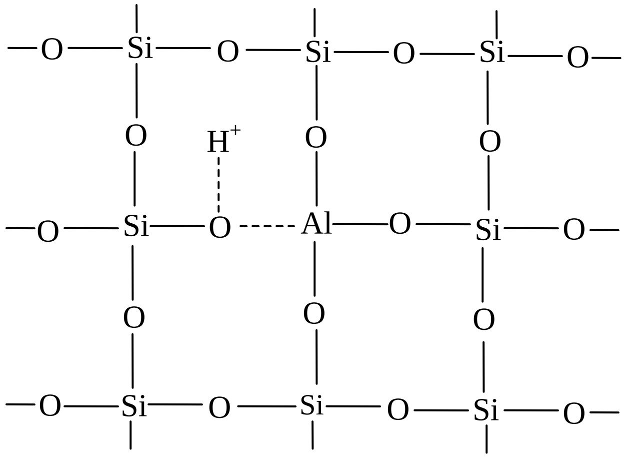

Figure 2.2 Zeolite with Brønsted acid center in the lattice structure.

The acid strength of the individual centers determines the activity of the catalyst and concomitantly on the catalyzed reaction. It can be influenced by the following parameters:

- Module M zeolites (module M is defined as the ratios between SiO_2 to AlO_3 units)
- Type of trivalent cation other than Al^{3+} (e.g. Fe^{3+}, Ga^{3+})

ZSM5 can have a minimum module value of 10 [5]. Investigations have shown [5, 6] that an increase in module is connected with a reduction of the number of acid centers, however the strength of the individual centers rises. This fact can be explained by Sanderson electronegativity [7]. Other trivalent ions than Al are sometimes used to build up the zeolite structure. In this case, an increase in the electronegativity of the metal ($\chi_{Fe} > \chi_{Ga} > \chi_{Al}$) will decrease the strength of the Brønsted centers in the zeolites [8]. Lewis centers may also be present in zeolites. They can be formed from a missing oxygen bridge between a silicon and an aluminium atom. These lattice defects are formed from the dehydration of two Brønsted center by temperature treatment.

2.1.4 Zeolites of type ZSM5

ZSM5 is the best catalyst for the direct hydroxylation of benzene to phenol process by using N_2O as oxidant. ZSM5 is mainly used for the interconversion of hydrocarbon like, m-xylene to p-xylene. ZSM5 is a zeolite with high silica to alumina ratio. To increase the activity, substitution of an Al^{3+} for a Si^{4+} requires an additional proton. ZSM5 is a highly porous material and has an interesting two-dimensional pore structure. ZSM5 has two types of pores; both are formed by 10 membered oxygen rings. The first type is straight and elliptical in cross section with channel dimensions 5.1 Å x 5.5 Å. The second type intersect the straight pore type at right angles, in a zigzag pattern and are circular in cross section with dimensions 5.4 Å x 5.6 Å [9]. Figure 2.3 gives the schematic pore structure of ZSM5.

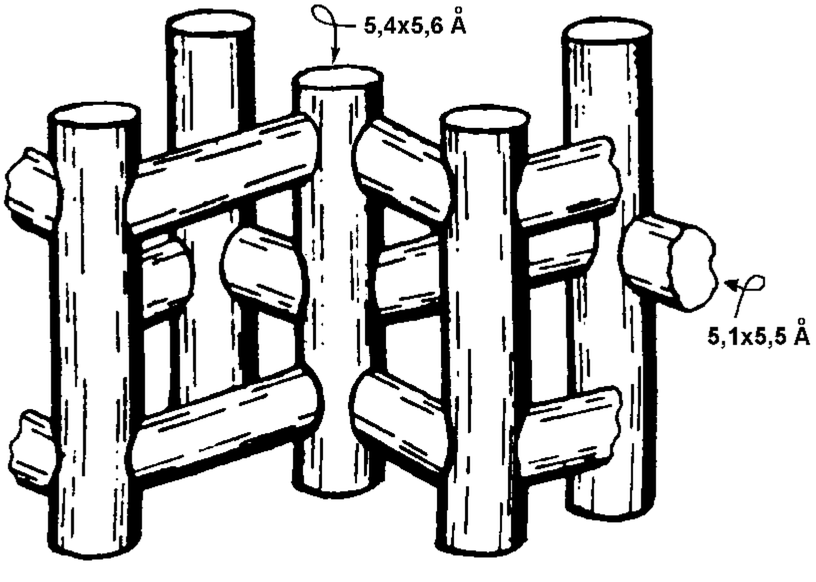

Figure 2.3 Pore structure of ZSM5 zeolite.

2.2 Fe-ZSM5 as SCR catalyst for NO_x removal

In recent years, a number of papers have appeared on catalytic NO abatement by zeolites. Many of these studies are aimed at using zeolites for the removal of NO_x from mobile exhaust gases (diesel and lean-burn exhaust gas). The selective catalytic reduction of NO_x with ammonia (NH_3-SCR), which is extensively applied to stationary NO_x sources [10], is a very effective method, because NH_3 reacts much more selectively with NO than hydrocarbons. This can be attributed to an intrinsic high reactivity of NH_3 towards NO_x species with a direct formation of the N–N bond and low activity towards a reaction with O_2 compared with hydrocarbons [11]. The commercial catalysts that are used today are based on V_2O_5 promoted by WO_3 and supported on TiO_2 [12, 13]. Various H-form and metal exchanged zeolite were tested for NH_3-SCR [14-17], among them Fe-ZSM5 is regarded as a potential alternative to the established vanadia based catalysts, because it functions at temperatures up to 700 °C, the risk to emit volatile vandyl species is avoided and no disposal problems occur.

Byrne et al. [18] from Engelhard Corporation developed a commercial SCR catalyst for high temperature applications. This catalyst is based on a Fe promoted zeolite with three dimensional pore structures and a high module. The catalyst was highly selective towards SCR NO_x reaction, yielding high NO_x removal efficiency over a wide temperature range from 300 °C to 600 °C. Feng and Hall prepared an over exchanged Fe-ZSM5 catalyst using Fe oxalate precursor salt [19]. They found the catalyst to be highly active at 500 °C and stable in the presence of 10 % H_2O and 150 ppm of SO_2. Only minimal loss in DeNOx was observed after ageing for 2500 h^{-1}.

Long and Yang studied the catalytic performance of Fe-ZSM5 catalyst for SCR by NH_3 [20]. A series of Fe exchanged molecular sieves were studied as catalyst for the SCR reaction. Both Fe-ZSM5 and Fe-mordenite catalysts were highly active for the SCR reaction. Nearly 100 % NO conversion was obtained at 400-500 °C at high space velocity. However, Fe-Y and Fe- MCM41 with larger pore sizes showed lower activities for this reaction. For Fe-ZSM5 catalyst, the SCR activity decreased with increasing Si/Al ratio. As the Fe exchange level increased from 58 % to 252 %, NO conversion increased at lower temperatures (e.g. 300 °C), but decreased at high temperatures (e.g. 600 °C). The catalyst also showed substantially lower activity for SO_2 oxidation to SO_3. Other groups like Ma and Grünert [21] and Chen and Sachtler [22] have reported high activity for Fe-ZSM5 catalysts for NH_3-SCR. Krishna et al. [23] have shown that a modified sublimation technique for preparing Fe-ZSM5 results in improved DeNOx activity.

Eng and Bartholomew examined the kinetics and the mechanism of NO_x reduction by NH_3 over H-ZSM5 [24, 25]. Steady-state kinetic experiments were performed at temperatures above 330 °C with and without H_2O, which indicated that H_2O does not affect SCR at these temperatures. Analysis of the kinetic data showed that SCR has a positive reaction order with respect to NO and O_2, but is inhibited by NH_3. The overall mechanism proposed by them is shown in figure 2.4.

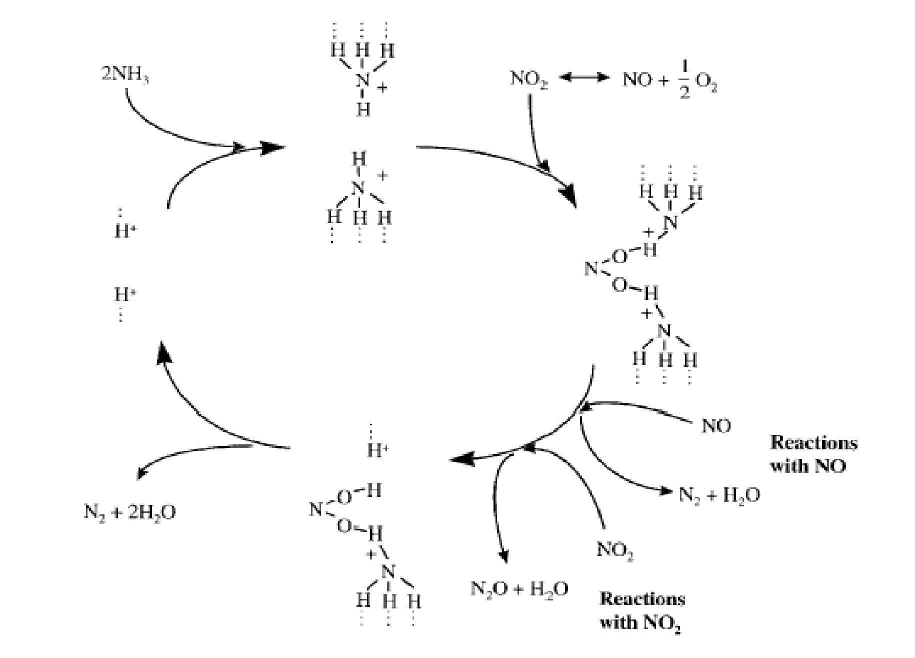

Figure 2.4 Reaction mechanism of SCR of NO_x with NH_3 over H-ZSM5.

The initial step in the proposed reaction mechanism is the adsorption of NH_3 onto neighboring acid sites and rearrangement of the NH_4^+ complexes to the 3H structure. The next step involves the reaction of adsorbed NH_3 with NO_2 to form an active complex.

This active complex reacts rapidly with NO or NO_2 to form N_2 or N_2O respectively, leaving a residual complex. The residual complex then decomposes to form additional N_2 and H_2O. The proposed reaction mechanism explains the following observations:

- 1:1 NO_2:NO ratios are optimal for maximum NO_x conversion to N_2
- Optimum reactant stoichiometries for NO reduction by NH_3 are 4 NO:4 NH_3:1 O_2
- Only N_2 is formed during NO reduction in the presence of O_2
- The reduction of NO_2 leads to the formation of 50 % N_2 and 50 % N_2O

Stevenson et al. examined the kinetics of the selective catalytic reduction of NO by NH_3 over H-ZSM5 [26]. They observed that the reaction was in first order with respect to nitric oxide and oxygen, but that the reaction is inhibited by the presence of ammonia resulting in a negative order. The degree of inhibition decreases as the temperature is increased. This is attributed to competitive adsorption of ammonia i.e. ammonia blocks sites that are needed for the oxidation of NO.

Richter et al. [27] reported that the ammonium ions in the zeolites are effective for the SCR reaction at low temperatures as low as 373 K. A reaction mechanism is proposed for NO_x conversion involving ammonium ions in the zeolite lattice. Their mechanism basically assumes the combination of N^{3+} (from the anion) and N^{3-} (from ammonium cation) to form neutral N_2. Sun et al. [28] used isotopic labelling to find out details of the reaction mechanism over Fe-ZSM5. Isotopic labelling with ^{15}NO shows that the preferred path for the reduction of NO_x with NH_3 is via NH_4NO_2. This nitrite decomposes to $N_2 + 2\ H_2O$. A 100 % pure $^{15}N^{14}N$ product is obtained by circulating a 1/1 mixture of ^{15}NO and $^{15}NO_2$ over a catalyst covered with adsorbed $^{14}NH_3$.

Long and Yang also proposed a mechanism for Fe-ZSM5 catalyst [29, 30], based on various catalyst characterizations. These included X-ray photoelectron spectroscopy (XPS), hydrogen temperature programmed reduction (H_2-TPR), electron spin resonance (ESR), temperature programmed desorption of ammonia (NH_3-TPD), temperature programmed surface reaction (TPSR) and Fourier transform infrared spectroscopy

(FTIR). XPS and ESR results indicated that iron cations were present mainly as Fe^{3+} ions with tetrahedral coordination, along with a small amount of Fe^{2+} and aggregated Fe^{3+} ions. The Fe^{3+} ions could be partially reduced to Fe^{2+} ions by H_2 at 300 - 600 °C, but reoxidation was possible when O_2 was fed to the reduced catalyst at 500 °C. FTIR spectra showed that NO molecules were oxidized by O_2 to adsorbed N_2O_3, NO_2, and nitrate. The NO_x adspecies were not stable above 300 °C in He, but adsorbed NO and NO_2 could be observed in flowing $NO+O_2/He$. NH_3 molecules were adsorbed on Brønsted acid and Lewis acid sites of Fe-ZSM5 thus generating NH_4^+ ions (majority) and coordinated NH_3 (minority). The NH_4^+ ions with three hydrogen atoms (3H structure) bonded to AlO_4 tetrahedra of ZSM5 were more stable at high temperatures (300-400 °C) than those with two bonds and coordinated NH_3. At 300 °C, the NH_4^+ ions with 3H structure were active in reacting with NO and $NO+O_2$, but the reaction rate with $NO+O_2$ was much higher than that with NO alone. The results indicated that NH_4^+ as well as NO and NO_2 adspecies play an important role in the SCR reaction on the Fe-ZSM5 catalyst. With NH_3 and NO_x coadsorbed on Fe–ZSM5, TPSR with gaseous He, NO, and NO_2 showed two kinds of reactions for N_2 formation. One reaction near 55 °C originated from decomposition of ammonium nitrite, which was not affected by the Fe^{3+} content. The other reaction at higher temperatures (170-245 °C) was due to an adsorbed complex, probably $[NH_4^+]_2NO_2$, reacting with NO or NO_2. The proposed reaction mechanism is shown in figure 2.5.

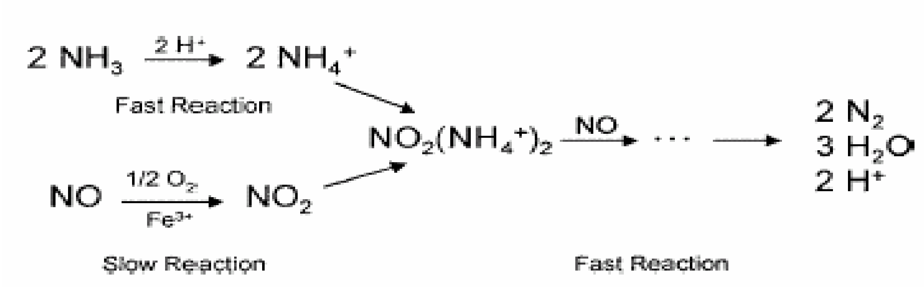

Figure 2.5 Reaction scheme of SCR of NO with NH_3 on Fe-ZSM5.

Delahay et al. [31] concluded that the sublimation method is the best method to prepare high efficient catalyst Fe-ZSM5 catalysts for the NH_3-SCR. Their reaction mechanism is shown in figure 2.6. In the catalytic cycle an Fe^{2+} specie is oxidized by O_2 to an iron III oxo/hydroxo species. The extra-framework oxygen then reacts with NO to form a surface nitrogen oxide intermediate bound to iron. Finally this later species reacts with ammonia to form water and nitrogen with concomitant reduction of Fe^{3+} to Fe^{2+} species.

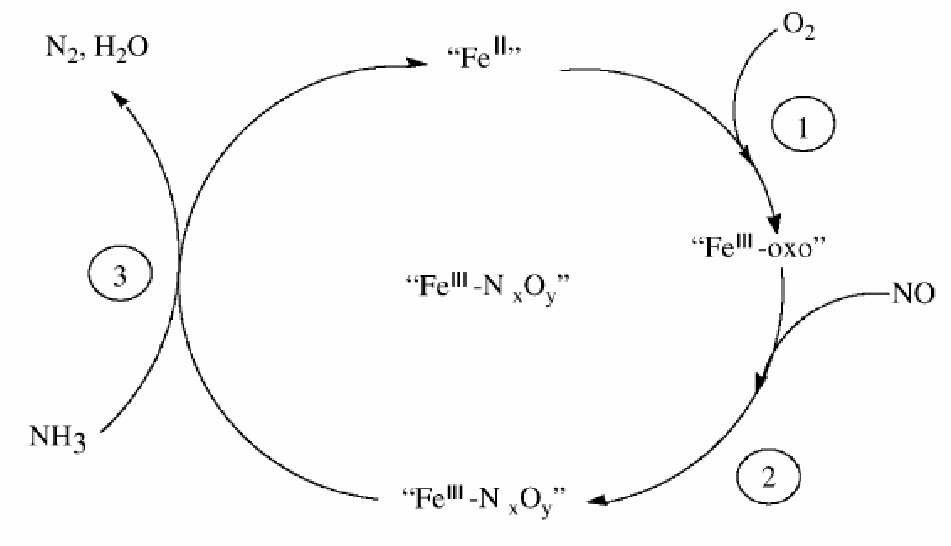

Figure 2.6 Catalytic cycle of NH_3-SCR on Fe-ZSM5.

The nature of the active site on Fe-ZSM5 for NH_3-SCR (and also HC-SCR) is still under strong debate by the scientific community. Panov et al. [32] and Sobolev et al. [33] found a particular state of adsorbed oxygen called α-oxygen in Fe-ZSM5 with low iron loadings, whereby the α-oxygen was associated with binuclear Fe-complexes. For high loading of Fe ("over-exchanged" ZSM5) various researchers [19, 22, 34-35] have proposed an oxygen bridged binuclear complex $[HO\text{-}Fe\text{-}O\text{-}Fe\text{-}OH]^{2+}$ as the active site, whereas Kucherov et al. [36] suggested isolated FeO^+ ions in tetrahedral and distorted sites. Joyner et al. [37] reported that Fe_4O_4 nano-clusters are the active sites for the selective catalytic reduction of NO_x with hydrocarbons. More recently, Schwidder et al. [38] correlated the SCR activity with the concentration of Fe sites determined by UV-vis spectroscopy. They found that mononuclear Fe ions are active for the SCR reaction, but confirmed that also oligomers contribute to the SCR activity. In the case of NH_3-SCR, they concluded that oligomeric Fe-oxo species contribute to the SCR activity with high efficiency.

2.3 References

[1] A. F. Cronstedt, Akademiens Handlingar, Stockholm, 17:120 (1756).

[2] J. L. Schlenker, G. H. Kühl, J. B. Higgins, Proceedings from the 9th International Zeolite Conference, Butterworth-Heinemann, Boston (1993) 3.

[3] R. M. Milton, ACS Symp. Ser., 398 (1989) 1.

[4] D. E. W. Vaughan, “The Synthesis and Manufacture of Zeolites”, Chem. Eng. Progress 25 (1988).

[5] W. Mortier, J. Catal. 55 (1978) 138.

[6] P. Jacobs, Catal. Rev. 24 (3) 415.

[7] M. Häfele, Dissertation, University of Erlangen-Nürnberg, Erlangen, 2000.

[8] C. Chu, C. Chang, Phys. Chem. 89 (1985) 1569.

[9] D. W. Breck, “Zeolite Molecular Sieves: Structure, Chemistry and Use”, Wiley, New York, 1973.

[10] H. Bosch, F. Janssen, Catal. Today 2 (1988) 369.

[11] E. Ito, R.J. Hultermans, P.M. Lugt, M.H.W. Burgers, H. van Bekkum, C.M. van den Bleek, Stud. Surf. Sci. Catal. 96 (1995) 661.

[12] P. Forzatti, L. Lietti, Heterogen. Chem. Rev. 3 (1996) 33.

[13] M. Koebel, M. Elsener, M. Kleemann, Catal. Today 59 (2000) 335.

[14] D. T. Pence and T. R. Thomas, in “Proceddings of the AEC Pollution Control Conference”,CONF-721030. 1972.

[15] R. T Yang, J. P. Chen, E. S. Kikkinides, L. S. Cheng, J. E. Cichanowicz, Ind. Eng. Chem. Res. 31 (1992) 1440.

[16] R. Q. Long, R. T. Yang, J. Catal. 186 (1999) 254.

[17] R. T. Yang, T. J. Pinnavaia, W. Li, W. Zhang, J. Catal. 172, (1997) 488.

[18] J. W. Byrne, J. M. Chen, B. K. Speronello, Catal. Today 13 (1992) 33.

[19] X. Feng, W. K. Hall, J. Catal. 166 (1997) 368.

[20] R. Q. Long, R. T. Yang, J. Catal. 188 (1992) 332.

[21] A. Z. Ma, W. Grünert, Chem. Commun. 1 (1999) 71

[22] H. Y. Chen, W. M. H. Sachtler, Catal. Today 42 (1998) 73.

[23] K. Krishna, G. B. F. Seijger, C. M. van den Bleek, M. Makkee, G. Mul, H. P. A. Calis, Catal. Lett. 86 (2003) 121.

[24] J. Eng, C. H. Bartholomew, J. Catal. 171 (1997) 27.

[25] J. Eng, C.H. Bartholomew, J. Catal. 161 (1996) 14.

[26] S. A. Stevenson, J. C. Vartuli, C. F. Brooks, J. Catal. 190 (2000) 228.

[27] M. Richter, R. Eckelt, B. Parlitz, R. Fricke, Appl. Catal. B 15 (1998) 129.

[28] Q. Sun, Z. Gao, H.Y. Chen, W.M.H. Sachtler, J. Catal. 201 (2001) 89.

[29] R. Q. Long, R. T. Yang, J. Catal. 194 (2000) 80.

[30] R. Q. Long, R. T. Yang, J. Catal. 198 (2001) 20.

[31] G. Delahay, D. Valade, A. G. Vargas, B. Coq, Appl. Catal. B 55 (2005) 149.

[32] G. I. Panov, A. K. Uriarte, M. A. Rodkin, V. J. Sobolev, Catal. Today 41 (1998) 365.

[33] V. I. Sobolev, G. Panov, A. Kharitonov, V. Romannikov, A. Volodin, K. Ione, J. Catal. 139 (1993) 435.

[34] W. K. Hall, X. Feng, J. Dumesic, R. Watwe, Catal. Lett. 52 (1998) 13.

[35] T. V. Voskoboinikov, H. Y. Chen, W. M. H. Sachtler, Appl. Catal. B 19 (1998) 279.

[36] A. V. Kucherov, C. N. Montreuil, T. N. Kucherova, M. Shelef, Catal. Lett. 56 (1998) 173.

[37] R. Joyner, M. Stockenhuber, J. Phys. Chem. B 103 (1999) 5963.

[38] M. Schwidder, M. S. Kumar, K. Klementiev, M. M. Pohl, A. Brückner, W. Grünert, J. Catal. 231 (2005) 314.

3

Physico-Chemical Characterization Techniques

3.1 Introduction

Characterization is an integral part of any worthwhile catalytic research and development program. The characterization of catalyst provides information of three distinct but related sorts. They are chemical composition and structure, texture and mechanical properties and catalytic activity [1].

Chemical composition and chemical structure, refers to matters such as elemental composition, structure, proportions of individual phases which may be present, surface composition and the nature and proportions of functional groups which may be present on the surface. The texture of the catalyst refers to its geometric structure and morphology, ranging from the grossest macroscale down to finest microscale. This deals with instance, size and shape of individual catalyst units, pore structure and total surface area. Mechanical properties refer to those which are important to the integrity of the catalyst in an industrial application. This refers to matters such as abrasion or attrition resistance, strength, and thermal shock resistance. The characterization of a catalyst in terms of its activity is a quantitative measure of the ability of a catalyst to carry out a particular chemical transformation under specified conditions.

In this thesis the following characterization techniques were used:

- X-ray Diffractometry
- Low Temperature N_2 Adsorption
- Inductively Coupled Plasma Emission-Atomic Spectroscopy
- Transmission Electron Microscopy

- Temperature Programmed Desorption of Ammonia
- Temperature Programmed Reduction by Hydrogen
- Nuclear Magnetic Resonance Spectroscopy
- Electron Paramagnetic Resonance Spectroscopy
- Ultraviolet Visible Spectroscopy
- Diffuse Reflectance Infrared Fourier Transform Spectroscopy

3.1.1 X-ray diffraction (XRD)

When X-ray radiation passes through matter, the radiation interacts with the electrons in the atoms, resulting in scattering of the radiation. If the atoms are organized in planes (i.e. the matter is crystalline) and the distances between the atoms are of the same magnitude as the wavelength of the x-rays, constructive and destructive interference will occur [2]. This results in diffraction where x-rays are emitted at characteristic angles based on the spaces between the atoms organized in crystalline structures called planes. Most crystals can have many sets of planes passed through their atoms. Each set of planes has a specific interplanar distance and will give rise to a characteristic angle of diffracted x-rays. The relationship between wavelength, atomic spacing and angle was solved as the Bragg equation (equation 3.1) [3]. If the illuminating wavelength is known (depends on the type of X-ray tube used and if a monochromator is employed) and the angle can be measured (with a diffractometer) then the interplanar distance can be calculated from the Bragg equation. A set of 'd-spaces' obtained from a single compound will be represent the set of planes that can be passed through the atoms and can be used for comparison with sets of d-spaces obtained from standard compounds.

$$n\,\lambda = 2d\cdot\sin\theta \qquad (3.1)$$

where n = order of reflection (n = 0 1, 2 3 …), λ = wavelength of x-ray (Å), d = lattice distance (Å) and θ = angle of diffraction (°).

X-ray diffraction patterns were recorded with a Philips X`Pert powder diffractometer with FeKα radiation. Measurements were carried out in the 2θ range 0-70° using a step size of 0.05°. Peak identification was performed with the “Powder Diffraction File™” from ICDD.

3.1.2 Low temperature N_2 adsorption

Low temperature nitrogen adsorption is based on the physisorption of a chemically inert gas, e.g. nitrogen, on the surface of solid substances. The physisorbtion is a function of the partial pressure of the gas at the condensation point of that gas. By using the so-called adsorption isotherm the total number of adsorbed molecules can be determined, from which the total surface of the solid can be derived [3]. Micorporous materials have a pore size of less than 2 nm, mesoporous materials have a pore size between 2 nm and 50 nm and macroporous materials have pore size greater than 50 nm [3]. The surface area is calculated by the Brunauer-Emmett-Teller (BET) method [4]. There are two stages in the application of the BET procedure. First it is necessary to derive the monolayer capacity n^a_m, defined as the amount adsorbate required to form a complete monolayer of the adsorbent on the surface. The BET surface area (equation 3.2) is then obtained from n^a_m by taking a value for the average area a_m, occupied by the adsorbate molecule in the filled monolayer [1].

$$a_s(BET) = n^a_m * L * a_m \qquad (3.2)$$

where L is the Avagadro constant ($6.0221*10^{23}$ mol^{-1})

A Micromeritics ASAP 2000 analyzer was used to measure the N_2 adsorption isotherms of the sample. The specific surface area was determined from the BET plot. Prior to the experiment the sample was pretreated overnight under vacuum at 250 °C.

3.1.3 Inductively coupled plasma emission-atomic spectroscopy (ICP-AES)

Inductively coupled plasma is a very high temperature (7000-8000 °C) excitation source that dissolves, vaporizes and ionises atoms. Molecular interferences are reduced with this excitation source but are not eliminated completely. ICP sources are used to excite atoms for atomic emission spectroscopy and to ionise atoms for mass spectrometry. It can be used in quantitative analysis of trace elements in organic and inorganic compounds, simultaneously semi quantitative analysis of inorganic elements, analysis of trace elements in rocks, accumulations, analysis of metals in drinking water or waste water, measurement of contaminant in pure inorganic compounds and analysis of metals in living matters [5].

The instrument was a Varian Vista AX Spectrometer. The sample was dissolved in a mixture of 1 ml HF, 0.5 ml HCl, 2.5 ml HNO_3 and 10 ml H_2O. Then the mixture was placed in a water bath at 95 °C for 3 h. For analysis, H_3BO_3 is added to 1 ml of the dissolved mixture and filled up to 25 ml with water.

3.1.4 Transmission electron microscopy (TEM)

Electron microscopy is simple technique to determine the size and shape of the supported particle. In TEM, a primary electron beam of high energy and high intensity passes through a condenser to produce parallel rays that impinge on the sample. As the attenuation of the beam depends on the density and thickness of the sample mass, this is subsequently magnified by the election optics to produce a so called bright field image. With reference to morphology we get the size, shape and arrangement of the particles which make up the specimen as well as their relationship to each other on the scale of atomic diameters. With reference to crystallographic information we get the arrangement of atoms in the specimen and their degree of order, detection of atomic-scale defects in areas a few nanometers in diameter and with reference to compositional information we get the elements and compounds the sample is composed of and their relative ratios, in areas a few nanometers in diameter [3].

Transmission electron microscopy measurements were performed on a JEOL 2010 microscope equipped with a LaB_6 cathode and with high-tilt objective lenses. The acceleration voltage was 200 kV and vacuum pressure level was 10^{-6} bar.

3.1.5 Temperature programmed desorption of ammonia (NH_3-TPD)

Temperature programmed desorption (TPD) studies employ probe molecules to examine interactions of surfaces with gas or liquid phase molecules. The probe molecules are chosen with respect to the nature of the adsorbed species believed to be important in the catalytic reaction under study or chosen to provide information on specific types of surface sites. TPD of simple bases used method assess the total number of strength of acid sites [6]. Ammonia and pyridine are widely used probe molecules, but for TPD ammonia is preferred than pyridine because pyridine at higher temperatures decomposes and not desorbs.

In a typical TPD experiment, catalyst is contained in a reactor that can be heated at a linear rate. After pretreatment, the catalyst is saturated with a probe molecule under well defined adsorption conditions. After the excess gas is flushed out of the reactor the sample is heated in a flowing inert gas stream. A thermocouple inserted in the catalyst measures the temperature and a detector downstream measures the effluent gas composition. The concentration of the desorbing gas in the effluent gas is monitored by thermal conductivity. Inert gas flow rate, catalyst particle size, catalyst pore size and catalyst bed depth affect the TPD spectra. TPD studies of porous catalysts are generally carried out using reactors designed to minimize the concentration gradients in the reactor.

Temperature programmed desorption (TPD) of NH_3 was carried out in a TPD/TPR 2900 analyser of Micromeritics measuring ammonia with a thermal conductivity detector. 50 mg sample were degassed at 550 ° C for 1 h in a He flow and cooled down to 100 °C. At this temperature adsorption of NH_3 took place until saturation. Afterwards, the catalyst was flushed with He for 30 min. TPD measurements were performed from 100 °C to 650 °C with a heating rate of 20 °C/min, with He as carrier gas.

3.1.6 Temperature programmed reduction with hydrogen (H_2-TPR)

H_2-TPR was carried out in order to characterize the redox reactions of iron in the zeolite sample. Based on TPR patterns, the temperatures needed for the complete reduction of a catalyst can be obtained. Important information which can be derived from the TPR pattern is the oxidation state as well as the reduction capacity of the metal cations [7].

H_2-TPR measurements were carried out by using a TPD/TPR 2900 analyser of Micromeritics. 100 mg sample were activated at 450 ° C for 1 h in Ar flow and cooled to room temperature. The gas flow was switched to 10 vol % H_2 in Ar at room temperature. The TPR was carried out with a heating rate of 10 °C/min up to 700 °C. A liquid N_2/iso-propanol trap placed before the TCD detector removes the water formed during reduction of Fe.

3.1.7 Nuclear magnetic resonance spectroscopy (NMR)

Nuclear magnetic resonance spectroscopy is used to characterize the chemical and structural environment of atoms in the catalysts or in species adsorbed at the catalyst surface [8]. In NMR spectroscopy the transition between magnetic spin energy levels of certain atomic nuclei can be induced in a magnetic field. The most common information obtained from a NMR spectrum concerns the coordination of nuclei investigated and the number of neighbouring equivalent nuclei. The basic principle of NMR is that the atomic nuclei which contains an odd number of protons and/or neutrons possess a nuclear spin I = 0 and consequently a magnetic moment $\mu = \gamma h I$, where h is Planck’s constant and γ is the gyromagnetic ratio which is constant for each type nucleus. When placed in an external magnetic field B_0, the Zeeeman interaction relieves the degeneracy of the energy levels, thus resulting in quantized orientations of the nuclear magnetic moments.

The nucleus can adopt $2I+1$ different magnetic orientations with energies represented by $E(m) = -m\gamma h B_0$, where $m = I, I - 1, \ldots -I$. Transitions between neighbouring energy states can be induced by the radiation energy $E = h\upsilon$, i.e. of frequencies given by the Larmor equation $\upsilon_0 = \gamma B_0/2\pi$. The Larmor frequencies are in the radio frequency region (1-600 MHz). The application of NMR to solids is affected by some difficulties. In particular, the low resolution of the spectra obtained for solid samples makes the interpretation of the results very difficult. In solids, the nuclear spin interactions are anisotropic (they depend on the orientation of the crystals) and not averaged, thus causing a large line broadening. One of the techniques available to reduce the line width in the spectra off solid samples is known as magic angle spinning (MAS). This technique was introduced in 1958 by Andrew et al. [9]. The principle of MAS consists of a rapid rotation of the sample around an axis in angle θ to the external magnetic field. The maximum line narrowing effect is reached for the magic angle of $\theta = 54.74°$, since under this condition, in the first order, all Hamiltonians containing the geometric term $(3\cos^2\theta - 1)$ becomes zero. However, narrowing by MAS depends on the thermal mobility of the nuclei under study. Narrowing the MAS can be reached only if the correlation time and thermal mobility is large in comparison with the period of the macroscopic rotation [10]. In the characterization of zeolitic material ^{27}Al MAS NMR is commonly used to investigate the coordination of Al atoms. Depending on the coordination number of the Al nuclei and the nature of the surrounding atoms, different types of Al species can be identified on the basis of the chemical shifts.

In this work, Magic angle spinning aluminium nuclear magnetic resonance (^{27}Al MAS NMR) spectra were obtained on a Bruker Ultrashield 500 spectrometer at a magnetic field of 11.7 T equipped with a 4 mm MAS head probe. The aluminium resonance frequency at this field is 130 MHz. The sample rotation speed was 12.5 kHz. The ^{27}Al chemical shifts were referenced to a saturated $Al(NO_3)_3$ solution. To obtain NMR spectra as quantitatively as possible in the presence of a heterogeneous distribution of quadrupolar coupling constants, the ^{27}Al nuclei were excited with a single 20° pulse of 1 μs. Excitation pulses longer than 3 μs were seen to overemphasize the extra-framework aluminium signal intensity relative to the framework aluminium signal. The relaxation delay between the scans was set to 1 s. No saturation effects were observed in the spectrum for relaxation delays longer than 0.5 s.

3.1.8 Electron paramagnetic resonance spectroscopy (EPR)

Electron paramagnetic resonance is powerful method which allows to obtain detailed information about paramagnetic centers (elements with one or more unpaired electrons) situated on the surface or in the bulk of solids. EPR is extremely sensitive, which makes it possible to detect and characterize very low abundant paramagnetic species [11]. The basic working principle in EPR is based on the Zeeman effect, i.e. the interaction energy of the electron magnetic moment μ with an external applied magnetic field B_0 ($E = -\mu B_0$). To obtain the energy operator, i.e. the spin Hamiltonian H_s in quantum mechanics, μ_e is replaced by the corresponding spin operator. The spin Hamiltonian is represented by the equation $H_s = g\beta B_0 S$, where β is the Bohr magneton, S is the electron spin operator, and g is the g-tensor, the energy difference between the states $m_s = +1/2$ and -1/2 [11, 12].

EPR transitions obey the selection rule, i.e. the spin flip from the lower ($m_s = +1/2$) to the higher ($m_s = -1/2$) energy spin state. The energy absorption is detected, amplified and plotted as a function of the magnetic field. Depending on the type and symmetry of paramagnetic species, its unpaired electron spins can undergo different interactions, which determine the number and energy of electronic sublevels and, thus, the number and magnetic field positions of observable EPR transitions. When paramagnetic species contain more than one unpaired electron ($S > 1/2$) dipolar interaction between the latter creates 2S+1 electronic sublevels and leads to fine structure of the EPR spectrum [13].

EPR measurements have been carried out using an ELEXYS Bruker spectrometer (at X-band microwave frequency), at temperatures of 20 °C and -150 °C.

3.1.9 Ultraviolet-visible spectroscopy (UV-vis)

In UV-vis spectroscopy, the electrons are transferred from low energy to high energy atomic or molecular orbitals when the material is irradiated with light [14]. Such electron transfer process may take place in transition metal ions, and inorganic and organic molecules. Electronic transitions are of two types and involve orbitals or levels localized on the same metal atom or on two adjacent atoms [15]. The first type includes the following metal-centered (MC) transitions:

- d→d and (n-1)d→ns in transition elements
- f→f and 4f→d in rare earth elements
- ns→np in the main group of elements

The second class involves charge transfer (CT) transitions from an occupied level centered on a donor atom to a vacant one centered on an acceptor [15, 16]. This type includes:

- Ligand to metal (LMCT) and metal to ligand (MLTC) charge transfers
- Metal to metal charge transfers (MMCT)
- Transitions between molecular orbitals ($n \rightarrow \pi^*$ and $\pi \rightarrow \pi^*$)

LMCT, MLTC and MMCT transitions depend on the symmetry and the oxidation state of metal and on the nature ligand or of the other metal atom [15]. The energy of the CT band increases with the optical electro negativity differences between the metal and the ligand.

In solid catalysts or turbid solutions, most of the light is reflected and not transmitted. For the investigation of such materials, diffuse reflectance spectroscopy is used. In this technique, the light reflected by the sample is collected by an integrating sphere, coated wih a highly reflecting layer on the inside (e.g. MgO or $BaSO_4$), and then conveyed to the detector. The reflectance is given by $R = I/I_0$, where I and I_0 are the intensities of the incident and reflected light respectively. For a non-transparent think layer, R is called $R\infty$. As reflectance of the sample is compared to that of reference compound, the relative quantity $R`\infty$ is $R\infty$(sample)/ $R\infty$(reference). The measurable reflectance $R`\infty$ is used to calculate the Kubelka-Munk $F(R`\infty)$ function which is given as $F(R`\infty) = K/S = (1-R`\infty)^2/(2\ R`\infty)^2$, where K and S are the adsorption and reflection coefficients respectively. [3]. The diffuse reflectance UV-vis spectrum of the catalyst was measured on a Cary 400 UV-vis spectrometer equipped with a Praying Mantis sample stage from Harrick. $BaSO_4$ was used as reference.

3.1.10 Diffuse reflectance infrared Fourier transform spectroscopy (DRIFT)

Spectroscopic techniques play an important role in the study of zeolites because of the difficulties of applying diffraction methods to elucidate the structures of these substances. Infrared (IR) radiation is electromagnetic radiation that encompasses all the wavelengths between the visible and microwave regions of the electromagnetic spectrum. The term "infra red" covers the range of the electromagnetic spectrum between 0.78 and 1000 μm. In the context of infra red spectroscopy, wavelength is measured in "wave numbers", which have the unit's cm^{-1}. The wave number is represented as $1/\lambda$, where λ is the wavelength (cm).

In all types of absorption spectroscopy the fundamental governor of intensity is the number of molecules sampled. A simple relationship between the intensity of the transmitted (I) and incident radiation (I_0) and the amount of sample in the beam (concentration or thickness) exists and is known as the Beer-Lambert law, which is given as $I = I_0 \exp(-\varepsilon cl)$, where c is the concentration, l is the cell thickness and ε is the frequency dependent extinction coefficient. The Beer-Lambert law is the foundation for all quantitative infrared spectroscopy. Absorption of IR is restricted to compounds with small energy differences in the possible vibrational and rotational states. For a molecule to absorb IR, the vibrations or rotations within a molecule must cause a net change in the dipole moment of the molecule. The alternating electrical field of the radiation interacts with fluctuations in the dipole moment of the molecule. If the frequency of the radiation matches the vibrational frequency of the molecule then radiation will be absorbed, causing a change in the amplitude of molecular vibration.

The following sample transmission sampling techniques are used IR spectroscopy:

- Transmission (general samples)
- Attenuated Total Reflectance (thick samples)
- Diffuse Reflectance Fourier Transform (powders)
- Reflection Absorption Infrared Spectroscopy (very thin samples)

Transmission is the most simple and basic infrared spectroscopic sampling technique. Essentially, infrared radiation is passed through a sample and the transmitted radiation is measured. The spectra obtained will be representative of the whole of the sampled area and 'localized' (e.g. surface) properties can quite easily be lost in the 'bulk' properties depending on the size and nature of the sample. It is only useful for thin (<10 µm) samples or when looking at weak bands, such as overtones, in thicker samples. Often sample preparation such as the manufacture of KBr discs is necessary which can be time consuming and difficult to reproduce.

For all samples which are powders (e.g. zeolites) a technique called Diffuse reflectance infra red spectroscopy (DRIFTS) is used. In DRIFTS the incident radiation beam is passed on to the flat mirrors from where it is reflected to two elliptical mirrors and from there it is further reflected to the sample. Once when it reached the sample the incident radiation gets refracted and passes on to the elliptical mirrors and from there it is reflected to the flat mirrors and finally it is passed on to the detector [3].

Diffuse Reflectance Infrared Fourier Transform (DRIFT) spectra were recorded with a Nexus 860 Thermo Nicolet spectrometer in a DRIFT cell equipped with ZnSe windows. The sample was pretreated at 450 °C for 1 h in flowing N_2. At each temperature the background spectrum was recorded and subtracted from the sample spectrum obtained at the same temperature. In the experiment the IR spectra were recorded at 200 scans at a spectral resolution of 4 cm^{-1}. The total gas flow entering the cell was 40 ml /min.

3.2 References

[1] M. Devadas, Master Thesis, University of Erlangen-Nürnberg, Erlangen, 2002.

[2] N. Heff, “Grundlagen und Anwendung der Röntgenstruktur-Feinanalyse”, Oldenbourg-Verlag, München, 1962.

[3] G. Ertl, H. Knözinger, J. Weitkamp, “Hand Book of Heterogeneous Catalysis” Volume 2, Wiley-VCH, Weinheim, 1997.

[4] S. Brunauer, P.H. Emmet, E. Teller, J. Amer. Chem. Soc. 60 (1938) 309.

[5] R. O. De Dios, Master Thesis, University of Erlangen-Nürnberg, Erlangen, 2000.

[6] J. R. Anderson, K. C. Pant, “Introduction to Characterization and Testing of Catalyst”, Academic Press, Boston, 1985.

[7] J. W. Niemantsverdriet, “Spectroscopy in Catalysis”, Wiley-VCH, Weinheim, 1995.

[8] G. Engelhardt, D. Michel, “High Resolution Solid State NMR of Silicates and Zeolites”, John Wiley & Sons, New York, 1987.

[9] E. R. Andrew, A. Bradbury, R. G. Eades, Nature 182 (1958) 1659.

[10] E. R. Andrew, A. Jasinski, J. Phys. C 4 (1971) 391.

[11] K. Dyrek, M. Che, Chem. Rev. 97 (1997) 305.

[12] B. M. Weckhuysen, P. Van Der Voort, G. Catana, “Spectroscopy of Transition Metal Ions on Surfaces”, University Press, Lueven, 2000.

[13] B. M. Wechuysen, “In-Situ Spectroscopy of Catalysis”, American Scientific Publishers, California, 2004.

[14] L. F. Gladden, P. Alexander, Meas. Sci. Technol. 7 (1996) 423.

[15] G. Blasse, Struc. Bond. 76 (1991) 153.

[16] C. K. Jorgensen, “Absorption Spectra and Chemical Bonding in Complexes”, Permgamon, New York, 1962.

4

Experimental Set Up & Catalyst Preparation

4.1 Experimental set up

The experimental set up used for catalytic investigation is shown in figure 4.1(Reprint from [1]).

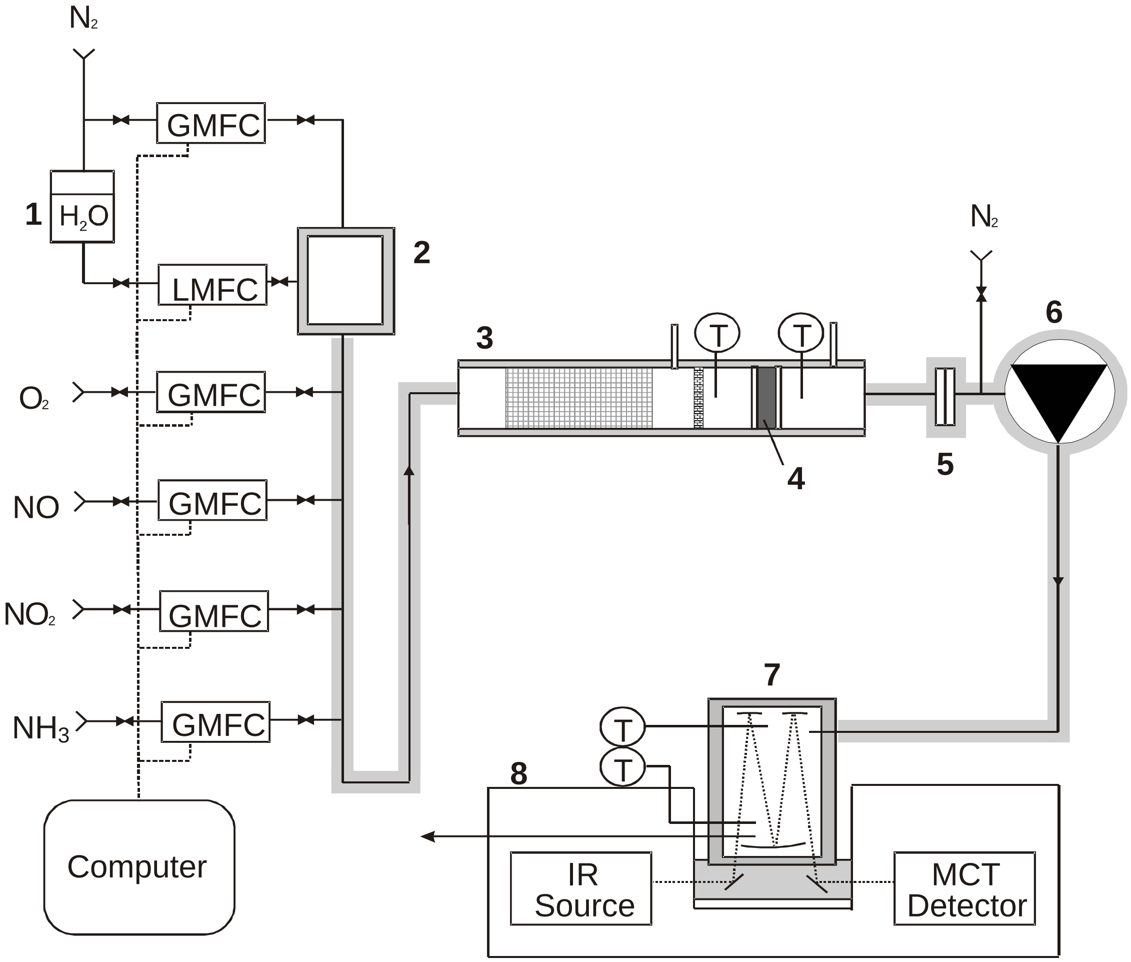

Figure 4.1 Plant set up (GMFC) gas mass flow controller, (LMFC) liquid mass flow controller, (T) thermocouple, (1) water reservoir, (2) water evaporator, (3) reactor, (4) catalyst sample, (5) filter, (6) diaphragm pump, (7) reflection gas cell, and (8) FTIR spectrometer.

In figure 4.1, the entire plant set up can divided into three sections namely: reactant gas dosing system, the reactor and finally the gas analyzer.

4.1.1 Reactant gas dosing system

The feed gases needed for the measurement were supplied by Carbagas. The purity of the reactant used is shown in table 4.1. The flow of each gas is controlled by mass flow controllers (Brooks 5850S). Since water is present in the feed, liquid water was dosed by means of a liquid mass flow controller (Brooks 5881) through a capillary tube into an electrically heated evaporator. The mass flow controllers were controlled by a computer. Nitrogen was used as a balance gas and was automatically adjusted to make up the total flow rate. The total flow rate could be varied between 350 and 450 L_N/h. The gas lines of the experimental set up were heated to 150°C-170 °C by heating tapes.

Table 4.1 Gas mixtures used for the preparation of the reactant feed gas.

Gases	Concentration	Purity
N_2	100 %	99.999 %
O_2	100 %	99.5 %
NO	5 % in N_2	99.9 %
NO_2	1 % in N_2	99 %
NH_3	5 % in N_2	99.997 %

4.1.2 Reactor for monolith catalyst testing

As shown in figure 4.1, the reactor used for testing monolith catalyst is a tubular glass reactor. The inner diameter of the glass reactor is 28 mm. The pre-heating zone of the reactor was filled with steatite pearls and the second zone was for the monolith catalyst. The entire reactor was heated independently by two separate heating tapes connected to individual temperature controllers. The temperature control was based on two thermocouples placed in front of the pre-heating zone and after the catalyst, respectively.

A third thermocouple was placed just in front of the catalyst entrance in order to measure the temperature of the gas feed.

4.1.3 Gas analyzer system

The gas which exits from the catalyst outlet is analyzed by Fourier transform infrared (FTIR) spectroscopy. The apparatus is a Nicolet Magna IR 560 spectrometer equipped with a liquid nitrogen cooled MCT detector. A multi-path gas cell (Graseby Specac G-2-4-BA-AU, 2 m path length, volume of 275 cm^3, gold mirrors) was used for the FTIR analysis. The cell could be heated up to 200 °C. The path length could be varied in the range 0.4-2.8 m (cell length = 10 cm) according to the number of reflections. A fixed path length of 2 m was used in the experiments. The cell was equipped with special sandwich-type windows in order to avoid the formation of nitrates by NO_2 contained in the test gas. All spectra were recorded with a resolution of 0.5 cm^{-1} and a wavelength range between 400 and 4000 cm^{-1}.

To quantify the various gaseous species, a software (Quant Pad) was used. This software is based on the CLS process (classic least square fit) and allows to correct the spectral adsorbance in the region of non linearity. Table 4.2 reports the ranges and the limits of detection of the various species. CO_2 was omitted from the test gas mixture as it interferes with N_2O, thus disturbing the measurement of this gas.

Table 4.2 Detection limits of various components in dry and wet feed conditions.

Gas	Detection Range [cm^{-1}]	Detection Limits without water [ppm]	Detection Limits with 5% vol. water [ppm]
NO	1850-1940	3	5
NO_2	1634-1678	1	3
N_2O	2134-2266	0.5	0.5
NH_3	831-1147	1	1
HNO_3	836-917	10	10
H_2O	2953-3017	300	-

4.2 Catalyst preparation

In the present work, a commercially available Fe-ZSM5 powder was used as a model substance. The catalytic material was coated on a cordierite honeycomb of the size 4.66" x 4.66" x 3" with a cell density of 400 cpsi by Umicore automotive catalysts, Germany. The Fe-ZSM5 was prepared by solid state ion exchange method. The active mass (catalyst loading) is 160 g/l. For the catalytic investigation, the cordierite monolith was cut into piece which fit to the sample holder of the tube.

4.3 Reference

[1] M. Kleemann, “Beschichtung von Cordierit-Wabenkörpern für die selektive Katalytische Reduktion von Stickodiden”, Thesis ETHZ No. 14301, Zurich, 1999.

5

Characterization of Fe-ZSM5

5.1 Introduction

As with any catalytic research, the characterization of the catalyst is an essential aspect for successful research. The complete and accurate knowledge of the properties of a catalyst is fundamental for evaluating its performance. A full characterization of the catalyst is needed if an optimization of the process conditions is desired, or if a change of the catalyst, of its texture or the dispersion of the active elements is needed. With characterization methods mentioned in chapter 3, fresh Fe-ZSM5 powder sample is characterized in order to get an insight into the catalytic and structural properties.

5.2 Experimental

Powder Fe-ZSM5 catalyst was provided by Umicore automotive catalysts, Germany. Fe-ZSM5 was prepared solid state ion exchange method.

5.3 Results

5.3.1 XRD

Figure 5.1 shows the XRD patterns of fresh Fe-ZSM5 sample. Fe-ZSM5 exhibited XRD patterns which are identical to MFI structures [1], indicating that the ZSM5 structure is maintained after ion exchange process. Low intensity diffraction lines at lines at 37.65° and 40.85° (denoted by * in figure 5.1) are attributed to traces of hematite (Fe_2O_3) particles.

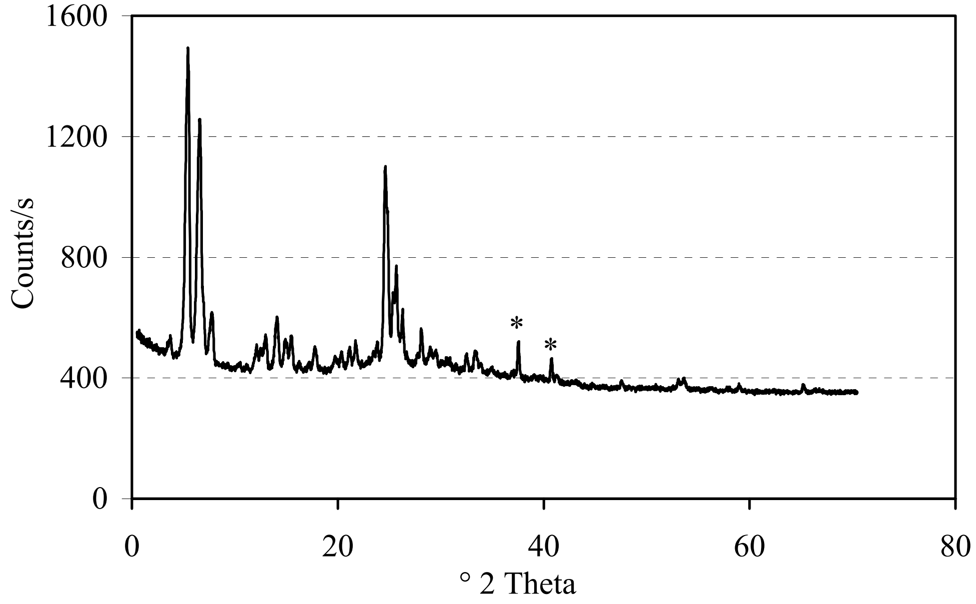

Figure 5.1 XRD of fresh Fe-ZSM5 catalyst.

5.3.2 ICP-AES & Low temperature N_2 adsorption

The BET surface area, micropore volume and elemental composition of Fe-ZSM5 are shown in table 5.1.

Table 5.1 Low temperature N_2 adsorption and ICP-AES results

	[a] BET surface are (m^2/g)	[a] Micropore volume (cm^3/g)	[b] Si/Al	[b] Fe/Al	[b] Fe wt (%)
Fe-ZSM5	301	0.089	23	0.75	4.97

[a] Determined from low temperature nitrogen adsorption analysis.

[b] Determined from ICP-AES analysis.

It is found from table 5.1 the Fe-ZSM5 has module (molar ratio of SiO_2/Al_2O_3) of 23 and the amount of Fe which got loaded into the zeolite is 4.97 wt %.

5.3.3 TEM

Figure 5.2 shows the TEM picture of the Fe-ZSM5 sample. Dark spots (marked by arrows) were observed in figure 5.2. These black spots of 10-20 nm size are attributed to Fe_2O_3 particles, which is supported by the XRD results.

Figure 5.2 TEM micrograph of fresh Fe-ZSM5 catalyst.

5.3.4 NH_3-TPD

Figure 5.3 display the NH_3-TPD profile of the Fe-ZSM5 sample. The spectrum of Fe-ZSM5 exhibited a double-peak characteristic of zeolites with the MFI-structure [2, 3]. The two peaks, named as low temperature (LT) peak and high temperature (HT) peak are centred at about 200 °C and 425 °C, respectively. Hidalgo et al. [2] found that the high temperature (HT) peak was always associated with ammonia adsorbed on acidic hydroxide groups. The low temperature peak is a subject of uncertainty, i.e. it could be physisorbed ammonia [4] or ammonia adsorbed on a non-zeolitic impurity [5].

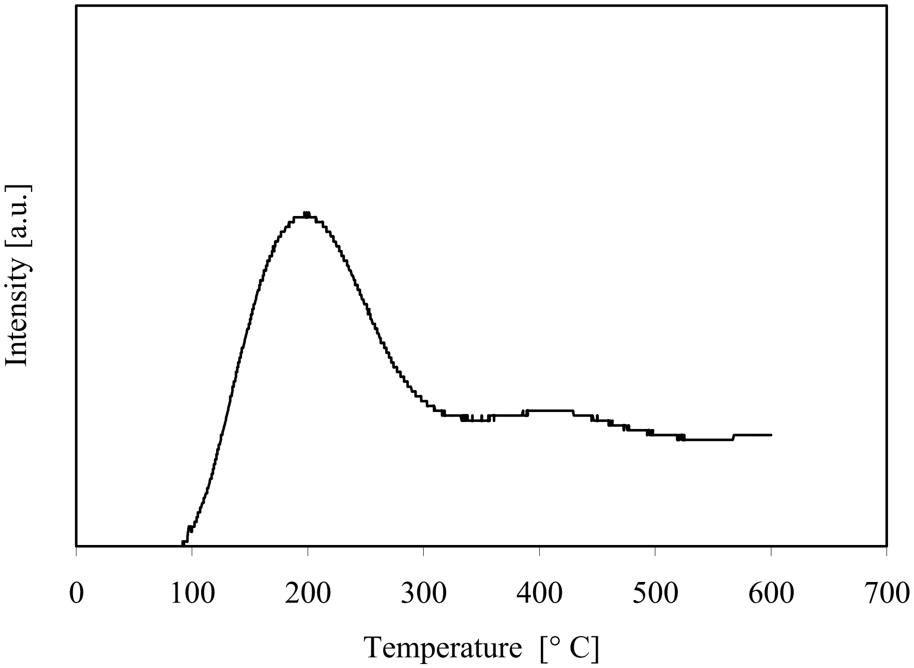

Figure 5.3 NH_3-TPD profile of fresh Fe-ZSM5.

5.3.5 H_2-TPR

Figure 5.4, shows the H_2-TPR profile for the fresh Fe-ZSM5 catalyst. Reduction proceeded in two stages. The first reduction peak around 480 °C corresponds to the reduction Fe^{3+} to Fe^{2+}. Integration of this peak yielded an H_2/Fe molar ratio of 0.44, which is close to the value of 0.5, required the reduction of Fe^{3+} to Fe^{2+}. The second peak around 550 °C corresponds to the reduction of Fe^{2+} to Fe^{0}. Integration of this peak yielded an H_2/Fe molar ratio of 0.10 and this small consumption of H_2 is attributed to the fact that most Fe^{2+} is hardly reducible in the Fe-ZSM5 [6], and only a small fraction exists in a easy reducible form.

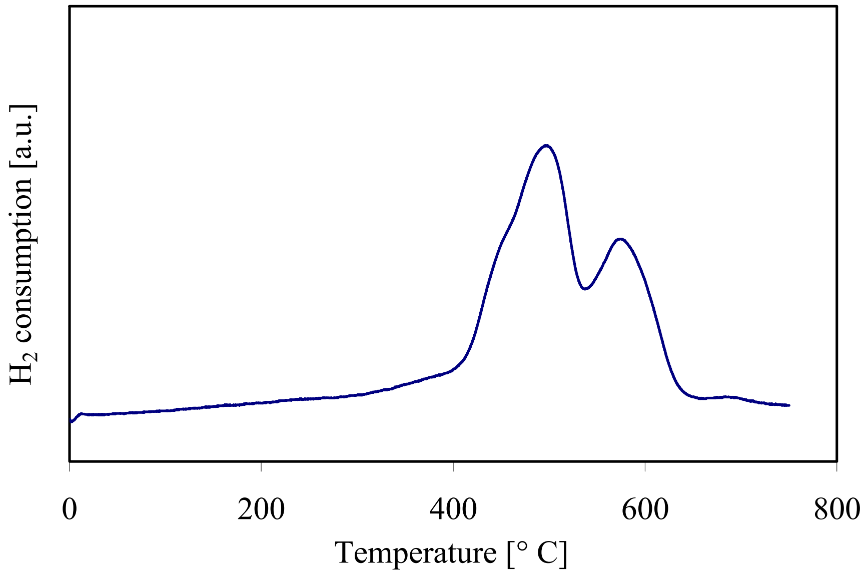

Figure 5.4 H_2-TPR profile of fresh Fe-ZSM5.

5.3.6 ^{27}Al MAS NMR

The ^{27}Al MAS NMR spectrum of the Fe-ZSM5 zeolite is shown in Figure 5.5. The signal at 55-60 ppm in the spectrum correspond to tetrahedrally coordinated alumina $Al(OSiO)_4$ in the framework lattice [7]. The signal at 0 ppm is created due to dealumination and it corresponds to aluminium in octahedral AlO_6 groups [8]. A broad signal in the range of 30-50 ppm is also often observed. However, the assignment of this signal is still under debate: some authors attributed this resonance line to penta coordinated aluminium [9, 10], whereas others assigned it to tetrahedral extraframework aluminium species [11]. Besides signal around 0 and 55 ppm, for Fe-ZSM5 weak signals around 185 and around -175 arise due to spinning side band and these bands depend upon the iron content [12].

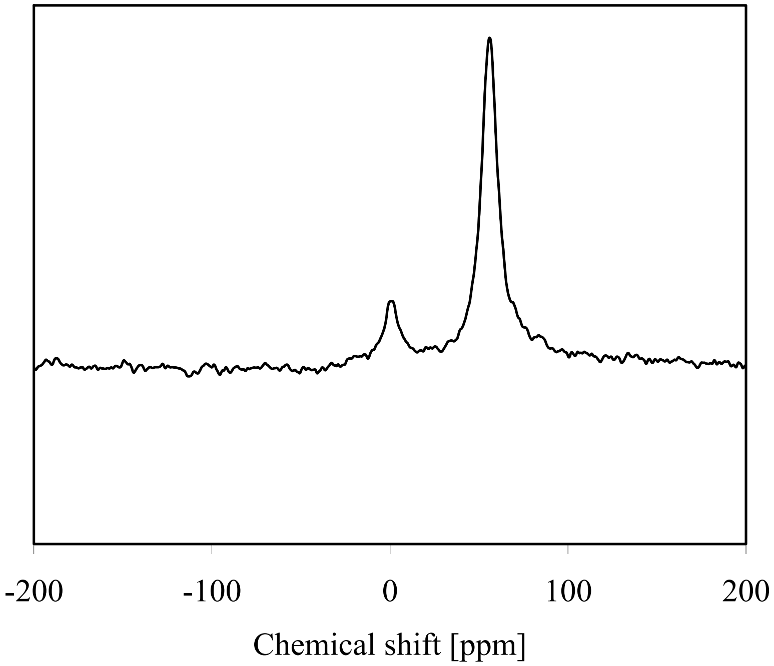

Figure 5.5 ^{27}Al MAS NMR spectra of FeZSM5.

5.3.7 EPR

In a generic sense when a Fe(III) ion is present in zeolitic lattices there are two possibilities of emplacements: either as a framework ion in tetrahedral or octahedral environment, or situated in extra-framework position as iron oxide, -hydroxide, with usually octahedral coordination. Depending on the concentration of Fe present in the zeolitic lattice and the preparation procedure, or further treatment, aggregates can be formed, as extra-framework components. The characterization of Fe(III) in zeolites is a rather difficult process due to the possible superposition of the EPR lines coming from different species and that the unambiguous attribution of these lines remains questionable. Moreover it is necessary to point out that all EPR measurements reveal only paramagnetic Fe species. The results of the EPR measurements are shown in figure 5.6. The spectra consist of signals in two regions, i.e. signals at $g \geq 4.2$ and signals at $g \geq 2.0$. In the region at $g \geq 4.2$ there is a main signal at $g \sim 4.2$ and others less intense at $g \sim 5.6$ and $g \sim 8.5$. The intensity of the signals at $g \geq 4.2$ increases with decreasing temperature. A second group of signals is located in the zone $g \sim 2.0$, for both spectra. At -150 °C, the signal at g ~ 2.3 is decreased in intensity and the signal at g ~ 2.3 is shifted to lower magnetic fields.

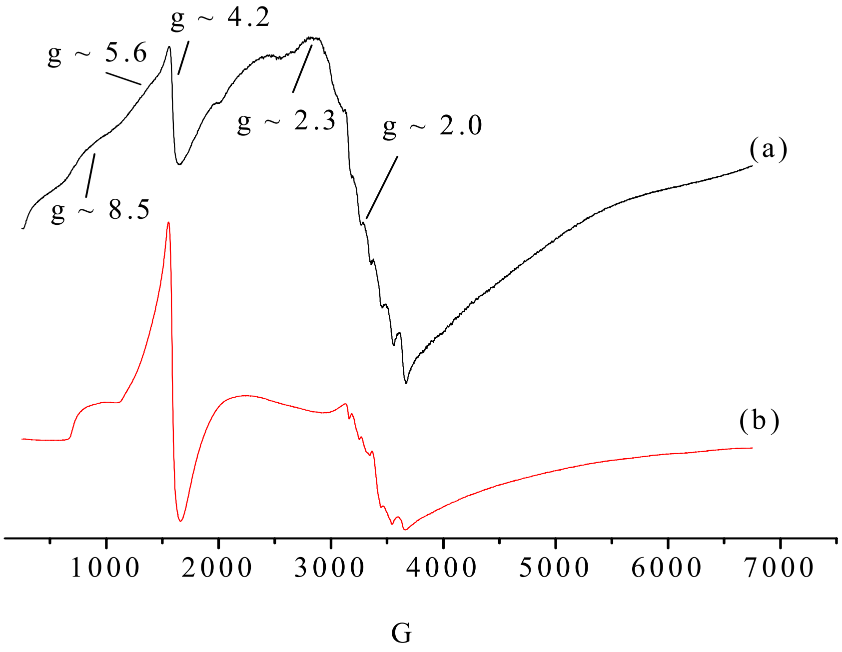

Figure 5.6 EPR spectra of fresh Fe-ZSM5 at (a) 20 °C and (b) -150 °C.

The observed signals are common for Fe-ZSM5 zeolites [13, 14] and also for Fe^{3+} ions in other oxide matrices. The number and positions of EPR transitions for Fe^{3+} ions observable in a powder spectrum depend sensitively on the local crystal powder spectrum of these sites and possible magnetic interactions between them. Goldfarb et al. [14] attributed the signals at g ~ 4.3 and $g \geq 6$ to arise from $| -½ > \leftrightarrow > ½ |$ transition of isolated Fe^{3+} sites in strong rhombic or axial distortion. Based on [14], M. S. Kumar et al. [15] implied that an Fe^{3+} species giving rise to a line at g ~ 4.3 is more strongly distorted than an Fe^{3+} site represented by a signal at g ~ 6 due to the difference in the magnitude of E. The signal at g ~ 4.3 is assigned to Fe^{3+} sites incorporated in tetrahedral positions while the line at g ~ 6 is assigned to isolated Fe^{3+} species in higher coordination numbers [14]. Signals at g ~ 2 can arise from isolated Fe^{3+} or from Fe_xO_y clusters. The broad line at g = 2.3 is attributed to small Fe_2O_3 particles [14]. The signal at g ~ 2.3 disappear at -

150 °C and do not follow the paramagnetic behaviour, indicating that the corresponding Fe^{3+} ions are in mutual magnetic interaction.

5.3.8 UV-vis

Figure 5.7 shows the UV-vis spectrum of Fe-ZSM5. A band at around 35,000 cm^{-1}, is accompanied with a shoulder around 45,000 cm $^{-1}$. In addition a band around 15,000 cm^{-1} and a strong absorption edge around 18,400 cm^{-1} were formed. Shoulders around 20,000 $cm^{-1}$and 28,000 cm^{-1} were also observed.

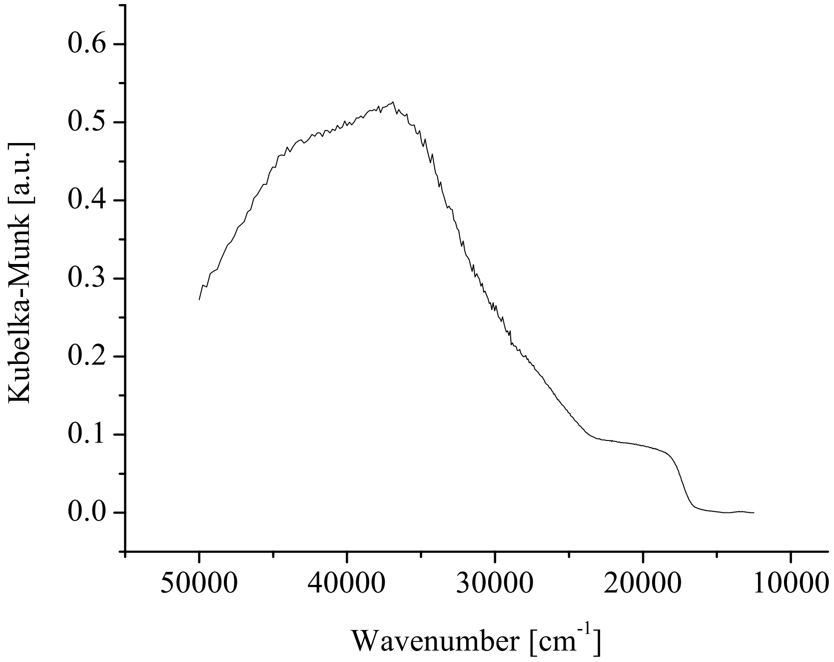

Figure 5.7 UV-vis spectrum of Fe-ZSM5.

For Fe^{3+} two ligand-to-metal charge transfer (CT) transitions, $t_1 \rightarrow t_2$ and $t_1 \rightarrow e$, are expected [16]. The bands at 35,000 cm^{-1} and 45,000 cm^{-1} are attributed to isolated Fe^{3+} sites at octahedral and tetrahedral positions, respectively [17]. The low intensity band at 15,000 cm^{-1} and the absorption edge around 18,400 cm^{-1} are assigned to Fe oxide like species. The strong absorption edge at 18,400 cm^{-1} corresponds to the d-d electron pair transition (EPT), which is unique for the presence of Fe^{3+} in Fe_2O_3 (hematite) [18, 19].

The position of the EPT band depends on the particle size of hematite [18]. From the EPT band in the range 18,200-18,900 cm^{-1} a hematite particle size of about 10-50 nm is derived, which confirms the results of the TEM analysis. For highly loaded Fe-MFI, the bands around 20,000 cm^{-1} are ascribed to Fe_2O_3 particles [20]. The shoulder at 28,000 cm^{-1} is characteristic for iron oxo dimmers, such as $[HO\text{-}Fe\text{-}O\text{-}Fe\text{-}OH]^{2+}$, which are bound to the zeolite framework via iron oxygen bridges [21].

5.3.9 DRIFT

5.3.9.1 OH stretching region

Figure 5.8 shows hydroxyl (OH) stretching region for the fresh Fe-ZSM5 sample. The spectrum was recorded with the empty cell as background.

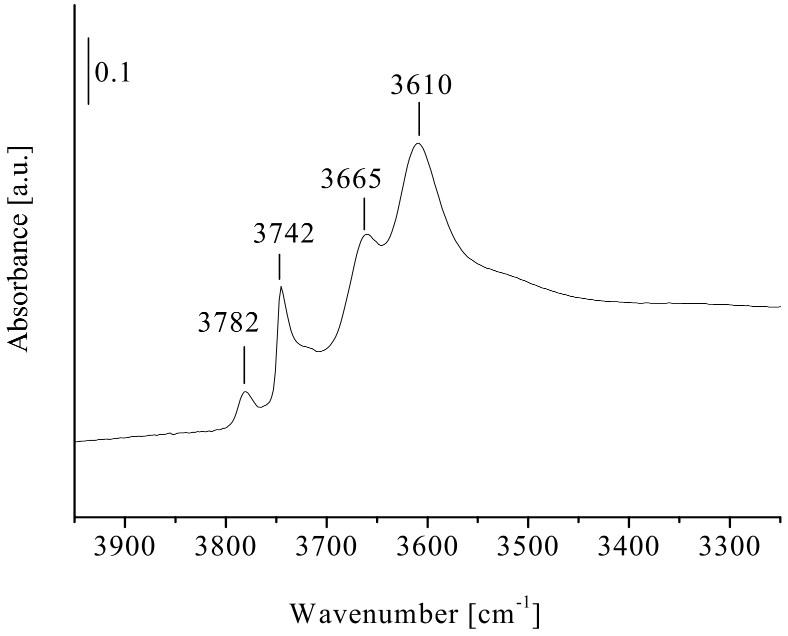

Figure 5.8 FTIR spectra of hydroxyl groups on fresh Fe-ZSM5 at 35 °C.

The band at 3610 cm^{-1} is characteristic for Brønsted acid sites. These sites are associated with framework aluminium (Si(OH)Al) [22], while the band at 3742 cm^{-1} is assigned to terminal silanol groups present in the channels and at the external surface [23]. Two additional bands at 3665 and 3782 cm^{-1} are attributed to the hydroxyl groups connected to extraframe work aluminium (Al-OH) species [24] and to hydroxyl groups attached to a tricordinated aluminium atom linked to the network via two oxygen bonds [25] respectively. The broad band around 3500 cm^{-1} is due to delocalized hydrogen-bonded groups where silanol groups are proximate to each other, typical of internal Si-OH groups on lattice defects [26, 27].

5.3.9.2 NO adsorption

Figures 5.9, 5.10, 5.11 and 5.12 represent the spectra evolved during NO treatment on Fe-ZSM5. In figure 5.9, NO was adsorbed for 30 min at 35 °C and then purged with N_2 for 60 min at the same temperature. After purging for 60 min, the spectra were recorded with increasing temperature in a nitrogen flow. The band at 1880 have been assigned to mono-nitrosylic species associated with isolated Fe sites either in the 3+ (Fe^{III}-NO) [28] or 2+ (Fe^{II}-NO) state [29].

Segawa et al. [28] assigned it to isolated Fe^{3+}-NO in Fe-Y zeolites, based on the presence of this band after treatment of the sample with O_2 at elevated temperatures. In addition to the 1880 cm^{-1} band, a shoulder at 1820 cm^{-1} is observed. This shoulder is assigned to species supported on Fe-oxide ions. The band at 2165 cm^{-1} is attributed to NO$^+$ species. This band is normally observed around 2145 cm^{-1} [30, 31]. The shift in NO$^+$ band, is attributed to the NO$^+$ stretching frequency dependency on the degree of electron transfer of the corresponding anion to the π^* orbital of NO$^+$ [33]. Therefore, the stretching frequency of NO$^+$ varies with nature and the extent of exchange with metal cation [32, 34]. The intensity of the band was decreased and the band was not stable at $T \geq 400$ °C.

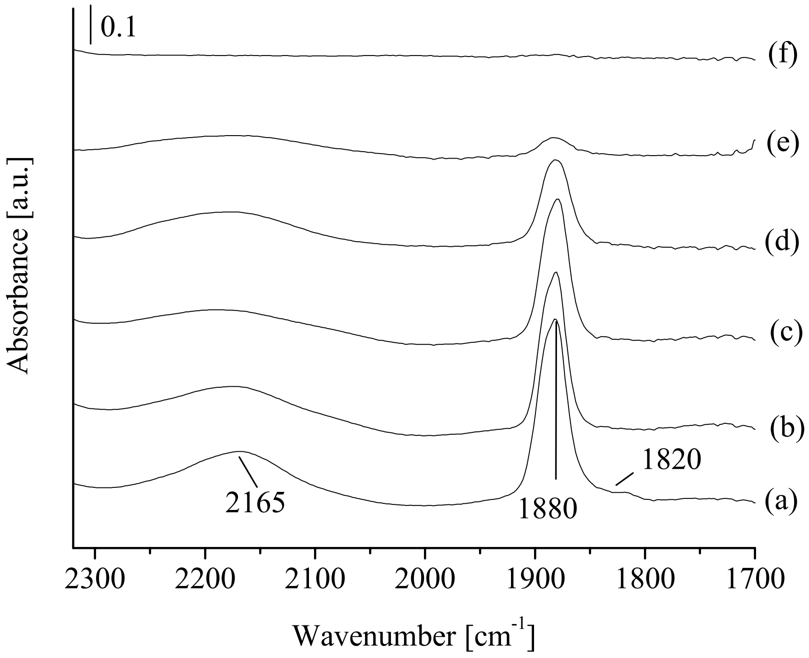

Figure 5.9 FTIR spectra of Fe-ZSM5 treated with 500 ppm NO. (a) NO adsorption at 35 °C, (b) after purging with N_2 for 60 min at 35 °C (c) 100 °C, (d) 200 °C, (e) 300 °C and (f) 400 °C.

Figure 5.10 shows the evolution of NO adspecies for increasing adsorption times. The intensity of the bands at 2165 cm^{-1} and 1880 cm^{-1} were increasing with time, but the increase of the later was relatively less compared to the 2165 cm^{-1} band.

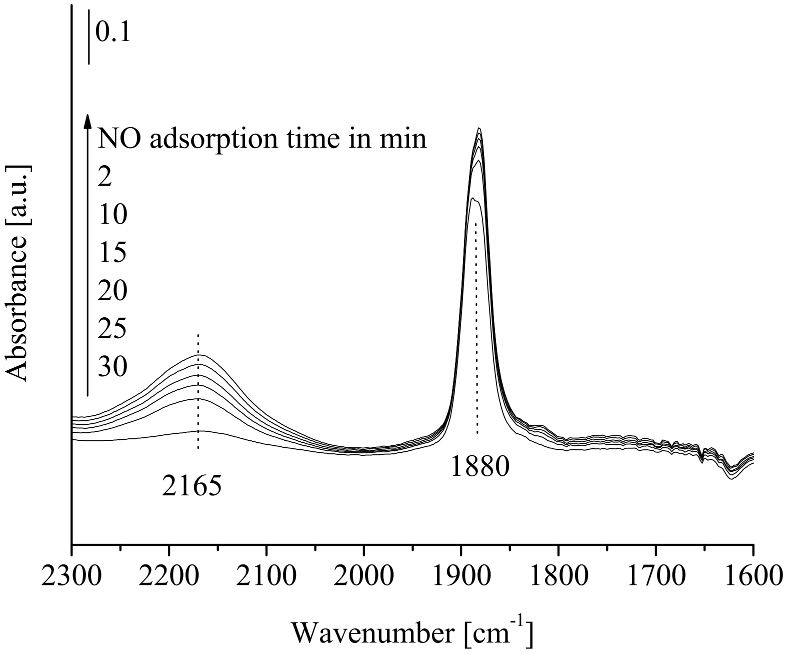

Figure 5.10 Evolution of NO adspecies on Fe-ZSM5 with adsorption times at 35 °C.

Bands in the region 800-1000 cm^{-1} are assigned to asymmetric internal stretching vibrations of the zeolite lattice: they indicate perturbation by transition metal cations located at exchange sites in zeolites. These bands shift when the oxidation state of the metal changes or when a substance is adsorbed. The changes in the T-O-T perturbation region are shown in figure 5.11. A distinct band at 933 cm^{-1} was formed. These skeletal bands which arise due to NO interaction with Fe-ZSM5 are typical for Fe ions located in cationic sites [35].

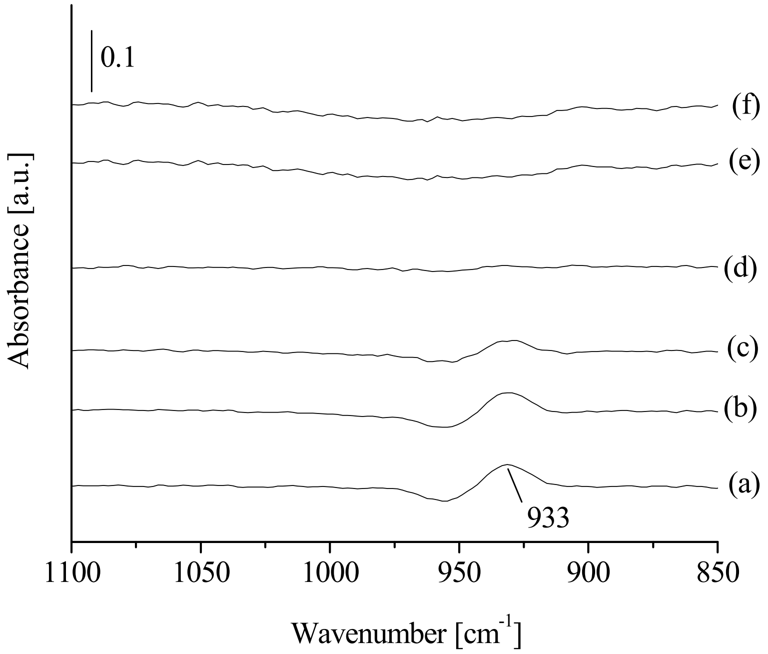

Figure 5.11 Changes in T-O-T region due to NO (500 ppm) treatment. (a) NO adsorption at 35 °C (b) after purging with N_2 for 60 min at 35 °C (c) 100 °C, (d) 200 °C, (e) 300 °C and (f) 400 °C.

The changes in the O-H stretching region during this experiment are shown in figure 5.12. Introduction of NO at 35 °C, resulted in a strong decrease in intensity of the band at 3605 cm^{-1}, which is attributed to the formation of NO^+ species on ion exchange positions. At the same time, the intensity of the band at 3665 cm^{-1} strongly decreased. The band at 3665 cm^{-1} increased with temperature. This band is attributed to hydroxyl groups connected to extraframe work aluminium (Al-OH) species. A plausible explanation might be, that NO adsorbs on extraframe work aluminium species at $T \leq 200$ °C as NO^+ and at higher temperatures this NO^+ reacts, resulting in an increase of the band at 3665 cm^{-1}.

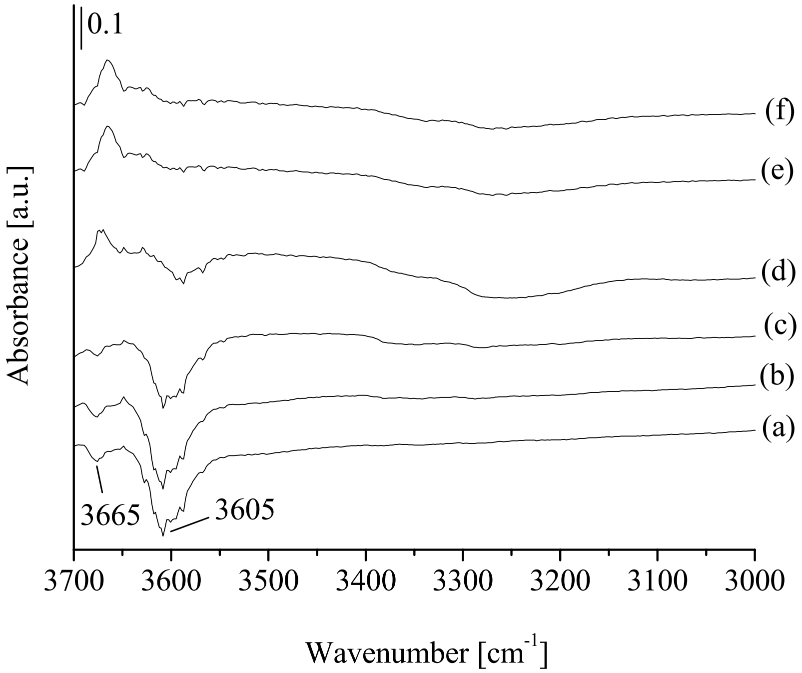

Figure 5.12 Changes in OH stretching region due to NO (500 ppm) treatment. (a) NO adsorption at 35 °C (b) after purging with N_2 for 60 min at 35 °C (c) 100 °C, (d) 200 °C, (e) 300 °C and (f) 400 °C.

5.3.9.3 NO_2 adsorption

Figure 5.13 depicts the IR spectra of NO_2 adsorption experiments on Fe-ZSM5. NO_2 was adsorbed for 45 min at 35 °C and purged with N_2 for 60 min at the same temperature. Then spectra were recorded at different temperatures in the flow of N_2. Bands at 1635 cm^{-1}, 1580 cm^{-1} and a shoulder at 1605 cm^{-1} were observed. The band at 1635 cm^{-1} is assigned to adsorbed NO_2 species [30]. The band at 1580 cm^{-1} is assigned to bidentate nitrates [36]. The assignment of the shoulder around 1605 cm^{-1} is to bridging nitrates [36]. All the species formed were not stable beyond $T \geq 400$ °C.

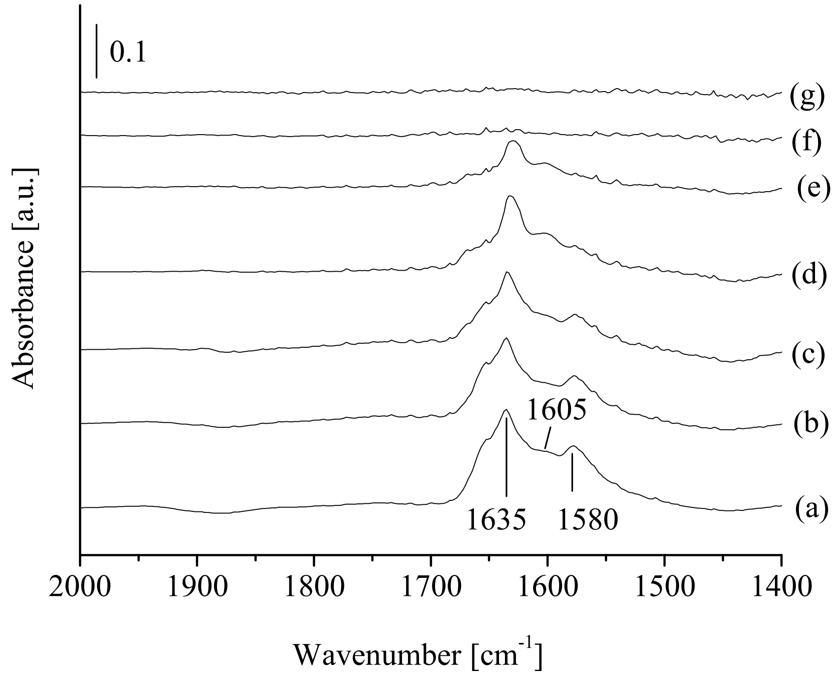

Figure 5.13 FTIR spectra of Fe-ZSM5 treated with 500 ppm NO_2. (a) NO adsorption at 35 °C, (b) after purging with N2 for 60 min at 35 °C (c) 100 °C, (d) 200 °C, (e) 300 °C, (f) 400 °C and (g) 450 C.

5.3.9.4 NO+O_2 adsorption

Figure 5.14 shows the IR spectra of NO + O_2 adsorption experiments on Fe-ZSM5. The oxygen concentration was 5 %. In figure 5.14, NO + O_2 was co-adsorbed for 45 min at 35 °C and then purged with N_2 for 60 min at the same temperature. Then spectra were recorded with increasing temperature in the flow of N_2. The band at 1635 cm^{-1} is assigned to adsorbed NO_2 species; the formation of this band is explained by the oxidation of NO to NO_2 in the presence of O_2. On N_2 purging and with increasing temperatures, the intensity of the bands decreased: the species formed were not stable beyond $T \geq 400$ °C. The nitrate species bands at 1605 cm^{-1} and 1578 cm^{-1} were also observed, confirming the oxidation of NO to NO_2, which is bonded as nitrate.

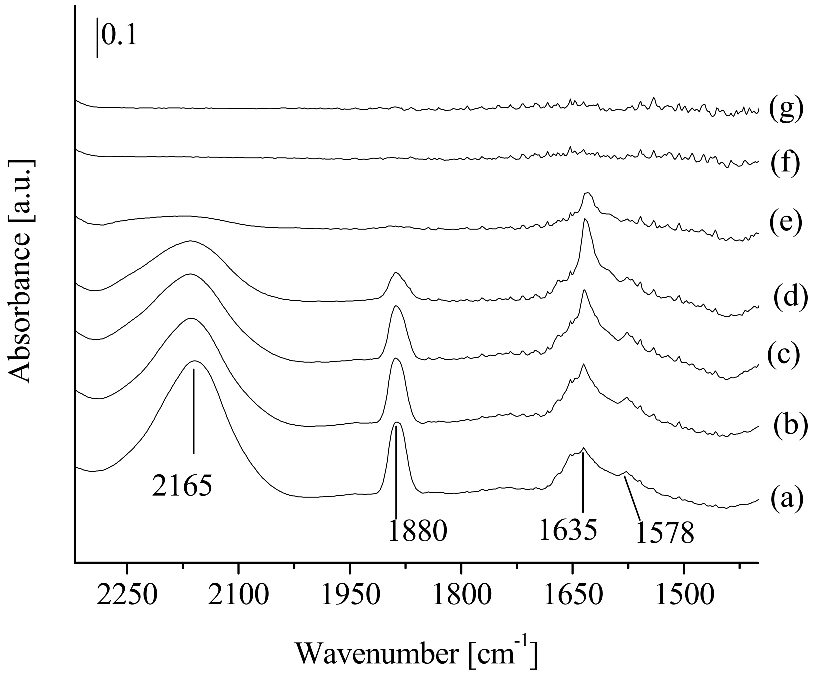

Figure 5.14 FTIR spectra of Fe-ZSM5 treated with 500 ppm NO + 10 % O_2. (a) Adsorption at 35 °C, (b) after purging with N_2 for 60 min at 35 °C (c) 100 °C, (d) 200 °C, (e) 300 °C, (f) 400 °C and (g) 450 C.

5.3.9.5 NH_3 adsorption

Figure 5.15 shows the IR spectra of the NH_3 adsorption experiments on Fe-ZSM5. The ammonia concentration was 500 ppm. Ammonia was adsorbed for 45 min at 35 °C and then purged with N_2 for 60 min at the same temperature. Subsequently, spectra were recorded with increasing temperature in the flow of N_2. Adsorption of ammonia on Fe-ZSM5 leads to the formation of bands at 1470, 3375, 3280, 3180 2925, 1590 and 1270 cm^{-1}. The broad bands between 2600-2900 cm^{-1} are assigned to physisorbed ammonia.

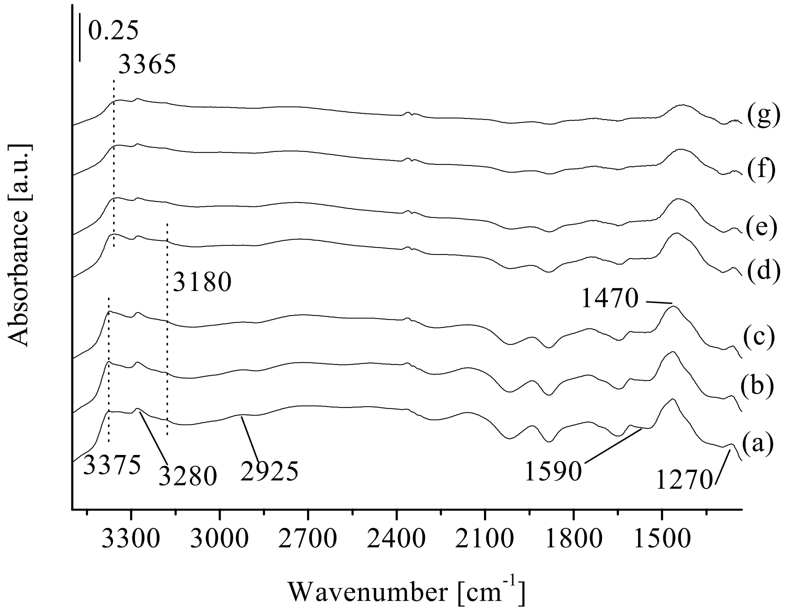

Figure 5.15 FTIR spectra of Fe-ZSM5 treated with 500 ppm NH_3. (a) Adsorption at 35 °C (b) after purging with N_2 for 60 min at 35 °C (c) 100 °C, (d) 200 °C, (e) 300 °C, (f) 400 °C and (g) 450 °C.

These bands decreased with increasing temperature. The strong band at 1470 cm^{-1} is due to the asymmetric bending vibration of NH_4^+ chemisorbed on Brønsted acid sites, while the bands at 1270 cm^{-1} and 1590 cm^{-1} are assigned to the symmetric and asymmetric bending vibrations respectively, of the N-H bonds in NH_3 coordinately linked to the Lewis acid sites [37]. The bands at higher wave numbers are associated with N-H stretching vibrations of NH_4^+ ions located at the AlO_4 tetrahedra of the ZSM5 framework. The bands at 3375 cm^{-1} and 3280 cm^{-1} can be assigned to NH_4^+ ions with three hydrogen atoms bonded to three oxygen ions of AlO_4 tetrahedra (3H structure) and the bands at 3180 cm^{-1} and 2925 cm^{-1} are attributed to NH_4^+ ions with two hydrogen atoms bonded to AlO_4 tetrahedra (2H structure) [38, 39]. In a flow of N_2, the band at 3375 cm^{-1} was slightly shifted to 3365 cm^{-1} with increasing temperatures. The bands which correspond to 3H structure were found to be stable at higher temperatures, whereas the bands of 2H structure were only stable at lower temperatures. The bands of Brønsted acid sites were relatively large compared to the bands of Lewis sites, indicating a large fraction of Brønsted acid sites in this sample.

5.3.9.6 NH_3 adsorption on pre-adsorbed NO

First, Fe-ZSM5 was treated with 500 ppm NO for 30 min at 100 °C (figure 5.16a). After stopping the NO dosage, NH_3 (500 ppm) was introduced and the spectra were recorded as function of time (figure 5.16b-e).

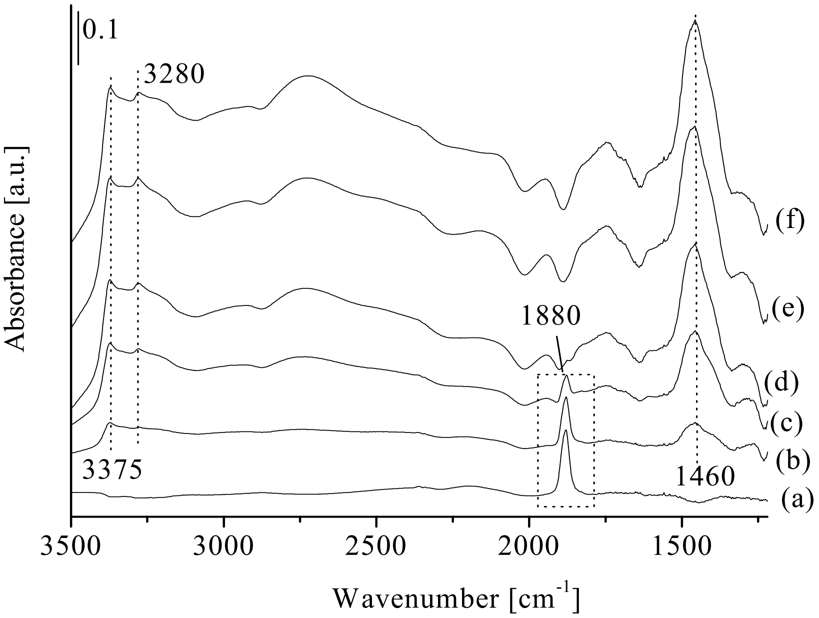

Figure 5.16 FTIR spectroscopy at 100 °C, by passing 500 ppm NH_3 over preadsorbed NO on Fe-ZSM5. (a) 0 min, (b) 2 min, (c) 5 min, (d) 10 min, (e) 15 min and (f) 30 min N_2 purging after 15 min flow of NH_3.

Finally, the NH_3 dosage was stopped and the catalyst was purged with N_2 for 30 min (figure 5.16f). As observed in figure 5.16, for longer NH_3 adsorption times, the bands at 3375 cm^{-1} and 3280 cm^{-1} are well developed and are stable even after purging with N_2. At the same time the band at 1880 cm^{-1} totally disappeared within 10 min of NH_3 flow indicating the reaction of the pre-adsorbed NO. The band at 1460 cm^{-1} was also observed with increasing NH_3 flow. The broad bands between 2600-2900 cm^{-1} are assigned to physisorbed ammonia.

The changes in the T-O-T vibration region are shown in figure 5.17a-f.

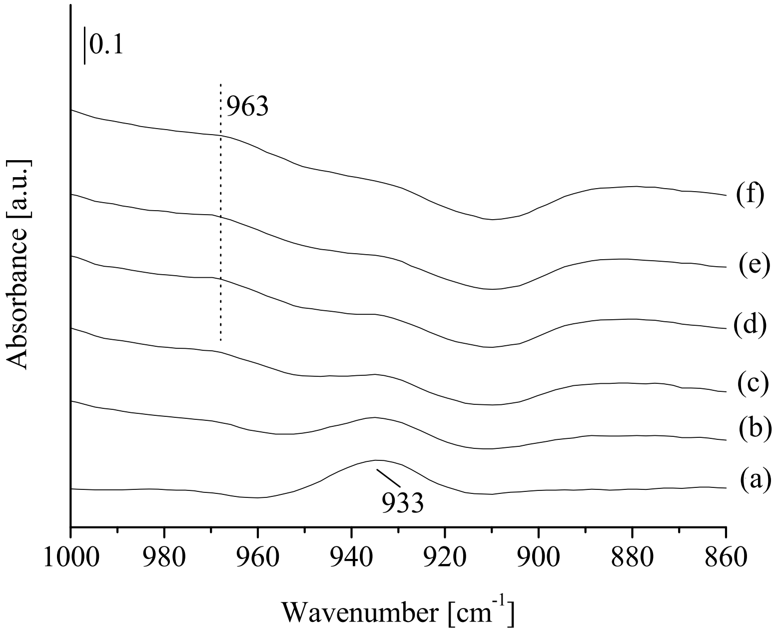

Figure 5.17 T-O-T vibration at 100 °C, after passing 500 ppm NH_3 over preadsorbed NO on Fe-ZSM5. (a) 0 min, (b) 2 min, (c) 5 min, (d) 10 min, (e) 15 min and (f) 30 min N_2 purging after 15 min flow of NH_3.

The band at 933 cm^{-1} was predominant when NO was preadsorbed on Fe-ZSM5. The band at 933 cm^{-1} which arise due to NO interaction with Fe-ZSM5 is typical for iron ions located in cationic sites [35]. On passing NH_3, the 933 cm^{-1} band started to disappear and a broad band centred at 963 cm^{-1} was formed. This broad band is assumed to be associated with the T-O-T band perturbed by Fe^{2+} species [40], most likely by $[Fe(NH_3)_n]^{2+}$ with n = 0, 1 or 2 . The same pattern was also observed for the T-O-T vibration region when NH_3 was dosed after pre-treatment with NO + O_2. The appearance of the 963 cm^{-1} band and the disappearance of 1880 cm^{-1} band during SCR indicate that

Fe is mainly in the 2+ state under reaction conditions. The spectra in figure 5.16 and 5.17 were obtained at 100 °C.

5.3.9.7 Under NO-SCR conditions

In order to investigate the oxidation state of iron at higher temperatures under SCR conditions also spectra at 200, 300, 400 and 450 °C were recorded (figure 5.18 & 5.19). Figure 5.18 clearly shows that NH_4^+ ions are present on the surface of Fe-ZSM5. In figure 5.18 the broad band centred at 963 cm^{-1} supports that Fe is in Fe^{2+} state under SCR conditions up to 300 °C. At T $\geq$ 400 °C, this characteristic band completely disappeared.

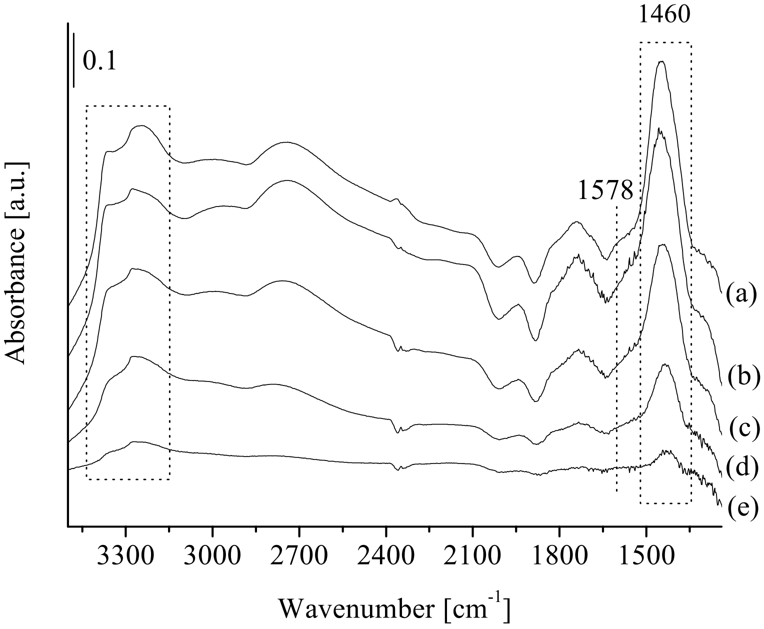

Figure 5.18 FTIR spectra recorded by flowing 500 ppm NO, 10 % O_2, 500 ppm NH_3 for 30 min on Fe-ZSM5. (a) 100 °C, (b) 200 °C, (c) 300 °C, (d) 400 °C and (e) 450 °C.

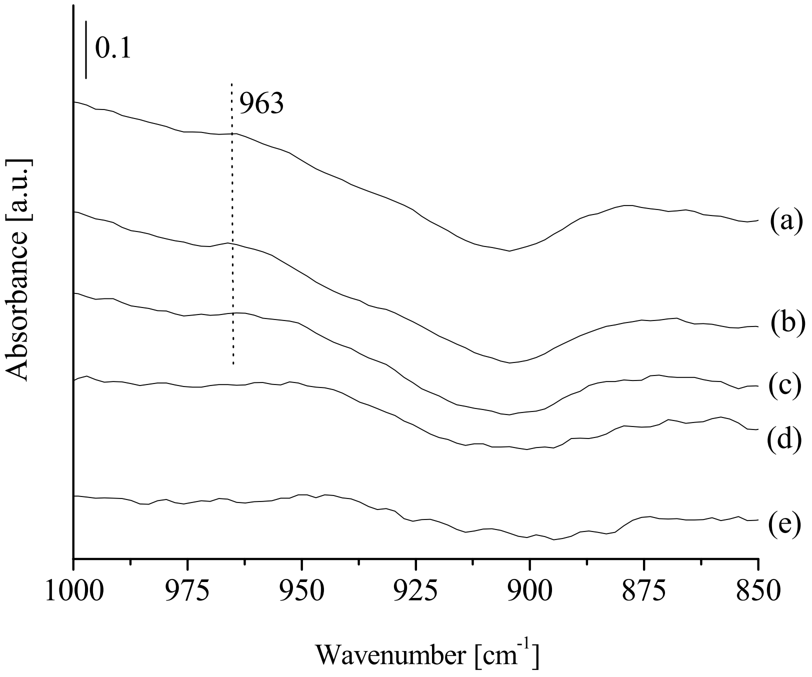

Figure 5.19 T-O-T vibration region. (a) 100 °C, (b) 200 °C, (c) 300 °C, (d) 400 °C and (e) 450 °C.

5.4 Discussion

From XRD (figure 5.1), the formation of iron oxide was observed. In principal the term overexchanged zeolites refers to Me/Al > 1. ICP-AES analysis showed a Fe/Al ratio of 0.75, which implies that this catalyst is not an overexchanged zeolite. The formation of iron oxide particles can be formed during washing and drying steps in the ion exchange process [41]. Two peaks were observed in the H_2-TPR experiment with Fe-ZSM5 (figure 5.4). These correspond to different iron species [42, 43]. The peak at 450 °C is corresponding to the reduction of Fe^{3+}, which could either be bare Fe^{3+} or oxo- or hydrocations such as FeO^{+}, $Fe(OH)^{2+}$ or $[(OH)\text{-}FeO\text{-}Fe(OH)^{2+}]$, into Fe^{2+}. The second peak at 550 °C is assigned to the reduction of FeO to Fe^{0}, which might be possible due to the presence of small of iron oxide aggregates [44]. From the many features found in the UV-vis spectrum isolated iron species in tetrahedral and octahedral environment, iron oxo species and iron oxo dimers could be clearly identified. The latter are assumed to be responsible for the oxidation of NO to NO_2. The iron oxide particles found in XRD and TEM investigations could also be detected.

In the DRIFT spectra, a strong band at 2165 cm^{-1} was obtained on adsorption of NO on Fe-ZSM5. The 1880 cm^{-1} band is often observed after NO adsorption on different Fe-exchanged zeolites [45, 46] and oxide supported Fe^{n+} ions [47, 48]. This band evolves in parallel with the NO^+ band at 2165 cm^{-1}. Based on these related peak intensities at 2165 cm^{-1} and 1880 cm^{-1}, Hadjiivanov et al. [49] suggested that oxidation of NO takes place by Fe^{3+} ions which leads to the simultaneous formation of NO^+ and Fe^{2+}-NO species. This statement was also supported by Lobree et al. [41], who found mono- and dinitrosyl species on different kinds of iron ions. When ammonia was dosed to NO species adsorbed on Fe-ZSM5, it was clearly discernible from the DRIFT spectra that NH_4^+ ions were generated and that at the same time NO^+ and Fe^{2+}-NO species were consumed, indicated by the disappearance of the characteristic bands at 2165 cm^{-1} and 1880 cm^{-1}. This implies that a selective reduction to nitrogen has taken place. However, the standard SCR reaction involves also oxygen, which was found responsible for the reoxidation of the catalytic centre during SCR, e.g. over vanadia based catalysts [50]. It is obvious, that under the oxygen-free conditions in the DRIFT experiment only the first reduction of the iron by NO can takes place. The iron remains in the reduced Fe^{2+} state and the catalytic cycle is not closed. These conclusions are corroborated by catalytic tests without oxygen showing only 0-6 % DeNOx from 200-450 °C [51]. From investigations of the redox behaviour of Fe-ZSM5, it is known that Fe^{3+} in Fe-ZSM5 is readily reduced to Fe^{2+}, even by simple evacuation at elevated temperatures. However, the reverse process takes place only in oxidizing media [52, 53], confirming our conclusions. It should be noted, that in reduced as well as oxidized materials always both forms of iron (Fe^{2+} and Fe^{3+}) are present [52, 54] and that oxidation or reduction treatment will just increase or decrease the Fe^{3+}/Fe^{2+} ratio, respectively.

The co-adsorption of $NO+O_2$ on Fe-ZSM5 (figure 5.14a) produced the same NO^+ and Fe^{2+}-NO species at 2165cm^{-1} and 1880 cm^{-1}, respectively, as observed during adsorption of NO (figure 5.9a). But additional bands were formed at 1635, 1605 and 1578 cm^{-1}, being indicative of adsorbed NO_2 and nitrates. As the same bands were found when NO_2

was adsorbed on Fe-ZSM5 (figure 5.13a), this proves that Fe-ZSM5 is able to oxidize NO to NO_2 and nitrates in the presence of oxygen [55]. When ammonia was passed over NO + O_2 adspecies, again NH_4^+ ions were generated and NO^+ as well as Fe^{2+}-NO species were consumed, but along with the disappearance of the adsorbed NO_2 species at 1635 cm^{-1}, corroborating that both NO and NO_2 are involved in the standard SCR mechanism over Fe-ZSM5. The negligibly capacity of H-ZSM5 for the oxidation of NO to NO_2 (~ 1 % at $T \leq 350$ °C and ~ 2 % at $T > 350$ °C) compared to the high NO_2 yields over Fe-ZSM5, proves the conclusion that the presence of iron in ZSM5 is responsible for the oxidation capacity of NO to NO_2 [51]. Our finding are also supported by the results of Long et al. [56], who performed a different method, i.e. NO_x TPD on H-ZSM5 and Fe-ZSM5. The observed relation between SCR activity and NO oxidation capability of Fe-ZSM5 and H-ZSM5 furnishes evidence that the negligible SCR activity of H-ZSM5 is due to its low NO oxidizing capability and that the formation of NO_2 is crucial step in the SCR mechanism on ZSM5 catalysts.

The changes in the T-O-T vibration region (800-1000 cm^{-1}) shown in figures 5.11 & 5.17 allows us to draw conclusions about the active iron centres during reaction. The disappearance of 1880 cm^{-1} band (Fe^{2+}-NO) and the appearance of the 963 cm^{-1} band, likely caused by T-O-T band perturbations by $[Fe(NH_3)_n]^{2+}$ during SCR indicate that Fe is mainly in the 2+ state under reaction conditions. However, the band at 963 cm^{-1} was only observable up to 300 °C.

The complexity of the different iron species found by the different characterization methods makes the identification of the active site for SCR difficult. Different kinds of iron sites appear to coexist in Fe-ZSM5: Fe_2O_3 clusters, isolated iron ions and iron oxo dimmers. Among them, iron oxo dimers are supposed to be the active SCR sites. In order to explain this, we would like to come back to the NO adsorption experiments without oxygen, where the band at 2165 cm^{-1} was attributed to NO^+ species at cation exchange positions. Hadjiivanov et al. [31] demonstrated for metal free ZSM5, that NO^+ is formed by the following reaction scheme:

$$NO + NO_2 + 2H^+ \rightarrow 2\ NO^+ + H_2O \qquad (5.1)$$

However, for this reaction NO_2 is required, which is not present in the gas feed. Thus, the NO_2 can only be formed if part of the NO reacts with bridging oxygen in binuclear iron complexes [57]. Thereby, the oxygen bridge is transferred to NO, leaving an iron dimer fragment:

$$[\text{HO-Fe}^{3+}\text{-O-Fe}^{3+}\text{-OH}]^{2+} + \text{NO} \rightarrow [\text{HO-Fe}^{2+}\text{-}\square\text{-Fe}^{2+}\text{-OH}]^{2+} + \text{NO}_2 \qquad (5.2)$$

When NO and O_2 are both present in the gas phase, the formation of both nitro and nitrate groups were observed. Other researchers [43, 58-59] also support the theory of oxygen bridged binuclear iron complex to be the active center. The results obtained by us, showed close similarities to that observed in the literature mentioned above, even though the Fe-ZSM5 sample prepared by us was entirely different. Based on our experimental results and the literature data, it is likely that oxygen bridged binuclear Fe complexes are active sites for NH_3-SCR, although the discussion is not completed.

The inhibition of the SCR reaction over Fe-ZSM5 by ammonia was observed at lower and intermediate temperatures up to 350 °C (see chapter 6 for details). Stevenson et al. [60] who found the same effect on H-ZSM5 suggested that the ammonia inhibition is due to competitive adsorption of NH_3 and NO_x at the active sites with NH_3 dominating at lower temperatures. Based on our results, the inhibition effect for Fe-ZSM5 might also be explained by a stronger adsorption of ammonia compared to NO_x on active Fe sites. But another explanation is also possible: high SCR activity might be limited to Fe in the 3+ state. The inhibition effect could therefore be explained by an elevated reduction of Fe^{3+} to Fe^{2+} at higher concentrations of NH_3 at $T \leq 300$ °C under SCR conditions. In fact, based on XAFS measurements, Battiston et al. [61] observed an increase in oxidation state of iron from 2.3 to 2.9 after switching from the dosage of SCR reactants to the dosage of only NO in nitrogen at 350 °C. They suggested that the reoxidation might be due to the oxygen traces in the gas phase. Further, Voskoboinikov et al. [62] suggested the reoxidation of the iron complexes could have been caused by the oxygen from the zeolite matrix. At these high temperatures, Fe^{2+} might be instantaneously reoxidized in the catalytic cycle. Since Fe species are responsible for the formation of NO_2, the role of Brønsted or Lewis acid sites is subjected to ammonia storage, which is in line with the observed bands for adsorbed NH_4^+ in the DRIFT experiments. These results are supported by Schraml-Marth et al. [63] as well as Went et al. [64] who also found ammonia to be adsorbed on Brønsted or Lewis acid sites during NH_3 SCR.

5.5 Conclusions

The iron in Fe-ZSM5 was found to be present in various forms and in various positions. Extensive characterization results led to the conclusion that oxygen bridged binuclear iron complexes might be the active site for NH_3-SCR. The main role of the iron in NH_3-SCR is to oxidize NO to NO_2, whereas the Brønsted and Lewis acid sites seem to be responsible for binding ammonia on the catalyst surface. The inhibiting effect of ammonia on the SCR activity at lower and intermediate temperatures is attributed to the reduction of Fe^{3+} to Fe^{2+} by NH_3.

5.6 References

[1] M. Rauscher, K. Kesore, R. Mönnig, W. Schwieger, A. Tißler, T. Turek, Appl. Catal. A 184 (1999) 249.

[2] C. V. Hidalgo, H. Iton, T. Hattori, M. Niwa, Y. Murakami, J. Catal. 85 (1984) 362.

[3] J. G. Post, J. H. C. van Hoff, Zeolites 4 (1989) 9.

[4] N. Y. Topsøe, K. Pedersen, E. G. Derouane, J. Catal. 70 (1981) 41.

[5] K. Chao, B. Chiou, C. Cho, S. Jeng, Zeolites 4 (1984) 2.

[6] R. Q. Long, R. T. Yang, J. Catal. 194 (2000) 80.

[7] G. Engelhardt, D. Michel, High-Resolution Solid State NMR of silicates and Zeolites, Wiley, New York, 1987.

[8] J. A. van Bokhoven, D.C. Koningsberger, P. Kunkeler, H. van Bekkum, A. P. M. Kentgens, J. AM. Chem. Soc. 122 (2000) 12842.

[9] P. B. Bodart, J. B. Nagy, G. Debras, Z. Gabelica, P. A. Jacobs, J. Phys. Chem. 90 (1986) 5183.

[10] J. L. Motz, H. Heinichen, W. F. Hölderich, J. Mol. Catal. A. Chem. 136 (1998) 175.

[11] J. Sanz, V. Fornés, A. Corma, J. Chem. Soc., Faraday Trans. 84 (1988) 3113.

[12] G. Delahay, D. Valade, A. Guzmàn-Vargas, B. Coq, Appl. Catal B 55 (2005) 149.

[13] A. Brückner, R. Lück, W. Wieker, B. Fahlke, H. Mehner, Zeolites, 12 (1992) 380.

[14] D. Goldfarb, M. Bernardo, K. G. Strohmaier, D. E. W. Vaughan, H. Thomann, J. Am. Chem. Soc. 116 (1994) 6344.

[15] M. S. Kumar, M. Schwidder, W. Grünert, A. Brückner, J. Catal. 227 (2004) 384.

[16] H. H. Tippins, Phys. Rev. B 1(1970) 126.

[17] S. Bordiga, R. Buzzoni, F. Geobaldo, C. Lamberti, E. Giamello, A. Zecchina, G. Leofanti, G. Petrini, G. Tozzola, G. Vlaic, J. Catal. 158 (1996) 486.

[18] J. Torrent, V. Barrón, Clays Clay Miner. 51 (2003) 309.

[19] C. Scheinost, A. Chavernas, V. Barron, J. Torrent, Clays Clay Miner. 46 (1998) 528.

[20] G. Centi, F. Vazzana, Catal. Today 53 (1999) 683.

[21] G. D. Pirngruber, M. Luechinger, P. K. Roy, A. Cecchetto, R. Smirniotis, J. Catal. 224 (2004) 429.

[22] P. O. Fritz, J. H. Lunsford, J. Catal. 118 (1989) 85.

[23] A. Zecchina, S. Bordiga, G. Spoto, D. Scarano, J. Chem. Soc. Faraday Trans. 88 (1992) 2959.

[24] M. B. Sayed, R. A. Kydd, R. P. Cooney, J. Catal. 88 (1984) 137.

[25] A. Vimont, F. Thibault-Starzyk, J. C. Lavalley, J. Phys. Chem. B 104 (2000) 286.

[26] R. M. Dessau, K. D. Schmitt, G. T. Kerr, G. L. Woolery, L. B. Alemany, J. Catal. 109 (1998) 472.

[27] K. Yamagishi, S. Namba, T. Yashima, J. Phys. Chem. 95 (1991) 872.

[28 K. Segawa, Y. Chen, J. E. Kubsh, W. N. Delgass, J. A. Dumesic, W. K. Hall, J. Catal. 76 (1982) 112.

[29] M. Lezcano, V. I. Kovalchuk, J. L. d'Itri, Kinet. Katal. 42 (2001) 104.

[30] G. Mul, J. Pèrez-Ramirez, F. Kapteijn, J. A. Moulijn, Catal. Lett. 80 (2002) 129.

[31] K. Hadjiivanov, J. Saussey, J. L. Freysz, J. C. Lavalley, Catal. Lett. 52 (1998) 103.

[32] J. Szanyi, M. T. Paffet, J. Catal. 164 (1996) 232.

[33] Y. H. Yeom, B. Wen, W. M. H. Sachtler, E. Weitz, J. Phys. Chem B. 108 (2004) 5386.

[34] Y. H. Yeom, J. Henao, M. J. Li, W. M. H. Sachtler, E. Weitz, J. Catal. 231 (2005) 181.

[35] Z. Sobalik, J. Dedecek, I. Ikonnikov, B. Wichterlova, Micropor. Mesopor. Mater. 21 (1998) 525.

[36] D. Pozdnyakov, V. Filimonov, Kinet. Katal. 14 (1973) 760.

[37] N. Y. Topsøe, J. Catal. 128 (1990) 499.

[38] J. Eng, C. H. Bartholomew, J. Catal. 171 (1997) 27.

[39] E. H. Teunissen, R. A. van Santen, A.P. J. Jansen, F. B. van Duijneveldt, J. Phys. Chem. 97 (1993) 203.

[40] P. Kubánek, B. Wichterlová, Chem. Listy 96 (2002) 876.

[41] L. J. Lobree, In- Chul Hwang, J. A. Reimer, A. T. Bell, J. Catal. 186 (1999) 242.

[42] K. Krishna, G. B. F. Seijger, C. M. van den Bleek, M. Makkee, G. Mul, H. P. A. Calis, Catal. Lett. 86 (2003) 121.

[43] H. Y. Chen, W. M. H. Sachtler, Catal. Today 42 (1998) 73.

[44] A. Guzmàn-Vargas, G. Delahay, B. Coq, Appl. Catal B 42 (2003) 369.

[45] H. Y. Chen, T. V. Voskoboinikov, W. M. H. Sachtler, J. Catal. 180 (1998) 171.

[46] L. M. Aparicio, W. K. Hall, Sh.Fang, M. A. Ulla, W. S. Millman, J. A. Dumesic, J. Catal. 108 (1987) 233.

[47] F. Boccuzzi, E. Guglielminotti, F. Pinna, M. Signoretto, J. Chem. Soc. Faraday Trans. 91 (1995) 3237.

[48] S. Yuen, J. E. Kubsh, J. A. Dumesic, N. Topsoee, H. Topsoee, Y. Chen, J. Phys. Chem. 86 (1992) 3022.

[49] K. Hadjiivanov, H. Knözinger, B. Tsyntsarski, L. Dimitrov, Catal. Lett. 62 (1999) 35.

[50] M. Koebel, G. Madia, F. Raimondi, A. Wokaun, J. Catal. 209 (2002) 159.

[51] M. Devadas, O. Kröcher, M. Elsener, A. Wokaun, G. Mitrikas, N. Söger, M. Pfeifer, Y. Demel, L. Mussmann, Catal. Today, submitted.

[52] W. K. Hall, X. Feng, J. Dumesic, R. Watwe, Catal. Lett. 52 (1998) 13.

[53] J. O. Petunchi, W. K. Hall, J. Catal. 78 (1982) 327.

[54] L. M. Aparicio, J. A. Dumesic, S. M. Fang, M. A. Long, M. A. Ulla, W. S. Millman, W. K. Hall, J. Catal. 104 (1987) 381.

[55] L. J. Lobree, I. C. Hwang, A. Reimer, A. T. Bell, Catal. Lett. 63 (1999) 233.

[56] R. Q. Long, R. T. Yang, J. Catal. 198 (2001) 20.

[57] H. Y. Chen, El-M. El-Malki, X. Wang, R. A. van Santen, W. M. H. Sachtler, J. Mol. Catal. 162 (2000) 159.

[58] A. A. Battiston, J. H. Bitter, D. C. Koningsberger, Catal. Lett. 66 (2000) 75.

[59] P. Marturano, L. Drozdová, A. Kogelbauer, R. Prins, J. Catal. 192 (2000) 368.

[60] S. A. Stevenson, J. C. Vartuli, C. F. Brooks, J. Catal. 190 (2000) 228.

[61] A. A. Battiston, J. H. Bitter, D. C. Koningsberger, J. Catal. 218 (2003) 163.

[62] T. V. Voskoboinikov, H. Y. Chen, W. M. H. Sachtler, Appl. Catal. B 19 (1998) 279.

[63] M. Schraml-Marth, A. Wokaun, A. Baiker, J. Catal. 124 (1990) 86.

[64] G. T. Went, L.J. Leu, R. R. Rosin, A. T. Bell, J. Catal. 134 (1992) 492.

6

Catalytic Investigation of NO-SCR on Fe-ZSM5

6.1 Introduction

Fe-ZSM5 has been reported to be an active and selective catalyst for the SCR reaction in [1-6]. Despite of the valuable information provided in these laboratory investigations, certain aspects have to be considered sufficiently for a reliable evaluation of Fe-ZSM5 as SCR catalyst:

1. Water must be present in the basic feed in order to measure the actual performance of the catalyst and to investigate the “real” functionality of the catalyst. However, omitting water may be useful in additional experiments to reveal the reaction mechanism.

2. For catalyst screening experiments dosing a constant amount of ammonia and measuring the activity of the catalyst as a function of temperature is a valuable tool. However with regard to dosage control in automotive applications a completed description of the catalyst performance is necessary. In our opinion, the temperature dependency of the catalyst activity is best expressed with respect to the allowable ammonia slip of 10 ppm independent of the ammonia to NO_x ratio dosed.

3. Currently, a broad range of engine development strategies are followed, resulting in either low exhaust gas temperatures, e.g. for engines using excessive exhaust gas recycling (EGR), or very high exhaust gas temperatures, e.g. for engines without EGR but with hot diesel particulate filter (DPF) regeneration. Thus, to cover the maximum range of exhaust gas temperatures, the activity and selectivity of the catalysts should be checked from 150-700 °C.

Based on the above mentioned considerations, SCR investigations are carried out on a monolith catalyst, which are indispensable for gaining experimental data and is representative of the situation in real world catalytic converters, i.e. low pressure drop, high geometric surface area and short diffusion distances [7].

6.2 Data analysis

Space velocity

Gas hourly space velocity (GHSV) is defined as:

$$\text{GHSV} = \frac{V_N^*}{V_C}\ [\text{h}^{-1}] \qquad (6.1)$$

V_N^* = volumetric gas flow in normal conditions [cm_N^3/h]

V_C = coated monolith volume [cm^3]

NO_x conversion

The NO_x conversion (DeNOx) is defined as follows:

$$\text{DeNOx} = \frac{NO_{x,IN} - NO_{x,OUT}}{NO_{x,IN}} \cdot 100\ [\%] \qquad (6.2)$$

The definition of DeNOx is based on the conversion of $NO_x = NO + NO_2$. The main product of the NO_x reduction is generally N_2, a high DeNOx indicating a high SCR activity of the catalyst.

Stoichiometric ratio

The stoichiometric ratio α represents the ratio between moles of nitrogen added as reducing agent and the moles of NO_x contained in the feed. If ammonia is used as reducing agent, then α is evaluated as follows:

$$\alpha = \frac{NH_{3,IN}}{NO_{x,IN}}\ [-] \qquad (6.3)$$

NO oxidation to NO_2

The oxidation of NO to NO_2 is calculated as follows:

$$\text{NO oxidation to NO}_2 = \frac{c_{NO_2,out}}{c_{NO,in}} \cdot 100\ [\%] \tag{6.4}$$

Selectivity for SCO reaction

The selectivitites are calculated by the equation:

$$S_i = \frac{\nu_{NH_3} \cdot \text{Product (i) formed}}{\nu_i \cdot NH_3\text{consumed}} \left[\frac{\text{mol}}{\text{mol}}\right] \tag{6.5}$$

where ν_{NH3} and ν_i are the stoichiometric coefficients of ammonia and product i of the respective reaction equation.

6.3 Experimental

For the catalytic investigation, the Fe-ZSM5 cordierite monolith was cut into a piece of the size 3.8 cm x 1.7 cm x 1.2 cm fitting to the sample holder of the tube reactor. The gas hourly space velocity (GHSV) was 52,000 h^{-1}, which represents the flow conditions in SCR converters on board of diesel vehicles. For tests of the standard SCR reaction, the composition of diesel exhaust gas was approximated by a model feed gas containing 10 % O_2, 5 % H_2O, 1000 ppm of NO and balance N_2. NH_3 was added in the range 100-2000 ppm.

The selective catalytic oxidation (SCO) reaction of ammonia to nitrogen was tested with a model feed consisting of 10 % O_2, 5 % H_2O, and 1000 ppm NH_3 but no NO. Water was omitted for supplementing investigations.

6.4 Results and Discussion

6.4.1 Standard SCR over Fe-ZSM5

A good SCR catalyst combines a high NO_x removal efficiency (DeNOx) with a high selectivity and low ammonia emissions after the catalyst. This means that suitable SCR catalysts must have acidic properties, which help to withdraw the ammonia in the catalyst and provide sufficiently high ammonia concentrations at the actives SCR sites at already low ammonia concentrations. Excessive ammonia dosage only slightly increases the ammonia concentration at the active sites. Therefore, the DeNOx remains nearly constant and all excessive ammonia is emitted. By plotting DeNOx versus ammonia slip (figure 6.1) these important catalyst properties are combined in one graph. These curves are obtained by increasing stepwise the ammonia concentration at a constant flow of 1000 ppm NO at a fixed temperature.

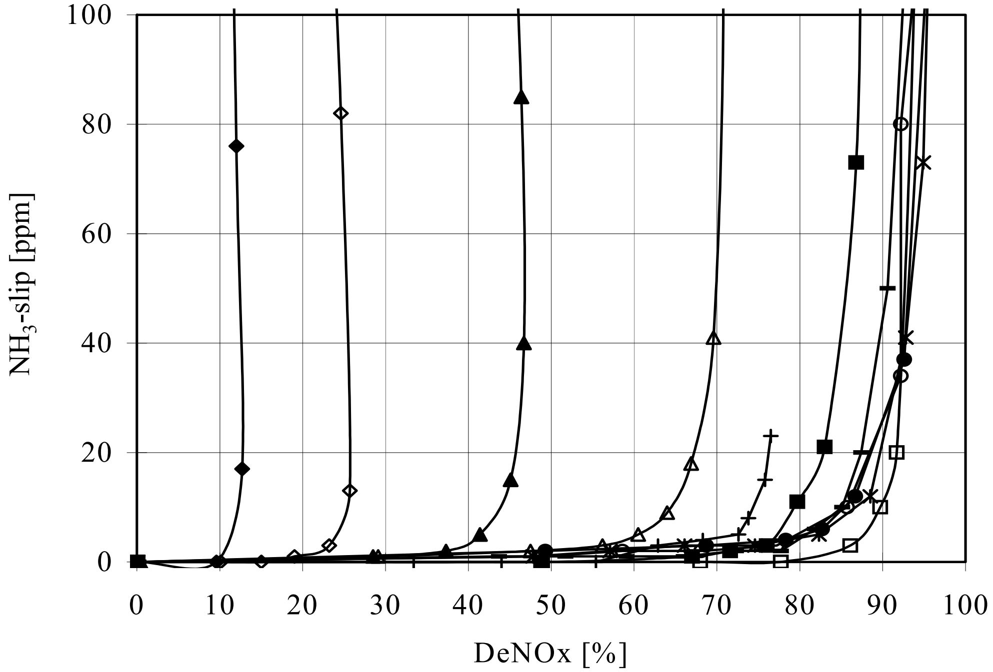

Figure 6.1 NH_3 slip vs. DeNOx for the fresh Fe-ZSM5 monolith catalyst at (♦) 200 °C, (◊) 250 °C, (▲) 300 °C, (Δ) 350 °C, (■) 400 °C, (□) 450 °C, (●) 500 °C, (o) 550 °C, (x) 600 °C, (-) 650 °C and (+) 700 °C.

The almost rectangular curve shape is a consequence of the high SCR activities at low ammonia slip through the catalyst. Usually, ammonia emissions of about 10 ppm in average are regarded as harmless for automotive applications [8]. This necessitates a dosage control for adding the right amount of ammonia relating to the NO_x concentration and the activity of the catalyst. From figure 6.1, the high SCR activity of Fe-ZSM5 is clearly discernible, especially at temperatures above 350 °C.

In accordance with the expected behaviour of a suitable SCR catalyst nearly all ammonia dosed goes into the SCR reaction, limited either by the activity of the catalyst at a given temperature or the stoichiometry of the SCR reaction. All additional ammonia causes an only marginal increase of the DeNOx. However, having a closer look at the ammonia slip at lower and intermediate temperatures up to 350 °C reveals an interesting behaviour. The steep part of the curves are slightly bent backward, indicating that the NO_x conversion first increases as expected but then decreases again if ammonia is overdosed and ammonia slip is forced. Obviously, the SCR reaction is inhibited by ammonia.

This effect is more pronounced in figure 6.2, where DeNOx values are plotted against the stoichiometric ratio α for different temperatures in the range 200-500 °C. In figure 6.2, at temperatures $\geq$ 400 °C shows an increase of DeNOx with increasing α. It can also be seen that the DeNOx decreases above $\alpha = 0.8$ at 350 °C, and for temperatures below 350 °C the inhibition occurs at lower values of α. These results suggest that the inhibition effect of ammonia could be due to competitive adsorption of ammonia and NO on the active sites. In fact, Eng et al. [9] and Stevenson et al. [10] observed a similar inhibition by ammonia on H-ZSM5, which was attributed to a competitive adsorption of ammonia and NO.

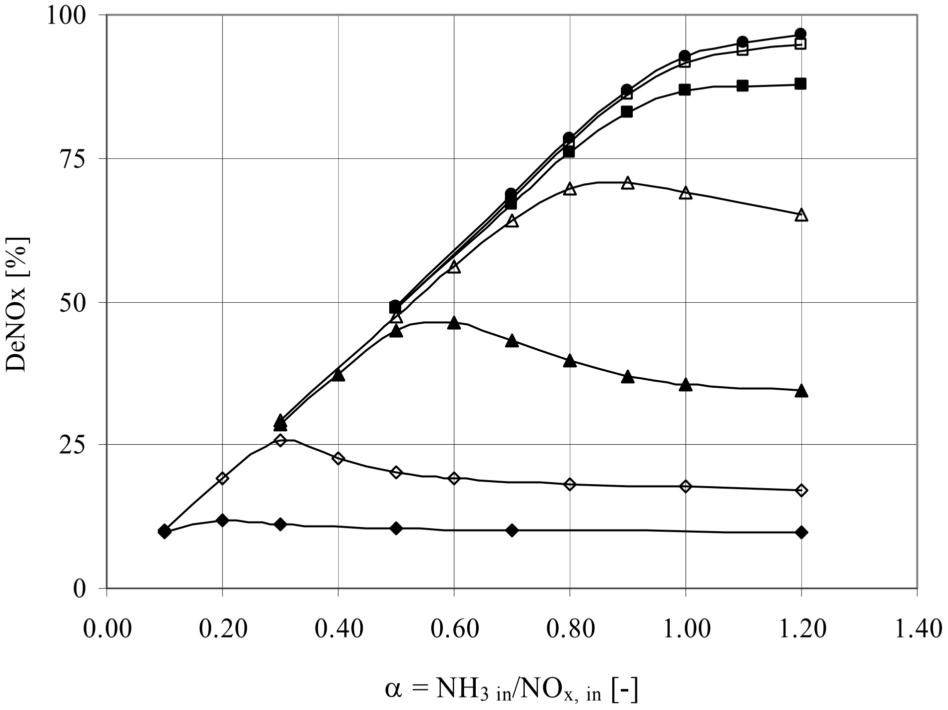

Figure 6.2 DeNOx vs. stoichiometric factor α for the fresh Fe-ZSM5 monolith catalyst at (♦) 200 °C, (◊) 250 °C, (▲) 300 °C, (Δ) 350 °C, (■) 400 °C, (□) 450 °C and (●) 500 °C.

Figure 6.3 illustrates the differences between the DeNOx at 10 ppm NH_3 slip and the maximum DeNOx, plotted vs. temperature in the range 200-700 °C. In accordance with figure 6.3, the difference between the maximum DeNOx and DeNOx at 10 ppm ammonia slip decreases for lower temperatures due to the ammonia inhibition effect, which prevents that the catalyst activity is increased by adding ammonia in excess. In this temperature range DeNOx is rather limited by the reaction temperature. The maximum DeNOx is steadily increasing from 200-600 °C, reaching $\geq$ 90 % for T $\geq$ 450 °C. It decreases at temperatures beyond 600 °C. However, at 700 °C still around 80 % of conversion was achieved.

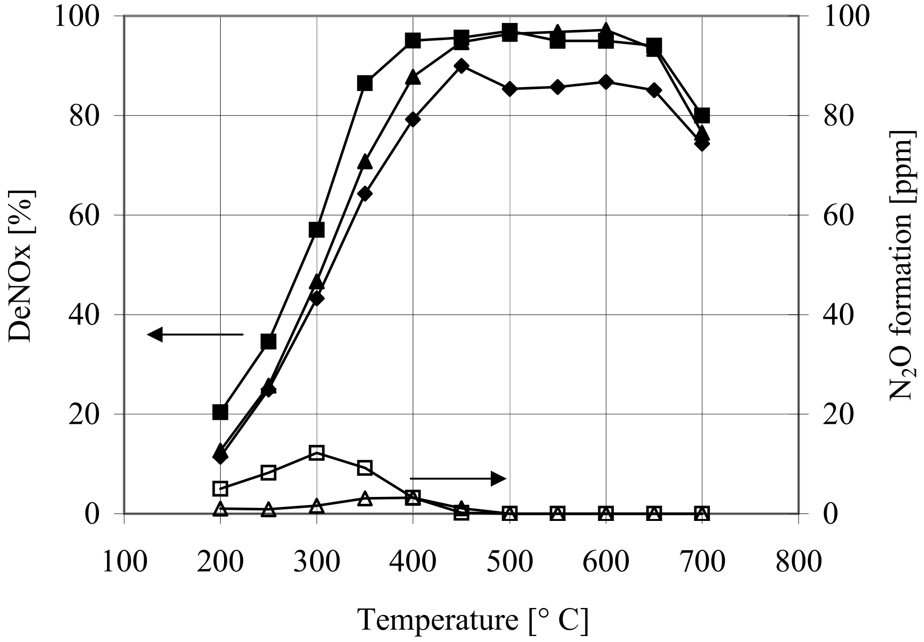

Figure 6.3 DeNOx vs. temperature for the fresh Fe-ZSM monolith (♦) at 10 ppm NH_3 slip with water in feed, (▲) at maximum conversion with water in feed, (■) at 10 ppm NH_3 slip without water. (Δ) N_2O formation at 10 ppm NH_3 slip with water in feed and (□) at 10 ppm NH_3 slip without water.

6.4.2 SCR stoichiometry

The problem for the investigation of the SCR reaction is that all reactions end up directly or via intermediates in nitrogen or NO, which cannot be distinguished from the feed components. Moreover, nitrogen cannot be detected by infrared spectroscopy. However, the contribution of all these side-reactions results in an increased consumption of ammonia relatively to the 1:1 stoichiometry of the SCR reaction.

This excess consumption is derived from the curves in figure 6.4, showing the ratio of consumed ammonia to consumed NO_x versus the ratio of dosed ammonia to dosed NO_x at 200-700 °C, which is a direct scale for the compliance of the SCR stoichiometry. The values of 1 to 1.1 between 200-600 °C clearly demonstrate, that Fe-ZSM5 follows the ideal SCR stoichiometry over a broad temperature range and that a maximum of 10 % ammonia is consumed by ammonia oxidation. However, at 700 °C, values of about 1.5-

1.7 were observed, indicating that the catalyst consumed an increasing part of ammonia mainly due to the oxidation to nitrogen at very high temperatures.

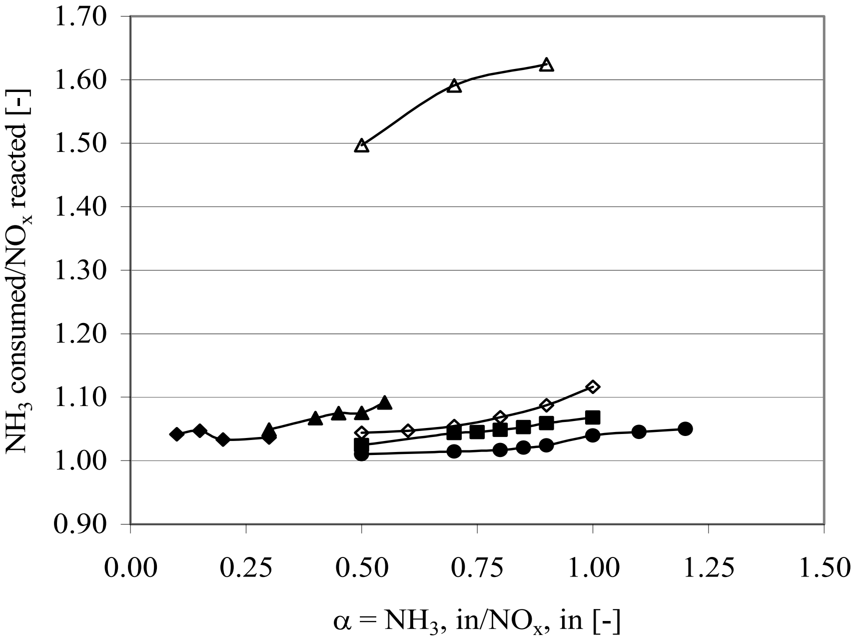

Figure 6.4 Observed ammonia to NO_x stoichiometry vs. dosed ammonia to NO_x ratio at (♦) 200 °C, (▲) 300 °C, (■) 400 °C, (●) 500 °C, (◊) 600 °C and (Δ) 700 °C.

6.4.3 Possible side-reactions during standard-SCR over Fe-ZSM5

Generally, DeNOx is expected to be limited by the catalyst activity at lower temperatures, the stoichiometry of the SCR reaction at intermediate temperatures and by the catalyst selectivity at high temperatures. With increasing temperatures different side-reactions are conceivable producing N_2O and NO_x as well as increased amounts of nitrogen [11].

For the production of N_2O the direct oxidation of ammonia,

$$2\ NH_3 + 2\ O_2 \rightarrow N_2O + 3\ H_2O \tag{6.6}$$

and the reaction of ammonia with NO_2 are discussed [11]:

$$2\ NH_3 + 2\ NO_2 \rightarrow N_2O + N_2 + 3\ H_2O \tag{6.7}$$

Other potential side-reactions of the SCR process are the selective catalytic oxidation of ammonia to nitrogen (SCO),

$$4\ NH_3 + 3\ O_2 \rightarrow 2\ N_2 + 6\ H_2O \qquad (6.8)$$

and the oxidation of ammonia to NO,

$$4\ NH_3 + 5\ O_2 \rightarrow 4\ NO + 6\ H_2O \qquad (6.9)$$

which itself may be further oxidized to NO_2.

6.4.4 N_2O formation

Figure 6.3 clearly shows that only negligible amounts of N_2O (~ 3 ppm) were formed during standard-SCR between 250-400 °C and that no N_2O was formed beyond 450 °C. This makes reaction 6.6 very unlikely, which is expected to produce increasingly amounts of N_2O formation at higher temperatures. The reaction of ammonia with oxygen over Fe-ZSM5 was investigated without the influence of the SCR reaction by dosing ammonia without NO (figure 6.5). No N_2O was formed at any temperature, ruling out the relevance of reaction 6.6 for the formation of this side-product. Moreover, according to this reaction equation the N_2O formation should be independent of the NO_2 content in the feed. However, experiments with increasing NO_2 fractions in the feed (Chapter 7) clearly showed the dependency of the N_2O emissions on the NO_2 concentration in the gas feed at 250-400 °C. This proves the relevance of reaction 6.7 for the formation of N_2O on Fe-ZSM5.

However, having a closer look at the underlying chemistry, the contribution of reaction 6.7 cannot be strictly ruled out, as N_2O might be formed as a short living intermediate at higher temperatures. In fact, Fe-ZSM5 shows strongly increasing N_2O decomposition activity at $T \geq 400$ °C.

$$2\ N_2O \rightarrow 2\ N_2 + O_2 \qquad (6.10)$$

and N_2O SCR activity at $T \geq 350$ °C [12]

$3\ N_2O + 2\ NH_3 \rightarrow 4\ N_2 + 3\ H_2O$ (6.11)

explaining the general absence of N_2O at higher temperatures independent of the reaction conditions or the feed composition.

6.4.5 SCO reaction and NO formation

The investigation of the ammonia oxidation over Fe-ZSM5 showed that ammonia conversion strongly increases with temperatures (figure 6.5).

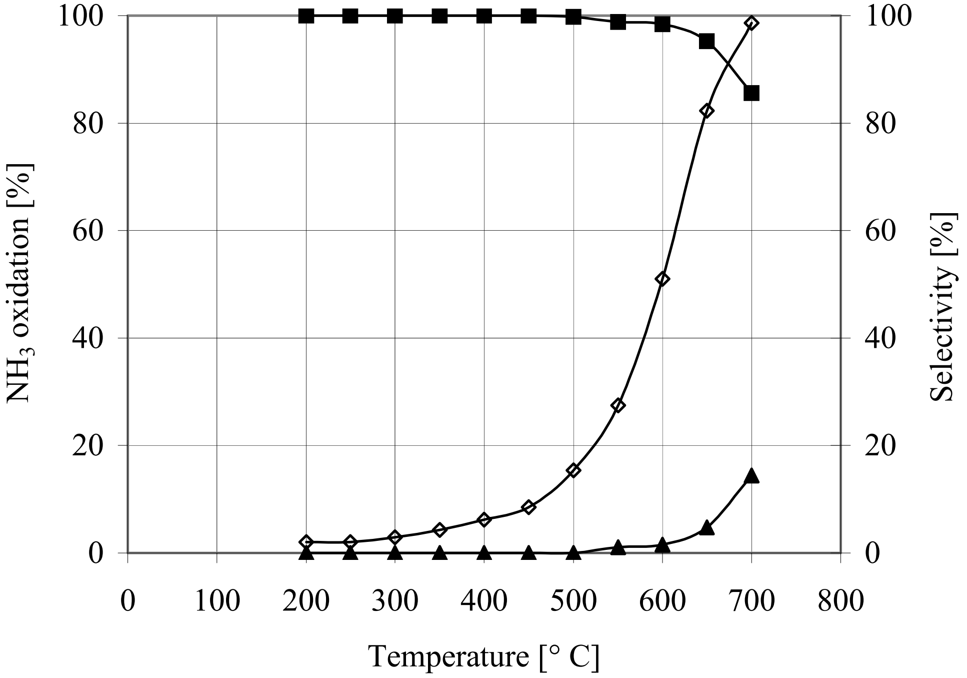

Figure 6.5 SCO properties of the fresh Fe-ZSM5 monolith vs. temperature (◊) NH_3 oxidized, (▲) selectivity towards NO and (■) selectivity towards N_2.

Around 50 % of the ammonia was oxidized at T = 600 °C and nearly 100 % at 700 °C. The selectivity towards N_2 was almost 100 % till 600 °C, but beyond 600 °C the selectivity towards nitrogen decreased accompanied with an increase in NO formation. The formation of NO beside the main product N_2 in the ammonia oxidation experiment gives occasion to the assumption that during SCR over Fe-ZSM5 NO is not only consumed but also produced on the catalyst by reaction of ammonia with oxygen. This NO cannot be distinguished from the NO in the feed and, especially, if it is formed at the catalyst entrance it may also react downstream in the standard SCR reaction. Based on the observed products, it is not possible to decide, if the oxidation of ammonia to nitrogen is a straightforward reaction or if proceeds via NO as intermediate.

6.4.6 NO_2 formation

Fe-ZSM5 has a distinct NO oxidation capability as shown in figure 6.6. The inlet NO concentration was 1000 ppm. No NH_3 was added. The NO_2 fraction increases with temperature as expected, but decreases again at higher temperatures due to the thermodynamic equilibrium between NO and NO_2 lying on the side of NO. NO_2 is essential for SCR activity of ZSM5-based catalysts [13], but, as the NO_2 formed from NO is not observed under standard-SCR conditions (figure 6.3) it may be concluded that it is only a short living intermediate, which is immediately consumed.

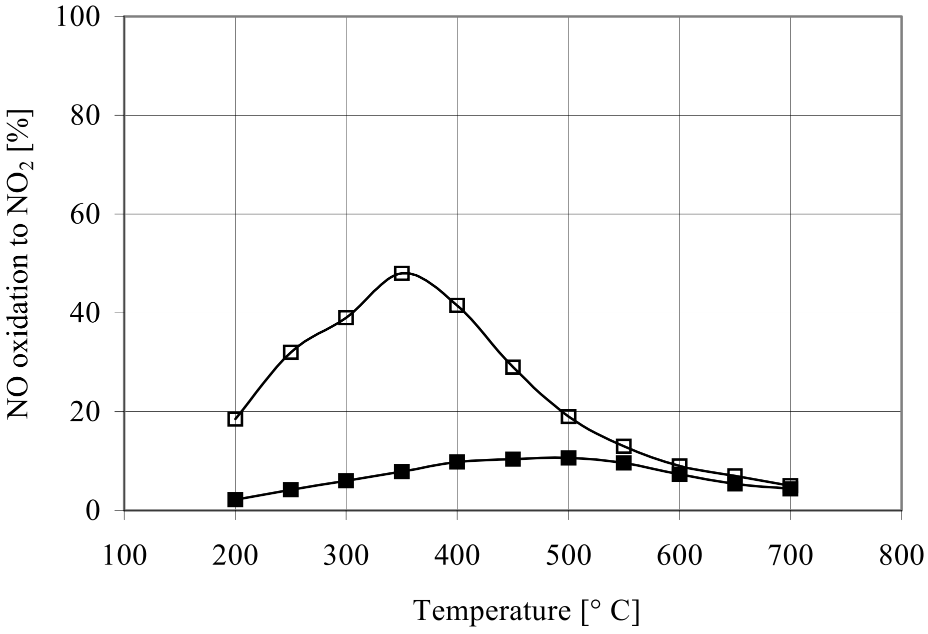

Figure 6.6 NO oxidation to NO_2 for the fresh Fe-ZSM monolith (■) with water in feed and (□) without water in feed.

The decisive function of NO_2 on the SCR reaction over Fe-ZSM5 was confirmed by adding NO_2 to the feed, which drastically increased the DeNOx values up to $NO_2/NO_x = 0.5$, especially at low temperatures [14]. The SCR reaction involving NO_2 is called fast-SCR [11]. It may be regarded as the *actual* and *general* SCR stoichiometry over zeolite based catalysts, because either NO_2 in the feed or the presence of an oxidation functionality in the zeolite for the oxidation of NO to NO_2 is a pre-requisite for SCR activity:

$$4\ NH_3 + 2\ NO + 2\ NO_2 \rightarrow 4\ N_2 + 6\ H_2O \tag{6.12}$$

6.4.7 Water-free experiments

In order to obtain a clearer picture of the functionality of the catalyst also water-free experiments have been performed. From figure 6.3 it is clearly discernible that Fe-ZSM5 shows a generally higher DeNOx activity if water is omitted. However, also much more N_2O is formed reaching a maximum of 12 ppm at intermediate temperatures. As stated above this side-product is typically formed in larger amounts at intermediate temperatures if NO_2 is present in the gas feed [14]. It is obvious from figure 6.6 that also much more NO_2 is formed under water-free conditions than with water in the feed. Thus, the increase in N_2O formation under water-free conditions is easily explained by the elevated concentration of NO_2 on the catalyst.

The higher oxidation capability of the catalyst under water free conditions, observable from the elevated NO_2 concentrations in figure 6.6, is also apparent in the investigation of the ammonia oxidation without water as shown in figure 6.7. By omitting the water, elevated NH_3 conversions are observed over the whole temperature range. At lower temperatures the occurrence of NO and N_2O is remarkable, which was not observed in the presence of water. Apparently, the ammonia oxidation to NO is promoted more than the following SCR reaction, resulting in the production of NO beside the main product N_2. With increasing temperature NO decreases as the SCR reaction accelerates faster than the ammonia oxidation. Long et al. [15] investigated the SCO reaction over powdered iron zeolites at temperatures up to 450 °C. They also found, that under water-free conditions the selectivity of the SCO reaction to nitrogen increases with temperature at the expense of a decrease in NO formation. This was explained by NO being the intermediate of the SCO reaction, which is reduced to nitrogen by NH_3 in the SCR reaction.

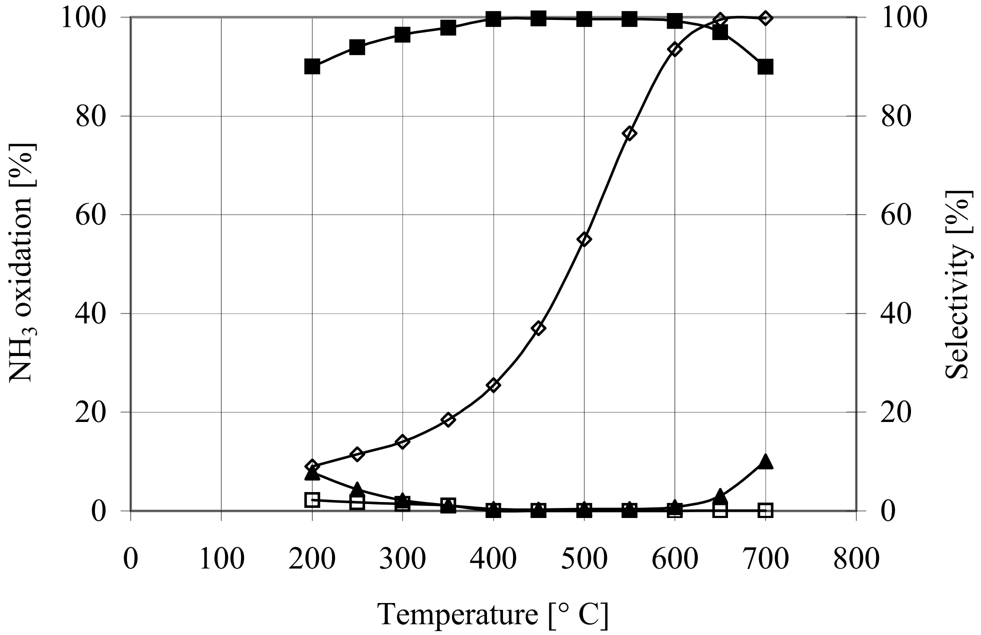

Figure 6.7 SCO properties of the fresh Fe-ZSM5 monolith vs. temperature without water in the feed. (◊) NH_3 oxidized (▲) selectivity towards NO and (■) selectivity towards N_2 and (□) selectivity towards N_2O.

The formation of N_2O seems to be coupled to the presence of gas phase NO. Due to the high oxidation capability of Fe-ZSM5, it is very likely, that part of the NO formed is further oxidized to NO_2 due to the strong oxidizing properties of the catalyst under water-free conditions. The NO_2, however, is not observable, as it is rapidly converted to nitrogen according to the “fast-SCR”reaction already at 200 °C [14]. Thus, the observed formation of N_2O would be a side-product of the “fast-SCR” reaction at low temperatures.

6.5 Conclusions

Fe-ZSM5 coated on cordierite proved to be active and selective for the catalytic reduction of NO in simulated diesel exhaust gas in the temperature region 250-650 °C. In order to obtain conversion efficiencies ≥ 90% temperatures of ≥ 400°C are necessary. Thus, the application of Fe-ZSM5 as urea SCR catalyst in a diesel vehicle with a low temperature operation window requires measures to promote the catalyst activity, i.e. elevating the NO_2 content in the exhaust gas for the utilization of the fast-SCR reaction or increasing the exhaust gas temperature. However, the high temperature activity suggest the use of this catalyst for the combination with a diesel particulate filter, which causes high exhaust gas temperatures during the regeneration process. Moreover, the usual platinum coating on the diesel particulate filter produces NO_2, which supports the fast-SCR reaction.

The observed DeNOx values are limited by the catalyst activity at low temperatures and by the selectivity at temperatures ≥ 700 °C, i.e. mainly the selective catalytic oxidation of ammonia to N_2 (SCO reaction) and the oxidation to NO. In order to exploit the full DeNOx potential of the catalyst accurate dosing of the reducing agent is required with respect to the catalyst activity and the stoichiometry of the reaction, as overdosing of ammonia inhibits the SCR reaction at low temperatures. Supplementing water-free experiments revealed that water deactivates the SCR activity of the catalysts by hampering the oxidation capability of Fe-ZSM5.

6.6 References

[1] A. Ma, W. Grünert, Chem Commun.1 (1999) 71.

[2] Q. Sun, Z. Gao, Y. Chen, W. M. H. Sachtler, J. Catal. 201 (2001) 89.

[3] R. Q. Long, R. T. Yang, J. Catal. 188 (1999) 332.

[4] K. Krishna, G. B. F. Seijger, C. M. van den Bleek, M. Makkee, G. Mul, H. P. A. Calis, Catal. Lett. 86 (2003) 121.

[5] M. S. Kumar, M. Schwidder, W. Grünert, A. Brückner J. Catal. 227 (2004) 384.

[6] M. Schwidder, M. S. Kumar, K. Klementiev, M. M. Pohl, A. Brückner, W. Grünert, J. Catal. 231 (2005) 314.

[7] H. Choi, S. Ham, I. Nam, Y. Kim, Ind. Eng. Chem. Res. 35 (1996) 106.

[8] M. Koebel, M. Elsener, G. Madia, SAE Technical Paper Series 3625 (2001) 01.

[9] J. Eng, C. H. Bartholomew, J. Catal. 171 (1999) 27.

[10] S. A. Stevenson, J. C. Vartuli, C. F. Brooks, J. Catal. 190 (2000) 228.

[11] G. Madia, M. Koebel, M. Elsener, A. Wokaun, Ind. Eng. Chem. Res. 41 (2002) 4008.

[12] B. Coq, M. Mauvezin, G. Delahay, J. B. Butet, S. Kieger, Appl. Catal. B 27 (2000) 193.

[13] Y. H. Yeom, J. Henao, M. J. Li, W. M. H. Sachtler, E. Weitz, J. Catal. 231 (2005) 181.

[14] M. Devadas, O. Kröcher, A. Wokaun, React. Kinet. Catal. Lett. 86 (2005) 347.

[15] R. Q. Long, R. T. Yang, J. Catal. 201 (2001) 145.

7

Influence of NO_2 on Fe-ZSM5

7.1 Introduction

During the last years, Fe-ZSM5 has been found to be an efficient catalyst for the selective catalytic reduction of nitrogen oxides in the exhaust of diesel vehicles by urea (urea-SCR) beside the established V_2O_5-WO_3/TiO_2 catalysts [1-3]. For both types of catalysts the reaction obeys the "standard-SCR" stoichiometry, involving equal amounts of NO and ammonia-the latter being the actual reducing agent, which is released from urea under the hydrothermal conditions in the exhaust pipe.

$$4\ NH_3 + 4\ NO + O_2 \rightarrow 4\ N_2 + 6\ H_2O \tag{7.1}$$

The main challenge for the application of Fe-ZSM5 in the urea-SCR process on board of diesel vehicles is to achieve high SCR activity and selectivity over a broad temperature range (150-700 °C). One possibility is the addition of NO_2 to the feed, whose promoting effect on the SCR reaction was already observed in the 1980's [4, 5]. Koebel et al., who investigated the influence of NO_2 on the SCR reaction over V_2O_5-WiO_3/TiO_2 in detail, pointed out the importance of having a 1:1 mixture of NO_2 and NO for reaching the maximum SCR activity [6, 7]. The high rates at this NO_2 to NO ratio are explained by SCR reaction (7.2), which is much faster than reaction (7.1), therefore called "fast-SCR".

$$4\ NH_3 + 2\ NO + 2\ NO_2 \rightarrow 4\ N_2 + 6\ H_2O \tag{7.2}$$

If the NO_2 : NO ratio is larger than 1:1 NO_2 reacts also via the "NO_2-SCR" route (7.3), which is even slower than the "standard-SCR" reaction over vanadia-based catalysts.

$$4\ NH_3 + 3\ NO_2 \rightarrow 3.5\ N_2 + 6\ H_2O \tag{7.3}$$

Very recently, the promoting effect of NO_2 was also reported for zeolite-based SCR catalysts by Rahkamaa-Tolonen et al. [8], who performed a screening of metal-exchanged zeolites. They added NO_2 and NO to the feed in the ratio 0.4:0.6, which is nearly ideal for the "fast SCR" stoichiometry, and found an increase in NO_x removal efficiency at lower temperatures compared to 100 % NO in feed.

The addition of NO_2 to the feed implies also some disadvantages. Thus, the formation of N_2O was observed over Fe-ZSM5 in the presence of NO_2 [8] and over Cu-ZSM5 even without NO_2 in the feed. On the basis of first performance tests the formation of N_2O over Fe-ZSM5 was generally attributed to ammonia oxidation [8]. Based on a more detailed investigation, Long et al. [9] tried to explain the elevated formation of N_2O by the reaction of NO_2 with the postulated intermediate species $NO_2(NH_4^+)_2$. Despite of this plausible explanation, many more reactions are conceivable to produce N_2O that have mainly been discussed for vanadia-based SCR catalysts [10], but cannot be ruled to take part on Fe-ZSM5 and other metal-exchanged catalysts.

The influence of NO_2 is described in detail on the SCR reaction over Fe-ZSM5 coated on a cordierite monolith, also comprising investigations on the formation of N_2O.

7.2 N_2O chemistry

Madia et al. [10] clearly explains the possible reactions schemes for the production of N_2O over the vanadia based catalyst. In the following, these reactions are summarized as a basis on which the observations in the present work are made.

The most important source of N_2O over vanadia-based SCR catalyst is the selective catalytic oxidation (SCO) of ammonia by oxygen (reaction 7.4):

$$4\ NH_3 + 4\ O_2 \rightarrow 2\ N_2O + 6\ H_2O \qquad (7.4)$$

At lower temperatures up to 350 °C, NO_2 which is a much stronger oxidant than O_2 is expected to contribute to the oxidation of ammonia to N_2O also by the following reactions:

$6\ NH_3 + 8\ NO_2 \rightarrow 7\ N_2O + 9\ H_2O \qquad (7.5)$

$4\ NH_3 + 4\ NO_2 + O_2 \rightarrow 4\ N_2O + 6\ H_2O \qquad (7.6)$

Due to the thermodynamic equilibrium

$NO + \frac{1}{2}\ O_2 \Leftrightarrow NO_2 \qquad (7.7)$

considerable amounts of NO are formed at T > 350 °C and low space velocities, facilitating the formation of N_2O by reaction 7.8, even if only NO is present in the feed gas.

$4\ NH_3 + 4\ NO + 3\ O_2 \rightarrow 4\ N_2O + 6\ H_2O \qquad (7.8)$

In the very low temperature region below 200 °C the formation of N_2O is explained by the decomposition of NH_4NO_3 as intermediate complex.

$NH_4NO_3 \rightarrow N_2O + 2\ H_2O \qquad (7.9)$

NH_4NO_3 itself is formed according to reaction 7.10 from NH_3 and N_2O_4 which is the stable dimerization product of NO_2.

$N_2O_4 + 2\ NH_3 + H_2O \rightarrow NH_4NO_3 + NH_4NO_2 \qquad (7.10)$

The simultaneously formed ammonium nitrite does not play an important role, as it is readily decomposed to nitrogen and water at T > 60 °C (reaction 7.11).

$NH_4NO_2 \rightarrow N_2 + H_2O \qquad (7.11)$

7.3 Experimental

The catalytic tests were carried out on fresh Fe-ZSM5 cordierite coated monolith in the laboratory test apparatus as described in chapter 4. The composition of diesel exhaust gas was approximated by a model feed gas containing 10 % O_2, 5 % H_2O, 1000 ppm of NO_x ($NO + NO_2$) and balance N_2. NH_3 was added in the range 100-1500 ppm. The gas hourly space velocity was 52,000 h^{-1}, except for the determination of the kinetic parameters, where a GHSV of 100,000 h^{-1} was used. Five different NO_2/NO_x ratios (0 %, 25 %, 50 %, 75 % and 100 %) were studied.

H-ZSM5 was used as iron-free comparable sample and coated on a cordierite monolith with a cell density of 400 cpsi by the procedure described in [11]. The active mass loaded on the monolith was 0.50 g. DRIFT measurements were carried out using fresh powder Fe-ZSM5 samples under the conditions mentioned in chapter 3.

7.4 Results

7.4.1 NH_3-SCR

Figure 7.1 shows the NO_x removal efficiency (DeNOx) of the Fe-ZSM5 monolith catalyst under varying $NO:NO_2$ ratios in the feed.

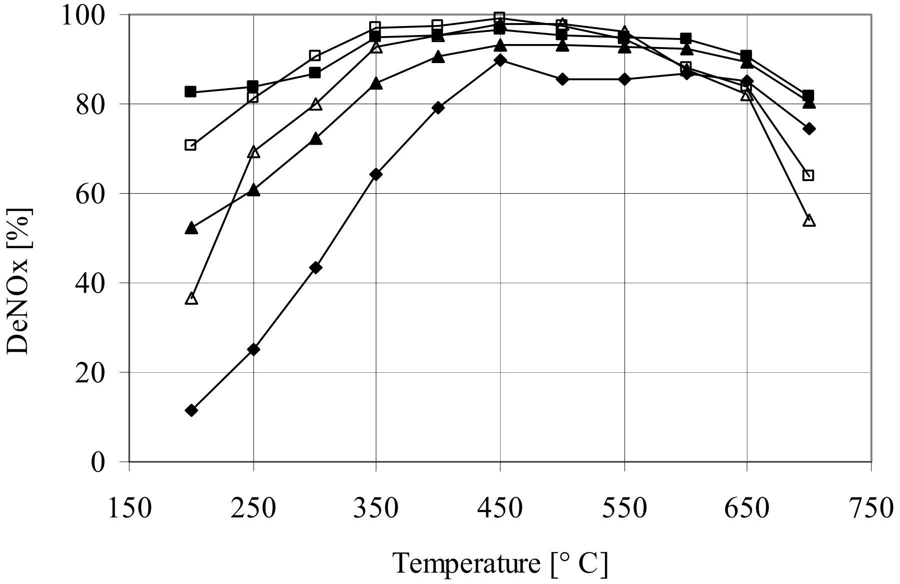

Figure 7.1 DeNOx vs. temperature at 10 ppm NH_3-slip for the Fe-ZSM5 monolith (GHSV = 52, 000 h^{-1}). (♦) $NO_{x,in}$ = 1000 ppm NO, (▲) 750 ppm NO + 250 ppm NO_2, (■) 500 ppm NO + 500 ppm NO_2, (□) 250 ppm NO + 750 ppm NO_2, and (Δ) 1000 ppm NO_2.

DeNOx increased drastically with the addition of NO_2 to the feed over the entire temperature range, most pronounced at lower and intermediate temperatures. Regarding the entire temperature range, NO_2/NO_x = 50 % resulted in the best DeNOx performance. However, it has to be noticed that the highest DeNOx values were achieved with 75 % NO_2 (250 ppm NO:750 ppm NO_2) in the temperature range from 300 to 450 °C and that also 100 % NO_2 (1000 ppm NO_2) was easily reduced at these intermediate temperatures. Due to the varying ammonia feed concentrations applied in figure 7.1 it is difficult to reliably assess the influence of NO_2 on DeNOx. In figure 7.2, plotted at the constant dosing rate $\alpha = NH_3/NO_x = 1$, the differences in DeNOx are much better discernible, demonstrating a clear maximum for NO_2/NO_x = 50 % followed by a decrease for higher NO_2 concentrations.

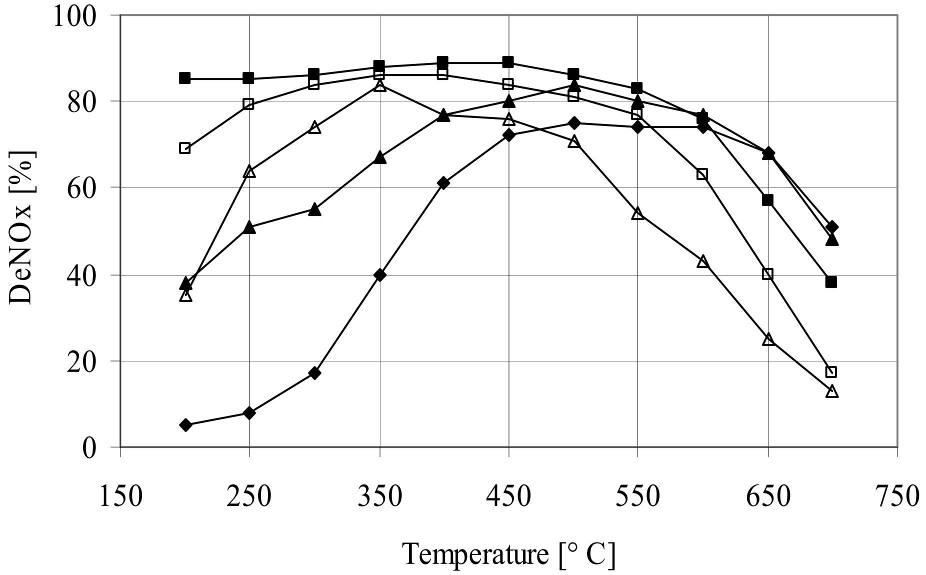

Figure 7.2 DeNOx vs. temperature at a constant feed ratio $\alpha = NH_3/NO_x = 1$ for the Fe-ZSM5 monolith (GHSV = 100,000 h^{-1}).

The weak decay in DeNOx performance for NO_2 shares above the optimum 50 % level found for Fe-ZSM5 clearly differs from that of vanadia-based SCR catalysts, who exhibit a *pronounced* DeNOx maximum at NO_2/NO_x = 50 % and a drastically reduced DeNOx activity for NO_2/NO_x > 50 % [6, 12]. The DeNOx values in figure 7.2 were measured at a high space velocity (GHSV = 100,000 h^{-1}) in order to avoid full conversion and to use them for the determination of the activation energy of the SCR reaction up to 450 °C. In this temperature range, ammonia is more readily adsorbed on the acidic surface than NO_x, as can be concluded from the very high ammonia storage capacity of Fe-ZSM5 [13], and thus it is present in excess on the catalyst surface for $\alpha = 1$. On that condition the reaction order of NO can be approximated to 1 in accordance with other research groups [14-16]. This makes the determination of the rate constants k_m quite simple, as the measured values of NO_x conversion could easily be calculated assuming a first order rate law and applying the well known equation for a plug flow reactor:

$$k_m = -\frac{V^*}{W} \cdot \ln\left(1 - \frac{X}{100}\right)$$

where k_m is the first order rate constant (referred to the catalyst mass) [$cm^3/g\cdot s$], V* is the gas flow at the actual conditions [cm^3/s], W is the active mass [g] and X is the conversion [%] (figure 7.3).

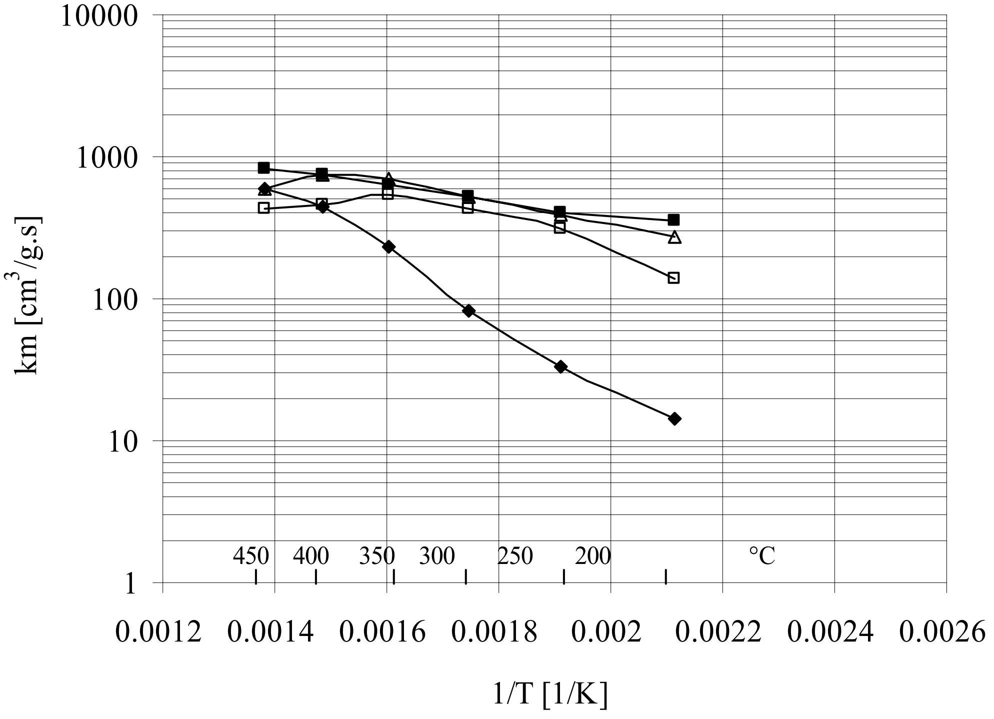

Figure 7.3 Arrhenius plot of the SCR rate constants for the feed ratios ($\alpha = 1$, GHSV = 100,000 h^{-1}). (♦) $NO_{x,in}$ = 1000 ppm NO, (■) 500 ppm NO + 500 ppm NO_2, (Δ) 250 ppm NO + 750 ppm NO_2, and (□) 1000 ppm NO_2.

The comparison of the different reaction rates were based on the values of k_m. Irrespective of the feed conditions, the curves level off at high temperatures due to a transition from reaction controlled to diffusion controlled regime. With respect to "standard-SCR" the found activation energy is quite low, but still typical for the reaction controlled regime, whereas all other activation energies are typical for diffusion controlled processes. The activation energies for the "standard" ($NO_{x,in}$ = 1000 ppm NO) and the "fast-SCR" reaction ($NO_{x,in}$ = 500 ppm NO + 500 ppm NO_2) were calculated from the slope of linear regression curves of the rate constants up to 350 °C (figure 7.4). The activation energies E_a were 39 kJ/mol (R^2 = 0.943) and 7 kJ/mol (R^2 = 0.967), respectively. Nearly the same values were obtained when the calculations were repeated with the SCR rates at GHSV = 52,000 h^{-1} (not shown here).

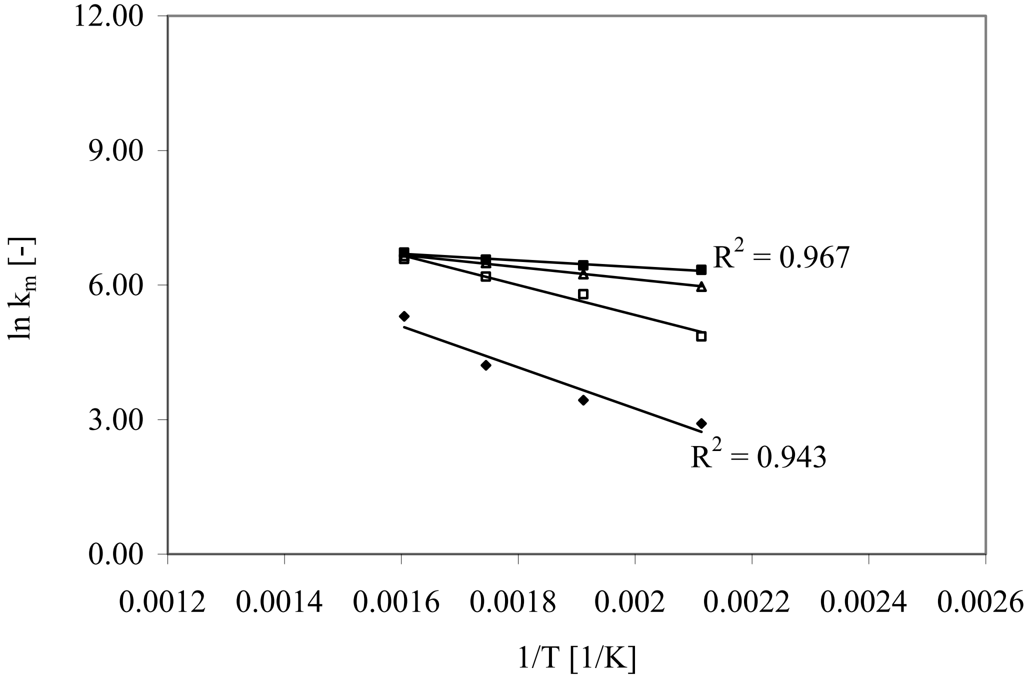

Figure 7.4 Linear regression of the SCR rate constants taken from the Arrhenius plot.

However, the regression constant for the "standard-SCR" reaction is quite low due to a non-linearity of data plot, which might be caused by the inhibiting effect of excessively adsorbed ammonia on the standard-SCR reaction for T ≤ 350°C [11, 13]. In order to suppress this inhibiting effect of ammonia on the “standard-SCR” reaction, the measurements were repeated at much lower inlet concentrations ($NO_{x,in}$ = 100 ppm NO, $\alpha = 1$). A much more linear data plot was obtained (not shown here), resulting in nearly the same E_a of 36 kJ/mol ($R^2 = 0.994$). The activation energies for the “standard-SCR” reaction determined in the present work (39 and 36 kJ/mol) with Fe-ZSM5 provided by Umicore are close to the values obtained with Fe-ZSM5 prepared at the Paul Scherrer Institute (45 kJ/mol) [11] and with Cu-ZSM5 (44 kJ/mol) [16].

By comparison of the NO oxidation over Fe-ZSM5 with H-ZSM5, we have shown in [17] that iron is required for the oxidation of NO to NO_2. By testing both zeolites also in the SCR reaction, the role of iron and zeolite framework should be further clarified. From figure 7.5, it is observable that H-ZSM5 is nearly inactive for the SCR reaction if only NO is present.

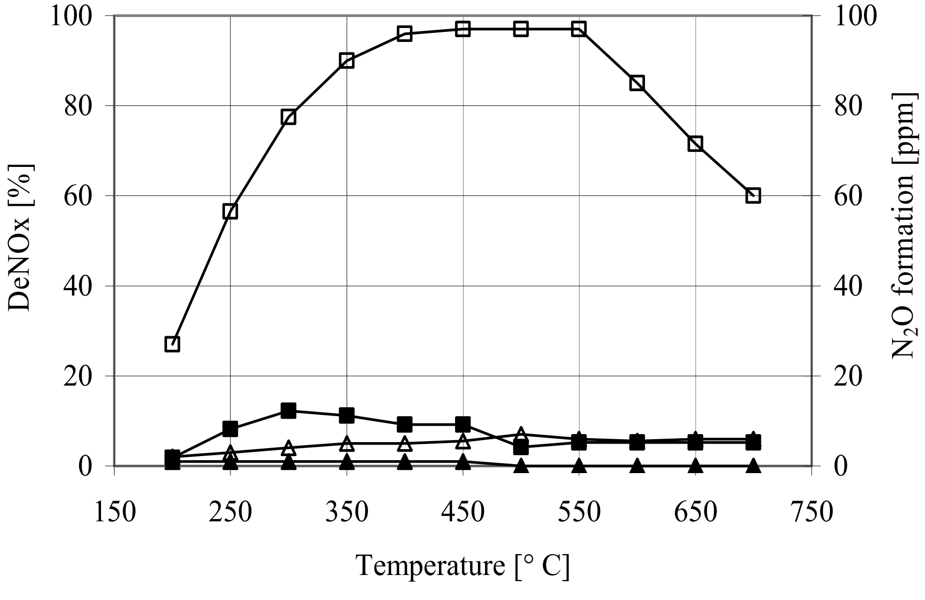

Figure 7.5 Maximum (Δ) DeNOx and (▲) N_2O formation over the H-ZSM5 monolith for $NO_{x,in}$ = 1000 ppm NO. Maximum (□) DeNOx and (■) N_2O formation for $NO_{x,in}$ = 500 ppm NO + 500 ppm NO_2.

However, by the addition of 50 % NO_2 to the feed DeNOx drastically increased at all temperatures, proving on the one hand that the oxidation of NO to NO_2 over iron is required to enable the SCR reaction and on the other hand that the SCR reaction itself takes place at the zeolite framework. However, is has to be noticed that the SCR activity is higher on Fe-ZSM5 than on H-ZSM5 even if the optimum NO_2/NO_x ratio of 50 % is dosed. This indicates that iron not only facilitates the NO oxidation but also promotes the SCR reaction over the zeolite framework.

In order to understand the role of water on DeNOx in dependency of temperature and the NO_2 fraction in the feed, experiments were performed with 0 % and 5 % water in a feed consisting of 10 % oxygen, 1000 ppm NH_3, 1000 ppm NO_x (NO_2/NO_x = 0 %, 25 %, 50 %, 75 %, 100 %) and balance N_2. Water had a very small effect on DeNOx, except for NO_2/NO_x = 0 % and NO_2/NO_x = 25 % where a reduction in DeNOx was observed up to 400 °C, shown in figure 7.6 & 7.7.

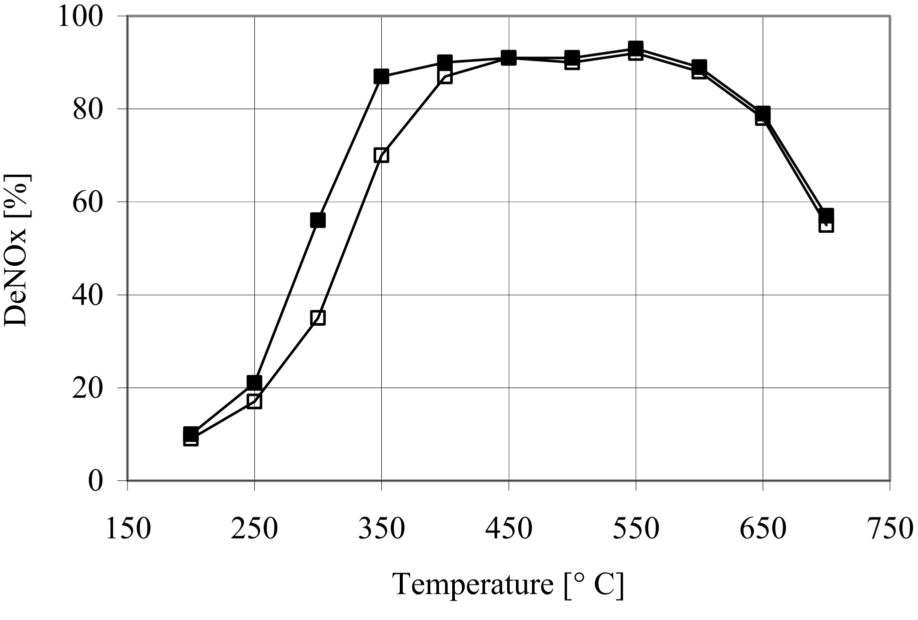

Figure 7.6 DeNOx at α = 1, (■) in the absence of water and (□) in the presence of 5 % water. $NO_{x,in}$ = 1000 ppm NO.

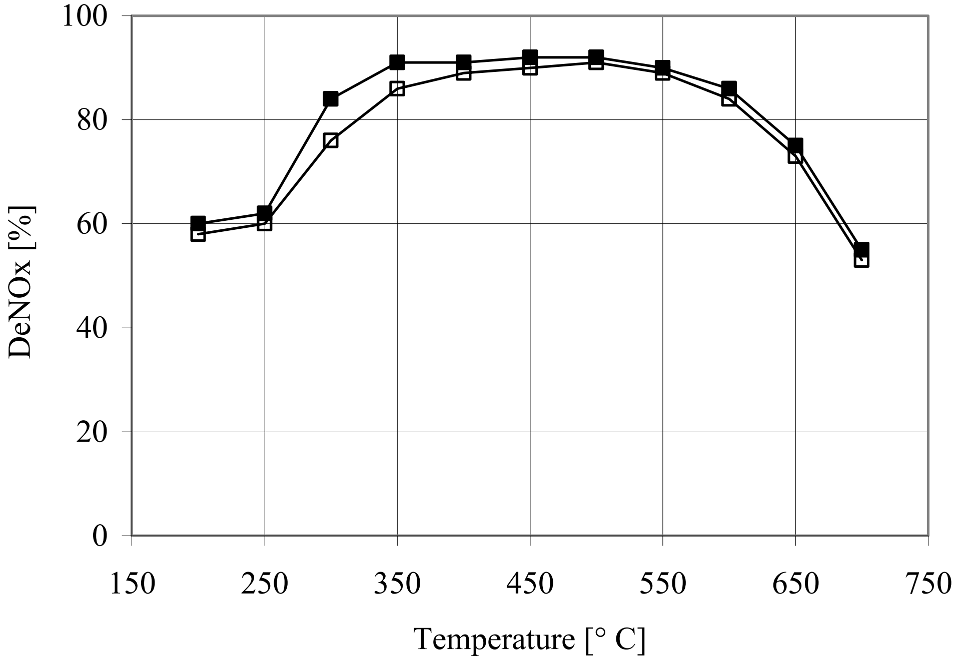

Figure 7.7 DeNOx at α = 1, (■) in the absence of water and (□) in the presence of 5 % water. $NO_{x,in}$ = 750 ppm NO + 250 ppm NO_2.

The influence of oxygen on the SCR reaction and the N_2O formation was investigated by additional tests in which oxygen was omitted (not shown here). Under such conditions with NO_x consisting of pure NO only 0-6 % DeNOx was achieved and no N_2O was formed from 200-450 °C, proving the crucial role of the NO oxidation step in the "standard-SCR" mechanism. For all ratios of $NO_2/NO_x \geq 50$ % the SCR activity as well as the N_2O formation was virtually the same over the whole temperature range.

7.4.2 N_2O formation

The SCR reaction over Fe-ZSM5 is accompanied by the formation of N_2O if NO_2 is present in the feed (figures 7.8 & 7.9). Up to NO_2/NO_x = 50 % only low amounts of N_2O are formed (figure 7.8), whereas an excess of NO_2 results in a steep increase in N_2O formation (figure 7.9). The highest N_2O concentration was formed for $NO_{x,in}$ = 100 % NO_2 at 250-300 °C.

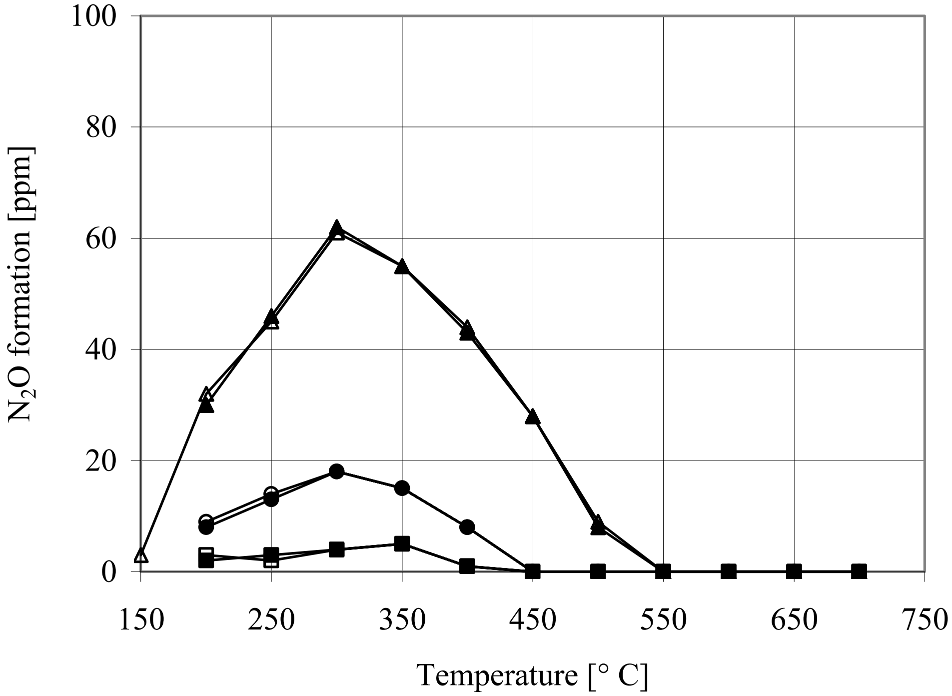

Figure 7.8 N_2O formation at $\alpha = 1$ (closed symbols) in the absence of water and (open symbols) in the presence of 5 % water. (□,■) 1000 ppm NO, (o,●) 250 ppm NO + 750 ppm NO_2 and (Δ,▲) 500 ppm NO + 500 ppm NO_2.

For higher temperatures the N_2O formation decreased and at 600 °C no N_2O was found irrespective of the amount of NO_2 in the feed. For $NO_2/NO_x \leq 50$ %, water does not influence the formation of N_2O at all temperatures. Since nearly the same N_2O concentrations were found with and without water in the feed for 25 % NO_2 and 50 % NO_2, the corresponding curves are overlaying each other.

However, on increasing the NO_2 fractions above 50 %, water was found to inhibit the formation of N_2O at lower and intermediate temperatures. The decline in N_2O concentration at higher temperatures does not implicitly mean that less N_2O is formed. On the contrary, N_2O might even be formed in higher concentrations at high temperatures but it should be readily converted to nitrogen under these conditions by N_2O decomposition [18] and/or the selective catalytic reduction of N_2O with NH_3 ("N_2O-

SCR") [19]. Therefore, investigation of the SCR chemistry on Fe-ZSM5 has been supplemented by experiments with N_2O dosage (See Chapter 8).

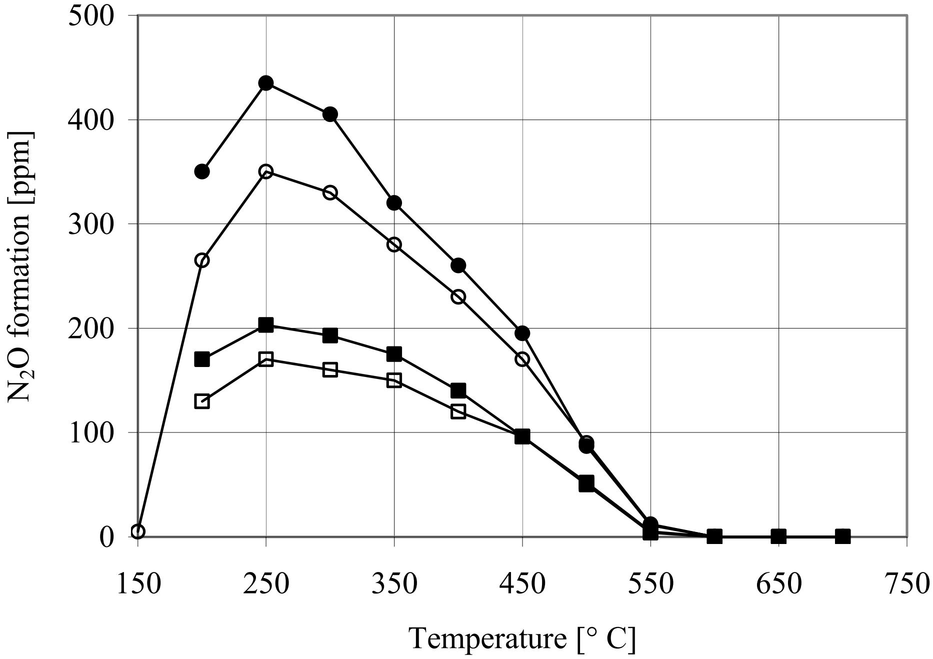

Figure 7.9 N_2O formation at $\alpha = 1$ (closed symbols) in the absence of water and (open symbols) in the presence of 5 % water. (□,■) 250 ppm NO + 750 ppm NO_2 and (o,●) 1000 ppm NO_2.

7.4.3 Pulse experiments

To investigate the role of water and oxygen in the NO oxidation, the SCR reaction and in N_2O formation, pulse experiments were carried out. First of all, the NO oxidation was studied. Figure 7.10 shows the outlet concentration profiles of NO and NO_2 at 450 °C and 200 °C which are formed as a response to switching oxygen and water on and off, in changing combinations. Small fluctuations and isolated spikes in the concentration profiles are due to disturbances in the water dosing system. The entire pulsing sequence is consisted of 5 steps. Step 1: after 2 min, 1000 ppm of NO are switched on. Step 2: oxygen (10 %) was supplied after 12 min and the outlet profile shows that NO_2 was formed by oxidizing NO. Step 3: by the addition of 5 % water after 25 min, the NO concentration was increased and the NO_2 concentration was decreased. Water clearly inhibits the oxidation of NO to NO_2. Step 4: after 37 min, the oxygen flow was stopped so that only NO and water remained in the feed. Consequently, no more NO_2 could be formed and the outlet NO concentration traces back to 1000 ppm, which is the inlet supply. Step 5: oxygen was supplied once again at 50 min, resulting in the same feed and outlet concentration profile as in step 3. N_2O was not formed at any time.

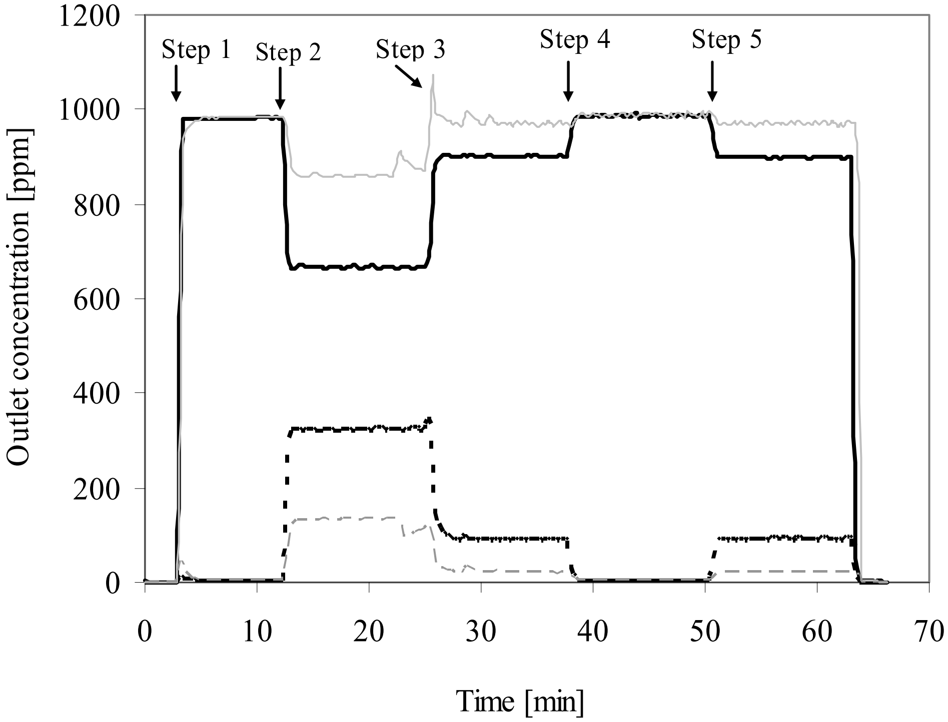

Figure 7.10 Influence of oxygen and water on the NO oxidation at (▬) 450 °C and (▬) 200 °C. (full line) NO concentration and (broken line) NO_2 concentration.

A similar pulsing experiment was carried out with ammonia and 50 % NO_2 in the feed mixtures in order to reveal more details of the SCR reaction (figure 7.11). Figure 7.11 shows the outlet concentration profile of NO, NO_2, N_2O and NH_3 at 350 °C, which is formed by sequentially switching ammonia, oxygen and water on and off. Step 1: after 2 min, 500 ppm NO + 500 ppm NO_2 were added to the basic nitrogen flow. Both the NO and NO_2 outlet concentration profile do not follow this step like switch-on of the gases.

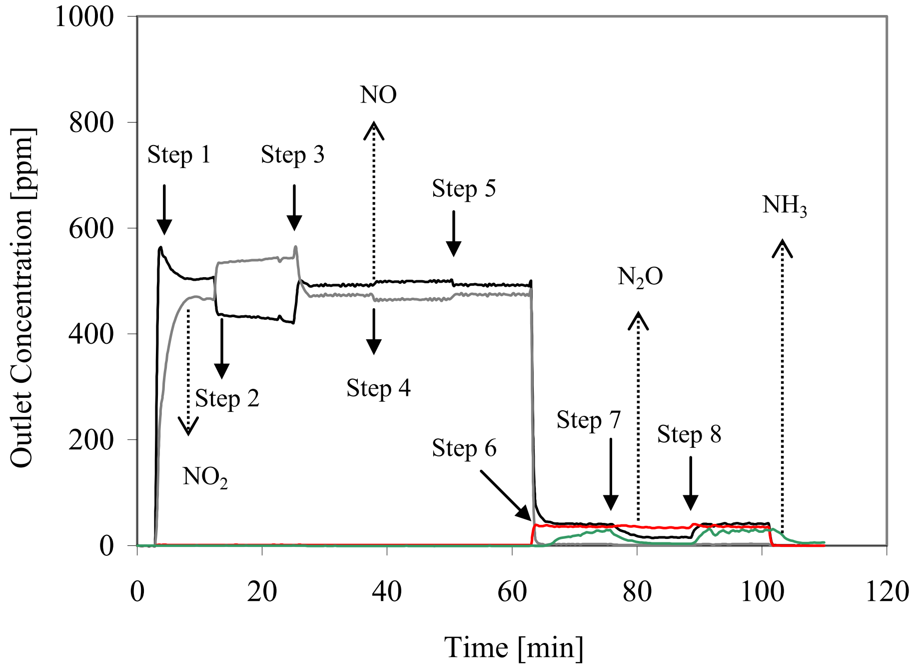

Figure 7.11 Influence of oxygen, water and ammonia on the reaction of NO and NO_2 over Fe-ZSM5 at 350 °C.

The NO_2 concentration reached its initial value after ~10 min indicating the adsorption of considerable amounts of NO_2 on the catalyst until saturation, whereas a concurrent desorption peak is found for NO. By integration of the peak areas the ratio of NO_2 adsorbed to NO desorbed was found to be around 3:1. This ratio is in accordance with a disproportionation reaction of NO_2, yielding nitrates bound to the surface and NO released to the gas phase.

$$3\ NO_2 \leftrightarrow NO + 2\ NO_3^- \qquad (7.12)$$

The same storage process was found for the highly active SCR catalyst Cu-ZSM5 [20], confirming the relevance of NO_2 adsorption for zeolite type SCR catalysts. Step 2: oxygen was supplied after 12 min. From the outlet profile, it can be seen that NO was oxidized to NO_2. Step 3: water was added after 25 min, which inhibited the oxidation of NO to NO_2 as expected. Step 4: after 37 min, oxygen dosing was stopped, which results in the original NO and NO_2 concentrations profiles of step 1. Step 5: oxygen was supplied again after 50 min and the outlet concentration recovered to the profile of step 3. Step 6: after 63 min, 1000 ppm of NH_3 was added to the feed with 500 ppm NO, 500 ppm NO_2, 10 % oxygen and 5 % water, representing “fast-SCR” conditions at $\alpha = 1$. A drastic drop in the NO and NO_2 profile was observed together with a low NH_3 concentration, indicating that these components have been consumed in the fast-SCR reaction. The formation of N_2O was also observed, typical for SCR over Fe-ZSM5 in the presence of NO_2. Step 7: after 75 min, the water inlet was stopped, resulting in a further decrease of NO, NO_2 and NH_3 concentrations, which corresponds to a small increase in DeNOx under water-free conditions. The N_2O concentration remains the same. Step 9: the water inlet was opened again after 88 min, and the outlet profiles recovered to that of step 6.

7.4.4 DRIFT measurements

DRIFT measurements were carried out under a flow of 500 ppm NO, 500 ppm NH_3, 5 % O_2 and balance N_2 (“standard-SCR” conditions) and in a flow of 500 ppm NO_2, 500 ppm NH_3, 5 % O_2 and balance N_2 (“NO_2-SCR”) at 200 °C. The resulting spectra in figure 7.12 look similar and most features are found under both standard- and NO_2-SCR conditions. The bands at 3372 cm^{-1} and 3275 cm^{-1} are associated to NH_4^+ ions with three hydrogen atoms bonded to three oxygen ions of AlO_4 tetrahedra (3H structure). Weaker bands at 3180 cm^{-1} and 2925 cm^{-1} are attributed to NH_4^+ ions with two hydrogen atoms bonded to AlO_4 tetrahedra (2H structure) [21, 22]. The band at 1460 cm^{-1} is due to the asymmetric bending vibration of NH_4^+ chemisorbed on Brønsted acid sites [23]. Under NO_2-SCR conditions (figure 7.12a), the additional weak bands at 2208 cm^{-1} & 2235 cm^{-1} indicate the presence of N_2O on the surface which might be formed from an intermediate species attacked by gas phase NO_2 as the formation of N_2O is exclusively observed in the presence of gas phase NO_2. These N_2O surface species are adsorbed via oxygen to Fe ions [24]. Apart from the N_2O bands, bands at 1634 cm^{-1}, 1578 cm^{-1} and 1604 cm^{-1} were observed. The band at 1634 cm^{-1} is assigned to adsorbed NO_2 [25], the band at 1578 cm^{-1} to nitrates species [26] and the band at 1604 cm^{-1} was assigned to another NO_2 species which reacts with NH_4^+ ions [9]. Figure 7.13 was recorded after flushing the sample with

N_2. All features remained the same, except for the N_2O band which was previously formed in the presence of NO_2 and now disappeared during purging with nitrogen.

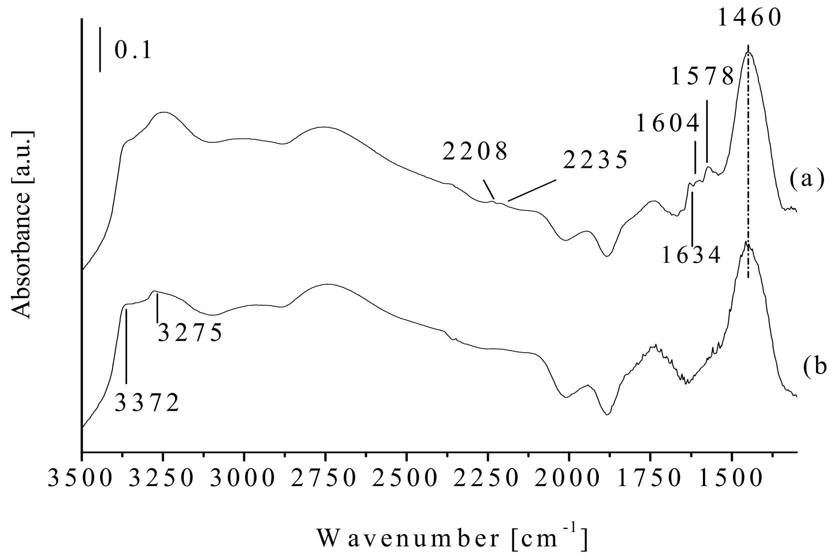

Figure 7.12 FTIR spectra of Fe-ZSM5 at 200 °C during (a) “NO_2-SCR” and (b) “standard SCR”.

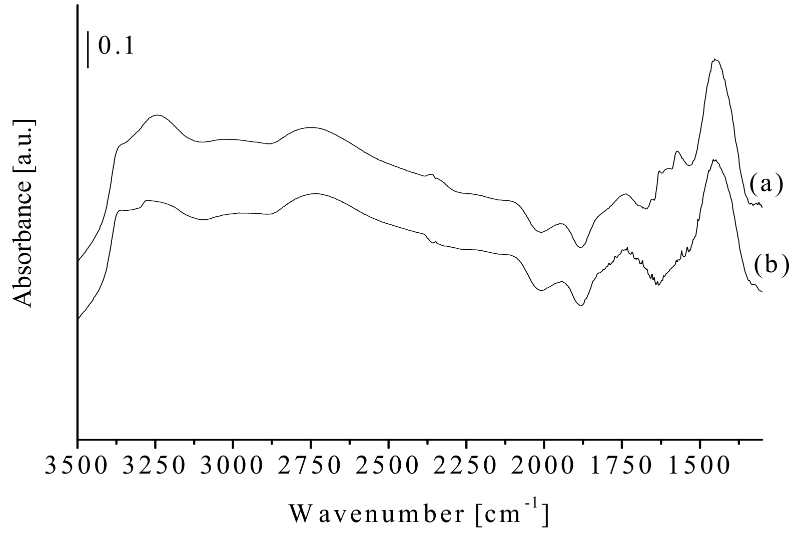

Figure 7.13 FTIR spectra of Fe-ZSM5 at 200 °C after purging with N_2 (a) for 15 min and (b) for 30 min.

7.5 Discussion

7.5.1 Standard-SCR

From the DeNOx measurements it is obvious that NO_2 is involved in the mechanism of the SCR reaction. In the case of "standard-SCR" (reaction 7.1), where no NO_2 is dosed, the reaction is able to proceed due to the capability of Fe-ZSM5 to oxidize NO to NO_2 [12]. When NO was dosed over Fe-ZSM5, first the NO_2 fraction increased with temperature but decreased again above ~ 350 °C due to the thermodynamic equilibrium between NO and NO_2, which shifts to the NO side for higher temperatures [12]. The capability of Fe-ZSM5 to oxidize NO to NO_2 was attributed to the iron [24], which was confirmed by our test of H-ZSM5, showing almost no activity under standard SCR conditions. The same conclusion was drawn in a very recent publication of Yeom et al. [27], who also attributes the inactivity of H-ZSM5 to the lack of NO oxidation capability. The necessity of NO_2 for the SCR activity is further supported by the tremendous increase in DeNOx activity over H-ZSM5, when NO_2 (NO_2/NO_x = 50 %) was added to the feed (figure 7.5). Regarding the "standard-SCR" reaction equation, NO_2 is not involved. However, all experimental results point out that NO_2 formed from NO takes part in the reaction scheme. Since NO_2 is not observed as product of the standard-SCR reaction, it must be a short living intermediate, which is immediately consumed. To sum up, it can be said that zeolite catalysts require NO_2 in the feed gas or an NO oxidation functionality to exhibit SCR activity.

As expected, DeNOx increased with the addition of NO_2 to the feed over the entire temperature range. It surprisingly arises from the measurements of the NO_x conversion, where ammonia is dosed in excess that the highest DeNOx values are reached for 75 % NO_2 in the feed, but for $\alpha = 1$ the highest DeNOx values are found at the expected ratio of NO_2/NO_x = 50 %. However, also for $\alpha = 1$ the DeNOx values for NO_2/NO_x > 50 % are only slightly lowered, which is in contrast to the dropping DeNOx values when NO_2 is overdosed on vanadia-based SCR catalysts [12]. A possible explanation for this observation might be the facile NO_2 storage on zeolites in form of nitrates accompanied by the release of NO, which we have found on Fe-ZSM5 (figure 7.11) and on Cu-ZSM5

[20]. These surface nitrates likely promote the SCR reaction on zeolites, because they serve as a NO_x supply nearby the active SCR sites. The storage of considerable amounts of the reactants ammonia and NO_2 on zeolites under SCR conditions, which is supported by our DRIFT experiments, is in contrast to vanadia-based systems, where only ammonia storage plays a significant role. From the results of our catalytic tests it is reasonable to conclude that the so-called "fast-SCR" reaction is the normal route on zeolites. Thus, the ideal mixture of NH_3, NO and NO_2 in SCR is always 2:1:1, which has to be provided by the gas feed or has to be produced by the catalyst itself. In parallel to the present research project the same general conclusion was drawn by Yeom et al. [27].

Oxygen enhances the oxidation of NO to NO_2 (figure 7.10) and thereby, the oxygen is an indirect promoter for DeNOx. Water has the opposite effect of oxygen. With water in the feed, the oxidation of NO to NO_2 is decreased, which is considered to be the rate limiting step in standard-SCR and thereby, the DeNOx is decreased. This decrease in oxidation of NO to NO_2 might be due to water blocking the active sites needed to oxidize NO to NO_2. Despres et al. [20] found this impeding effect of water on NO adsorption also on Cu-ZSM5 and attributed it to the competing nature of NO oxidation and H_2O adsorption on the same active site. The experimental results in figures 7.6 & 7.7 are in complete accordance with this explanation: the lower the NO_2 fraction in the feed the higher the water inhibiting effect. With increasing NO_2 fractions in the feed, the effect of water on DeNOx is considerably reduced and is only very small for NO_2/NO_x = 50 % or higher, because pre-oxidation of NO to NO_2 is no longer necessary.

7.5.2 Nitrous oxide production

General conclusions

The formation of N_2O is a critical issue for the application of a catalyst in a real-world SCR system. In this viewpoint, Fe-ZSM5 is harmless when used without any pre-oxidation catalyst, since NO_x in the raw Diesel exhaust gas is to over 90 % composed of NO, which does not produce N_2O over this type of catalyst. However, we have learned from the present investigation that a NO_2/NO_x ratio of 50 % is required to exploit the full potential of Fe-ZSM5 in the SCR process, especially at low temperatures up to 300 °C.

These exhaust gas temperatures are typical for Diesel vehicles under partial-load conditions. Therefore, Fe-ZSM5 is ideally applied in combination with a pre-oxidation catalyst in order to increase the NO_2/NO_x ratio upstream of the Fe-ZSM5 catalyst. From figure 7.8 it is clearly discernible that NO_2 fractions up to 50 % are uncritical, because only low amounts of N_2O are formed. Since NO_2 fractions over 50 % do not further increase the activity of Fe-ZSM5 and are detrimental regarding the N_2O formation (figure 7.9), in practice the oxidation catalyst is designed such, that 50 % NO_2 will never be exceeded. Combining the observations on the N_2O formation over vanadia-based SCR catalyst with our results, the following general conclusions are drawn about the formation of N_2O during SCR over Fe-ZSM5. Reaction 7.8 can be ruled out, since no N_2O was produced over Fe-ZSM5 in the “standard-SCR” reaction with NO in the feed (figures 7.8 & 7.9). In [13] we have shown that no N_2O is formed, if ammonia and oxygen is dosed over Fe-ZSM5, proving that also reaction 7.4 does not take place on Fe-ZSM5. Since the oxygen concentration did not influence the formation of N_2O, reaction 7.6 is excluded as well. As a consequence, reaction 7.5 remains, indicating that ammonia and NO_2 react with each other on the catalyst to form N_2O. The pulse experiments confirmed that N_2O is only formed when NH_3 and NO_2 are present in the feed. However, with the overall reaction equation 7.5 nothing is stated about the underlying elementary reaction mechanism, which has to be viewed in detailed.

N_2O formation at low and intermediate temperatures

On vanadia-based SCR catalysts, NH_4NO_3 could be identified as intermediate species formed from NH_3, NO_2 and water at temperatures below 200 °C [10]. Thermal decomposition of NH_4NO_3 starts at 170 °C to form either $HNO_3 + NH_3$ or $N_2O + 2\ H_2O$. At slow heating rates in the presence of water mainly $HNO_3 + NH_3$ is formed, whereas for fast heating rates and without water the formation of N_2O prevails. The different reaction paths end up directly or indirectly in the formation of the side-product N_2O. As N_2O was not formed over Fe-ZSM5 at 150 °C (figure 7.9), irrespective of the amount of NO_2 fraction in feed, but started to be produced at 200 °C in high amounts, the NH_4NO_3 mechanism might also be valid for Fe-ZSM5 in accordance with decomposition temperature of NH_4NO_3 at 170 °C: at 150 °C, NH_4NO_3 is formed and deposited at the catalyst surface, whereas at 200 °C decomposition of NH_4NO_3 occurs, resulting in the formation of N_2O. However, this mechanism only explains the absence of N_2O at 150 °C (figure 7.9) and the formation of N_2O at slightly higher temperatures, but not the huge amounts of N_2O found over Fe-ZSM5 at intermediate temperatures. Thus, another mechanism must significantly contribute to the formation of N_2O. We have learned from the catalytic tests that NO_2 is a key molecule, which is either fed directly in case of the "fast-SCR" reaction or is produced from the oxidation of NO in the "standard-SCR" reaction. Thus, the formation of N_2O might also be due to the presence of second intermediate species which is formed from NH_3 and NO_2 apart from NH_4NO_3. In accordance with the SCR experiments, N_2O was found on the catalyst surface in DRIFT measurements under "NO_2-SCR" conditions, but not under "standard-SCR" conditions, even though NO_2 (1635 cm^{-1}) is formed when NO + O_2 is fed to Fe-ZSM5 (not shown here) [28]. The most important feature of the NO_2-SCR spectrum is the band at 1604 cm^{-1}, which was assigned by Long et al. to be $NO_2(NH_4^+)_2$ [9]. This species may easily react with NO to yield nitrogen. The band at 1604 cm^{-1} could not be observed under "standard –SCR" conditions. Nevertheless, it is plausible to assume $NO_2(NH_4^+)_2$ to be a general intermediate in the SCR reaction over Fe-ZSM5 catalysts from which nitrogen is formed by reaction with NO and N_2O is formed by reaction with NO_2. The only difference between the presence and the absence of NO_2 in the gas phase is the low concentration of the intermediate species $NO_2(NH_4^+)_2$ on the catalyst surface.

In the absence of NO_2 in the feed, the oxidation of NO to NO_2 is rate limiting, whereupon the formed NO_2 immediately reacts on the surface to form $NO_2(NH_4^+)_2$, which itself reacts with NO to nitrogen. In the presence of NO_2 in the feed the intermediate $NO_2(NH_4^+)_2$ is easily formed, resulting in a much higher surface concentration of $NO_2(NH_4^+)_2$, which was, therefore, detectable by DRIFT spectroscopy (figures 7.12 & 7.13). Now, the consecutive reaction of $NO_2(NH_4^+)_2$ with NO becomes rate limiting thereby increasing the probability to form the side-product N_2O.

7.6 Conclusions

By the present study it was shown that the SCR activity of Fe-ZSM5 is tremendously improved by the addition of NO_2 to the feed gas. The maximum DeNOx was found for NO_2/NO_x = 50 %, but, surprisingly, higher NO_2 fractions resulted in similar high DeNOx values. This behaviour is explained by the assumption of $[NH_4^+]_2NO_2$ as intermediate complex species, which is formed fast from NH_3, NO and NO_2 in the optimum ratio 2:1:1 and reacts to the final product nitrogen. Higher NO_2 fractions are also easily converted to this intermediate species due to the pronounced ammonia and NO_2 storage capacity of Fe-ZSM5, providing high surface concentrations of the reactants.

Under practical conditions, i.e. the ammonia dosage was limited to 10 ppm ammonia emissions downstream of the catalyst, the best performance was found for a feed ratio NO_2/NO_x = 75 %. The addition of NO_2 to the feed was accompanied by the formation of N_2O, whose concentration depends on the NO_2 fraction in the feed. The maximum concentration of N_2O was always found at intermediate temperatures. The formation of N_2O is explained again by $[NH_4^+]_2NO_2$ as intermediate species, which is formed in the presence of gas phase NO_2 in high concentrations and may react not only to nitrogen but also N_2O. The N_2O formation at very low temperatures is reduced to the formation of NH_4NO_3, which is quantitatively formed at 150 °C and decomposed at 200 °C.

7.7 References

[1] M. Koebel, M. Elsener, M. Kleemann, Catal. Today 59 (2000) 335.

[2] R. Q. Long, R. T. Yang, J. Catal. 188 (1999) 332.

[3] R. Q. Long, R. T. Yang, Catal. Lett. 74 (2001) 201.

[4] A. Kato, S. Matsuda, T. Kamo, F. Nakajima, H. Kuroda, T. Narita, J. Phys. Chem. 85 (1981) 4099.

[5] G. Tünter, W. Leeuwen, L. Snepvangers, Ind. Eng. Chem. Res. Dev. 25 (1986) 633.

[6] M. Koebel, M. Elsener, G. Madia, Ind. Eng. Chem. Res. 40 (2001) 52.

[7] M. Koebel, G. Madia, M. Elsener, Catal. Today 73 (2002) 239.

[8] K. R. Tolonen, T. Maunula, M. Lomma, M. Huuhtanen, R. L. Keiske, Catal. Today 100 (2005) 217.

[9] R. Q. Long, R. T. Yang, J. Catal. 207 (2002) 224332.

[10] G. Madia, M. Koebel, M. Elsener, A. Wokaun, Ind. Eng. Chem. Res. 41 (2002) 4008.

[11] M. Devadas, O. Kröcher, A. Wokaun, React. Kinet. Catal. Lett., 86 (2005) 347.

[12] G. Madia, M. Koebel, M. Elsener, A. Wokaun, Ind. Eng. Chem. Res. 41 (2002) 3512.

[13] M. Devadas, O. Kröcher, M. Elsener, A. Wokaun, N. Söger, M. Pfeifer, Y. Demel, L. Mussmann, Appl. Catal. B. submitted.

[14] H.Y. Huang, R. Q. Long, R. T. Yang App. Catal. A 235 (2002) 241.

[15] S.A. Stevenson, J. C. Vartuli, C. F. Brooks, J. Catal. 190 (2000) 228.

[16] T. Komatsu, M. Nunokawa, I. S. Moon, T. Takahara, S. Namba, T. Yashima, J. Catal. 148 (1994) 427.

[17] M. Devadas, O. Kröcher, M. Elsener, A. Wokaun, G. Mitrikas, N. Söger, M. Pfeifer, Y. Demel, L. Mussmann, Catal. Today, submitted.

[18] T. Turek, Appl. Catal. B 9 (1996) 201.

[19] B. Coq, M. Mauvezin, G. Delahay, J. B. Butet, S. Kieger, Appl. Catal. B 27 (2000) 193.

[20] J. Despres, M. Koebel, O. Krocher, M. Elsener, A. Wokaun, Micropor. Mesopor. Mat. 58 (2003) 175.

[21] J. Eng, C. H. Bartholomew, J. Catal. 171 (1997) 27.

[22] E. H. Teunissen, R. A. van Santen, A.P. J. Jansen, F. B. van Duijneveldt, J. Phys. Chem. 97 (1993) 203.

[23] N. Y. Topsøe, J. Catal. 128 (1990) 499.

[24] A. Waclaw, K. Nowinska, W. Schweiger, A. Zielinska, Catal. Today 90 (2004) 21.

[25] G. Mul, J. Pèrez-Ramirez, F. Kapteijn, J. A. Moulijn, Catal. Lett. 80 (2002) 129.

[26] L. J. Lobree, I.- C. Hwang, J. A. Reimer, A. T. Bell, Catal. Lett. 63 (1999) 233.

[27] Y. H. Yeom, J. Henao, M. J. Li, W. M. H. Sachtler, E. Weitz, J. Catal. 231 (2005) 181.

[28] R.Q. Long, R.T. Yang, J. Catal. 198 (2001) 20.

8

Catalytic Investigation of N_2O Conversion on Fe-ZSM5

8.1 Introduction

Nitrous oxide (N_2O) is a pollutant which takes part in the greenhouse effect and the depletion of the ozone layer. At present, every year the N_2O concentration in the atmosphere is rising by 0.25 % [1]. At the Kyoto conference in 1997, the European Union committed itself to reduce the greenhouse gases by 2010. Catalytic decomposition of N_2O [2, 3] and the selective catalytic reduction of N_2O (N_2O-SCR) with reductants such as hydrocarbons [4, 5] and ammonia [6, 7] have been reported as an effective method for N_2O abetment.

From Chapter 7, it was found that the addition of NO_2 in feed mixtures not only improved the DeNOx but at the same time it caused an increase in N_2O formation as well. The N_2O was formed at lower and intermediate temperatures but more pronounced at intermediate temperatures. In order to check if N_2O decomposition and N_2O-SCR might take place at higher temperatures, investigations on N_2O conversions were carried out.

8.2 Experimental

Fresh Fe-ZSM5 cordierite monolith with catalyst volume of 7.7 cm^3 was used for catalytic investigation. The gas hourly space velocity (GHSV) was 52,000 h^{-1}. The composition of the feed was 10 % O_2, 5 % H_2O, 500 ppm of N_2O and balance N_2. NH_3 was added stepwise in the range 50-1500 ppm.

8.3 Results and Discussion

Figure 8.1 shows the NH_3-slip vs. N_2O conversion at different temperatures. It can clearly be seen that at higher temperatures the Fe-ZSM5 catalyst is active. The catalyst was inactive at T < 350 °C, not shown in the figure. With increasing temperatures, the N_2O conversion was steadily increasing and at T > 600 °C, 95 % conversion was achieved.

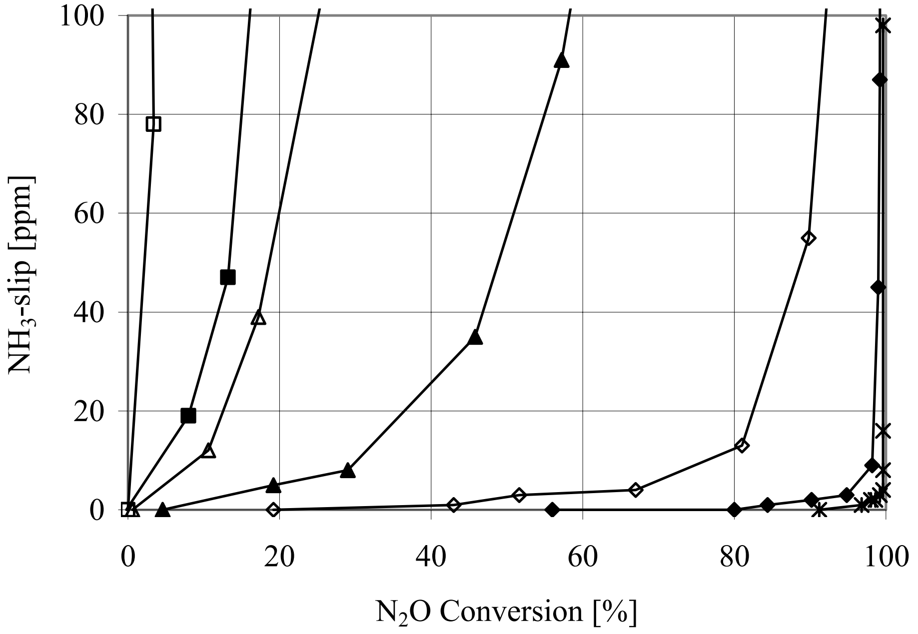

Figure 8.1 NH_3-slip vs. N_2O conversion for the fresh Fe-ZSM5 monolith catalyst at (□) 350 °C, (■) 400 °C, (Δ) 450 °C, (▲) 500 °C, (◊) 550 °C , (♦) 600 °C, (x) 650 °C.

Figure 8.2 depicts the N_2O conversion at different NH_3 inlet concentrations and different temperatures. At 350 °C, the N_2O conversion was going through a maximum for increasing NH_3 concentrations, which indicates an inhibition effect of NH_3 on N_2O removal. At higher temperatures, a steady increase in N_2O conversion was observed. Remarkably, N_2O conversion was also achieved without ammonia dosing (NH_3 inlet = 0 ppm). This is due to the catalytic decomposition of N_2O according to reaction 8.1, whereby the N_2O is decomposed to N_2 and O_2.

$$2\ N_2O \rightarrow N_2 + O_2 \qquad (8.1)$$

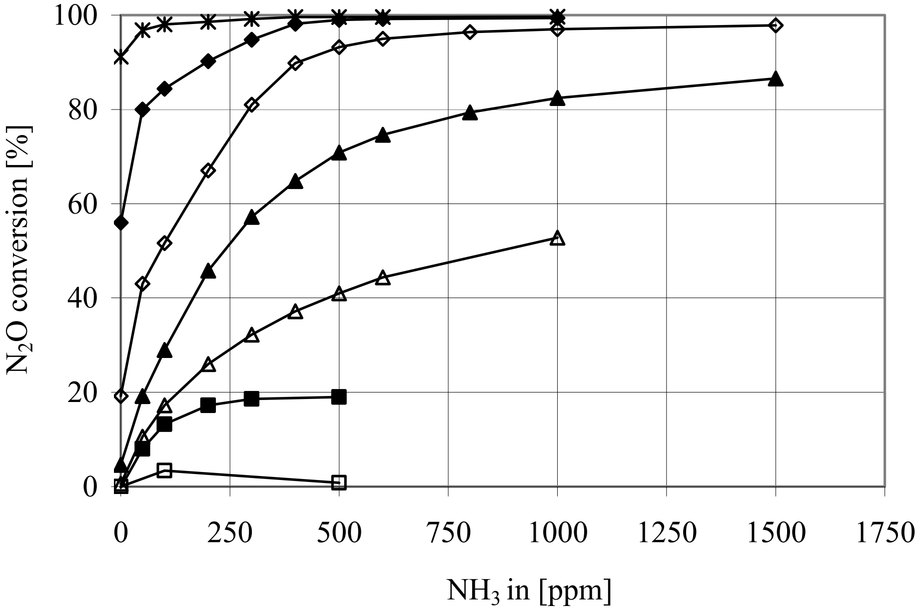

Figure 8.2 N_2O conversion vs. NH_3 inlet concentrations for the fresh Fe-ZSM5 monolith catalyst at (□) 350 °C, (■) 400 °C, (Δ) 450 °C, (▲) 500 °C, (◊) 550 °C , (♦) 600 °C, (x) 650 °C .

This particular effect is much better discernible in figure 8.3. Without dosing ammonia, N_2O started to decompose to nitrogen and oxygen at $T \geq 450$ °C reaching a maximum of 100 % conversion at 700 °C.

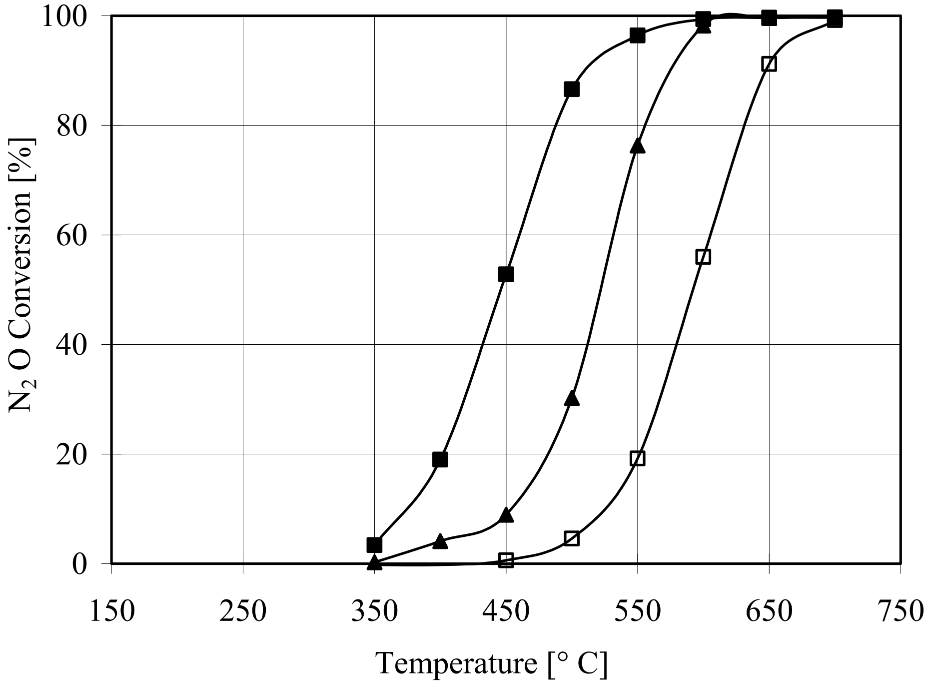

Figure 8.3 N_2O conversion vs. temperature. (■) Maximum N_2O conversion with NH_3 dosage, (▲) N_2O conversion at 10 ppm NH_3 slip and (□) N_2O conversion without NH_3 dosage.

In figure 8.4, the outlet concentrations of N_2O, NH_3, and NO_x ($NO+NO_2$) are shown at 550 °C. In the absence of ammonia (0 ppm NH_3 inlet in figure 8.4), the outlet N_2O concentration was 404 ppm, indicating that N_2O decomposition takes place according to reaction 8.1. At the beginning of the ammonia dosage, all ammonia was consumed and the NO_x concentration dropped. For 50 ppm of ammonia, an outlet concentration of 285 ppm N_2O and 20 ppm NO_x was found. Based on the stoichiometry of reaction 8.2, maximum 75 ppm N_2O consumption is expected, if 50 ppm NH_3 is dosed. This would result in an outlet concentration of 329 ppm N_2O assuming that the N_2O decomposition remains constant. However, only 285 ppm of N_2O were detected, which was less than the theoretical value. The only reasonable explanation for this effect is that ammonia dosage not only starts N_2O-SCR but also promotes the N_2O decomposition reaction. Thus, it is concluded that under SCR conditions at higher temperatures N_2O decomposition as well as N_2O-SCR play an important role in converting N_2O.

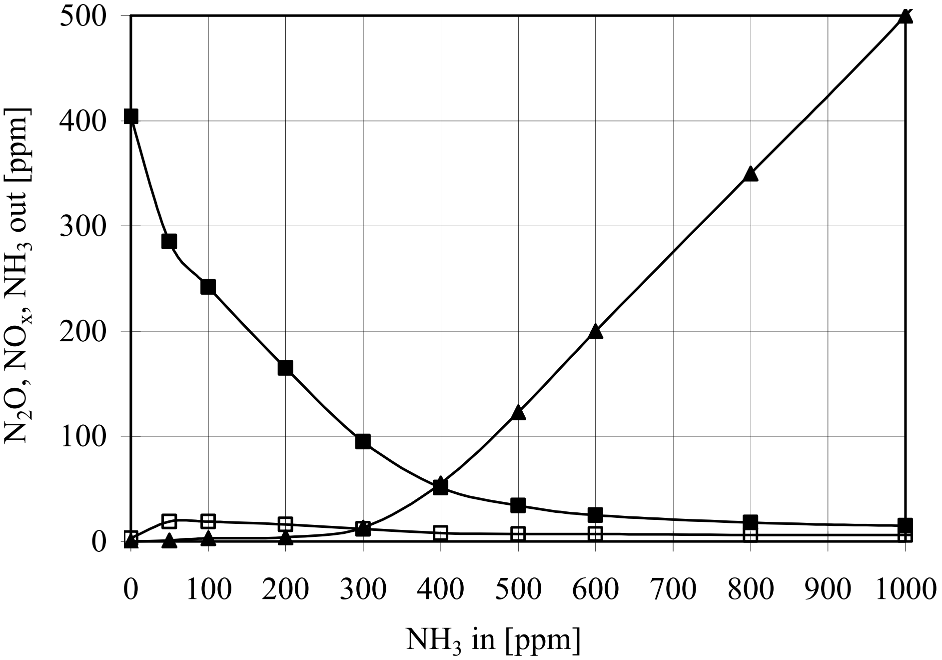

Figure 8.4 Outlet concentration of (■) N_2O, (□) NO_x and (▲) NH_3 vs. NH_3 dosage at 550 °C.

Kapteijn et al. [8] suggested a reaction sequence for the N_2O decomposition mechanism, in which N_2O is dissociatively adsorbed on an active iron site forming N_2 and a surface oxygen (O*). This surface oxygen is able to attack a second N_2O molecule releasing N_2, O_2 and the active site, which is now free to adsorb another N_2O molecule. This process is described by reactions 8.3 - 8.5, in which * represents an active iron site on the surface.

$$N_2O + * \rightarrow N_2 + O* \tag{8.3}$$

$$N_2O + O* \rightarrow N_2 + O_2 + * \tag{8.4}$$

$$2\,O* \rightarrow O_2 + 2* \tag{8.5}$$

The special property of the surface oxygen is that, it can easily be desorbed in different reactions, i.e. by reacting with another surface oxygen or by reaction with N_2O. Another possibility is the reaction of the surface oxygen with a reducing agent as observed for Fe-

ZSM5 [9]. Coq et al. [10] suggested that in the presence of $N_2O + NO + NH_3$, the surface oxygen can be removed by reaction (8.6), which is in accordance with our conclusion.

$$3\ O^* + 2\ NH_3 \rightarrow N_2 + 3\ H_2O + 3\ * \qquad (8.6)$$

8.4 Conclusions

The selective catalytic reduction of N_2O with NH_3 and N_2O decompositions over Fe-ZSM5 cordierite monolith was investigated. The catalyst was active for both reactions especially at higher temperatures. N_2O conversion was drastically enhanced when ammonia was dosed, reaching 100 % conversion at already 600 °C At higher temperatures, N_2O was completely converted, whereby the N_2O might have undergone N_2O decomposition as we N_2O-SCR by NH_3. Thus, if N_2O is formed on Fe-ZSM5 at higher temperatures during SCR conditions, it is also very easily decomposed under these conditions so that no N_2O is detected downstream of the catalyst exit.

8.5 References

[1] B. Coq, M. Mauvezin, G. Delahay, S. Kieger, J. Catal. 195 (2000) 298.

[2] J. Perez-Ramirez, F. Kapteijn, G. Mul, X. Xu, J. A. Moulijn, Catal. Today 76 2002) 55.

[3] A. Waclaw, K. Nowinska, W. Schweiger, A. Zielinska, Catal. Today 90 (2004) 21.

[4] G. Centi, F. Vazzana, Catal. Today 53 (1999) 683.

[5] R. W. van den Brink, S. Booneveld, J. R. Pels, D. F. Bakker, M. J. F. M. Verhaak, Appl. Catal. B 32 (2001) 73.

[6] G. Delahay, M. Mauvezin, B. Coq, S. Kieger, J. Catal. 202 (2001) 156.

[7] G. Delahay, M. Mauvezin, A. Guzman-Vargas, B. Coq, Catal. Commun. 3 (2002 385.

[8] F. Kapteijn, J. Rodriguez-Mirasol, J. A. Moulijn, Appl. Catal. B 9 (1196) 25.

[9] F. Kapteijn, G. Mul, G. Marban, J. Rodriguez-Mirasol, J. A. Moulijn in: J. W. Hightower, W. N. Delagass, E. Iglesia, A.T. Bell (Eds.), Proceedings of the 11th International Congress on Catalysis, Elsevier, Amsterdam, 1996, p. 641.

[10] B. Coq, M. Mauvezin, G. Delahay, J. B. Butet, S. Kieger, Appl. Catal. B 27 (2000) 193.

9

Influence of Ammonia Dosing

9.1 Introduction

The main challenge for the application of the SCR process in diesel vehicles was to improve the activity and selectivity over a wide temperature range (150 °C-700 °C). In case of vanadia based catalysts one of the major improvement was by the addition of NO_2 to the feed mixtures [1, 2]. As described in chapter 7, addition of NO_2 also caused an increase in DeNOx activity for zeolites. Apart from changing the inlet gas composition, DeNOx can be improved by changing the ammonia dosing strategy. Recently, Wallin et al. [3] studied the effects of a transient NH_3 supply on the selective catalytic reduction of NO_x over H-ZSM5 between 200 °C and 500 °C. They found that the activity for NO_x reduction was enhanced up to five times by pulsing NH_3 to the feed compared to continuous supply of NH_3. In order to check the ammonia dosing on Fe-ZSM5 catalysts, ammonia was dosed in different steps and pulse sequences.

9.2 Experimental

A fresh Fe-ZSM5 monolith catalyst with a volume of 7.7 cm^3 was used for both step and pulse experiments. Step experiments between 200 °C to 450 °C were carried out. The composition of the feed gas was adapted to a typical diesel exhaust gas, containing 10 % O_2 and 5 % H_2O with N_2 as balance. The concentration of NH_3 and NO were 1000 ppm whenever introduced. GHSV was 52,000 h^{-1}. The detection error for NO and NH_3 is about + 4 % at 1000 ppm.

In the case of pulse response measurements the concentration of NO_x was always kept constant at 500 ppm, but the NO:NO_2 ratio was varied. The total amount of ammonia dosed was in stoichiometric proportion to the amount of NO_x over each cycle. The concentration and duration of ammonia pulses are given in table 9.1.

Table 9.1 Concentration and duration of ammonia pulses (Average ammonia concentration was always 500 ppm).

Pulse Type	NH_3 Concentration [ppm]	NH_3 pulse Length [min]	Time without NH_3 [min]	Times Repeated
5/10	1500	5	10	2
5/5	1000	5	5	2
2/3	1250	2	3	5
5/1	600	5	1	5
1/1	1000	1	1	5
1/0.5	750	1	0.5	5
0.5/0.5	1000	0.5	0.5	5
0.5/0.25	750	0.5	0.25	5
0.25/0.25	1000	0.25	0.25	5

9.3 Results

9.3.1 Step response measurements

Figures 9.1 and 9.2 shows the inlet NO and NH_3 concentrations (constant for all temperatures). Figure 9.3 represents the outlet concentrations of NO, NO_2 and NH_3 at 450 °C. In the first 30 min (step 1), 1000 ppm of NO were dosed and a certain amount of NO_2 was formed, indicating that Fe-ZSM5 has the capability to oxidize NO to NO_2. The oxidizing capacity was increasing for higher temperatures.

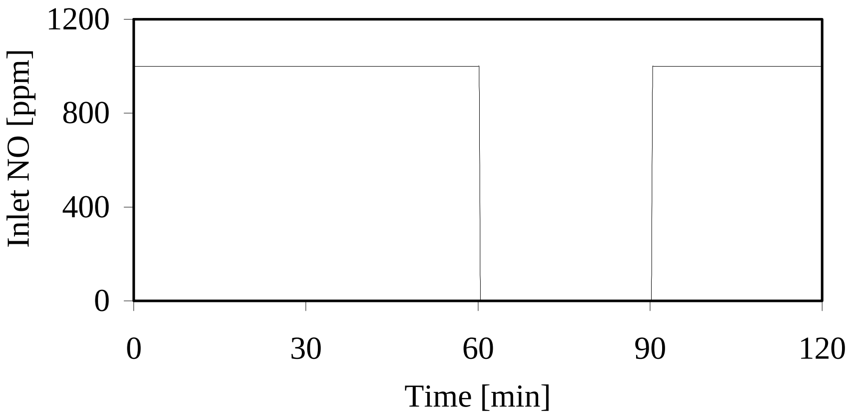

Figure 9.1 Inlet NO concentration vs. time.

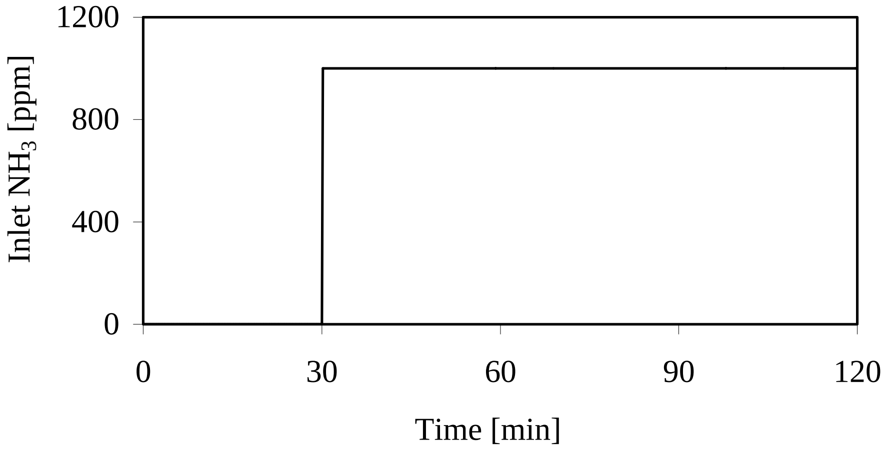

Figure 9.2 Inlet NH_3 concentration vs. time.

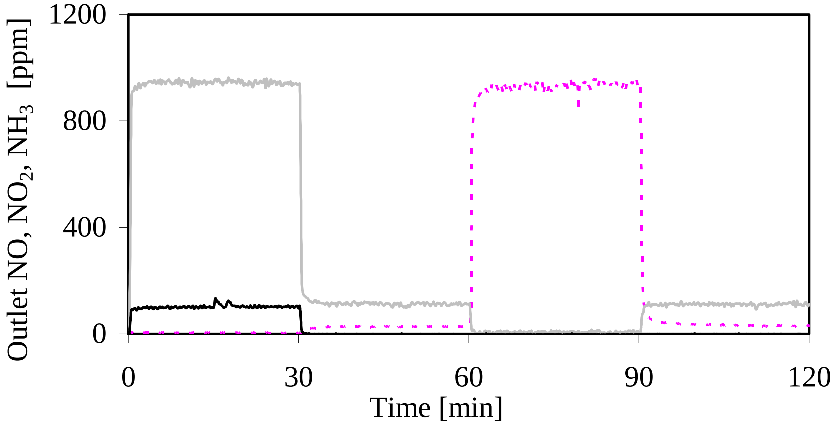

Figure 9.3 Outlet (—) NO, (▬) NO_2 and (--) NH_3 concentrations vs. time at 450 °C.

In the next 30 min (step 2), 1000 ppm of NH_3 were added to the catalyst, on which NO is preadsorbed. The outlet concentration of NO dropped with the start of the NH_3 dosage. A steady state NO_x conversion was observed after 5 min. After 60 min from the start of the experiment (step 3), NO was stopped and ammonia was dosed. The outlet NO concentration decreased and ammonia concentration increased and reached only 940 ppm, indicating that about 6 % of ammonia was oxidized. At 90 min (step 4), 1000 ppm of NO were added to the catalyst on which NH_3 is preadsorbed. As expected the outlet concentration of NO increased and the concentration of NH_3 decreased.

9.3.2 Pulse response measurements

From figure 9.4, it is seen that the inlet NO_x concentration was kept constant throughout the measurements, whereas ammonia was dosed according to the pulse types which are defined in table 9.1.

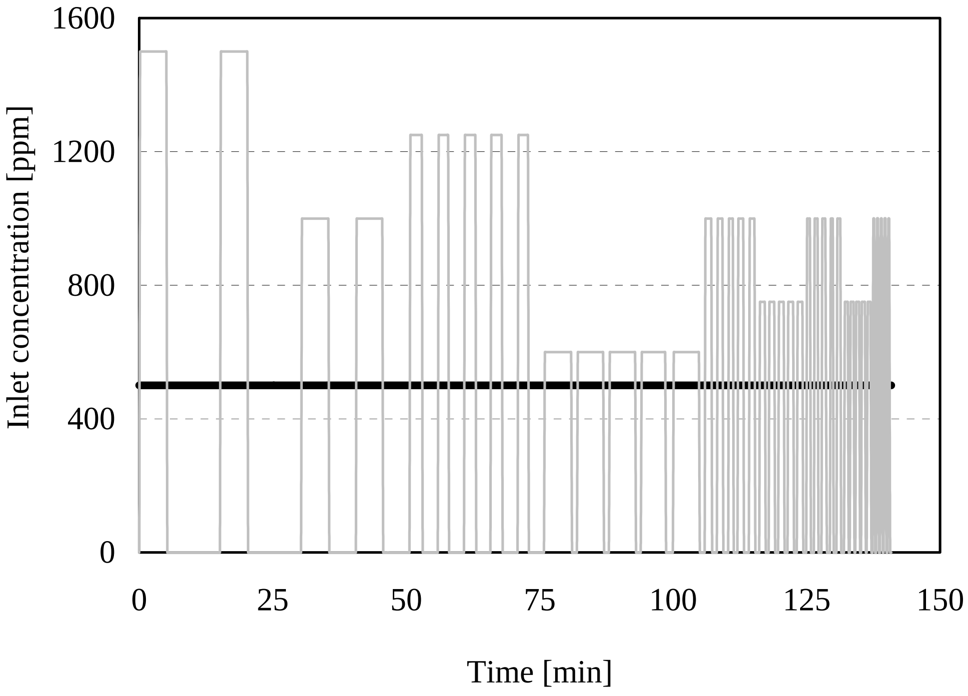

Figure 9.4 Inlet (▬) NH_3, (▬) NO_x concentrations vs. time.

9.3.2.1 100 % NO (NO_x = 500 ppm NO)

Figure 9.5 and Figure 9.6 show the system responses at 300 °C and 350 °C, when ammonia was dosed in the different pulse sequences. Table 9.2 and Table 9.3 summarize the average NO_x reduction and the average NH_3 slip for different pulse sequences and for the continuous supply of ammonia.

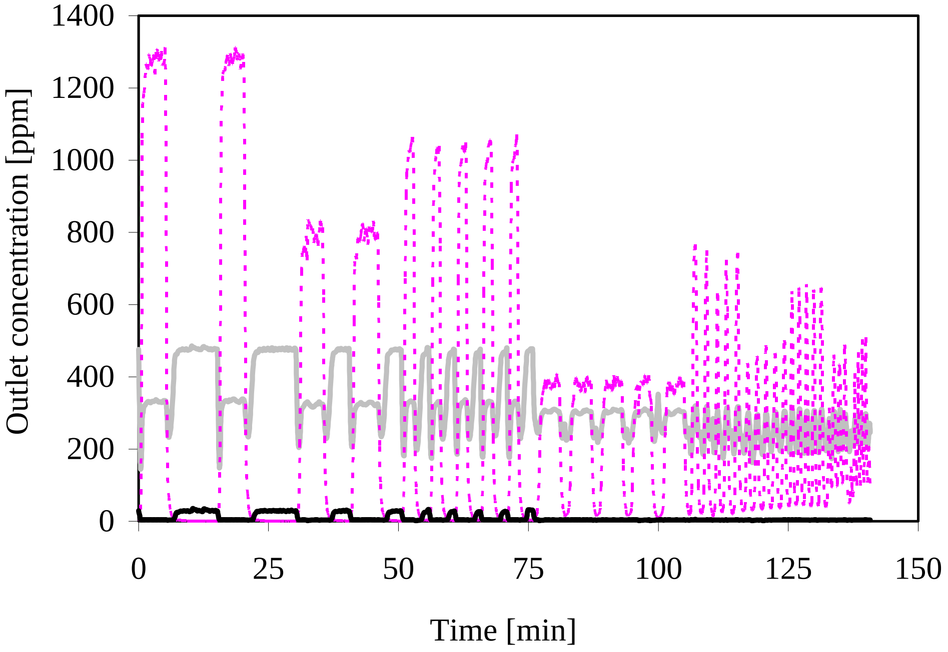

Figure 9.5 Outlet (—) NO, (—) NO_2 and (--) NH_3 concentrations vs. time at 300 °C.

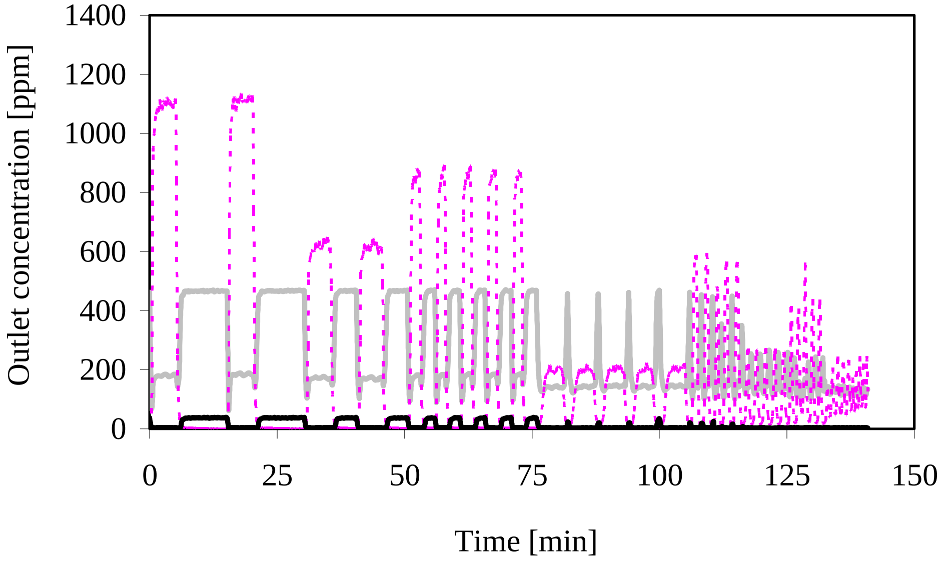

Figure 9.6 Outlet (▬) NO, (▬) NO_2 and (--) NH_3 concentrations vs. time at 350 °C.

Table 9.2 Average DeNOx (%) for 100 % NO.

Pulse Type	200 °C	250 °C	300 °C	350 °C	400 °C	450 °C
5/10	11	11	16	25	32	34
5/5	**13**	19	26	38	47	50
2/3	**12**	12	31	37	43	44
5/1	9	9	42	65	78	79
1/1	10	10	**49**	60	69	58
1/0.5	9	9	**51**	67	69	66
0.5/0.5	9	9	**56**	68	67	64
0.5/0.25	8	8	**51**	**73**	77	79
0.25/0.25	8	9	**49**	**74**	83	76
Continuous Supply	10	22	40	70	87	94

Table 9.3 Average NH_3 slip (ppm) for 100 % NO.

Pulse Type	200 °C	250 °C	300 °C	350 °C	400 °C	450 °C
5/10	443	433	402	351	325	315
5/5	**421**	421	376	282	237	230
2/3	**440**	440	346	305	276	276
5/1	446	446	254	134	91	91
1/1	471	471	241	194	229	203
1/0.5	417	417	**198**	99	104	114
0.5/0.5	488	488	**237**	163	152	177
0.5/0.25	456	456	**197**	**101**	77	104
0.25/0.25	478	476	**217**	121	83	125
Continuous Supply	390	340	235	80	35	30

With increasing temperature, the NO_x conversion was increased. At T $\geq$ 400 °C, continuous supply of ammonia resulted in better DeNOx and a reduced ammonia slip than pulsing of ammonia. The NO_x conversion improved for shorter pulses (e.g. 0.25/0.25) at intermediate temperatures and more pronounced at T = 300 °C. Longer pulses (e.g. 5/5) at T = 200 °C resulted in small increase DeNOx. At 300 °C and 350 °C, the average NH_3 slip was less for short pulses than for a continuous supply. N_2O could not be detected.

9.3.2.2 25 % NO_2 (NO_x = 375 ppm NO:125 ppm NO_2)

Figure 9.7 and Figure 9.8 show the system responses at 250 °C and 350 °C, when ammonia was dosed in the different pulse sequences. Table 9.4 and Table 9.5 summarize the average NO_x reduction and the average NH_3 slip for different pulse sequences and for the continuous supply of ammonia.

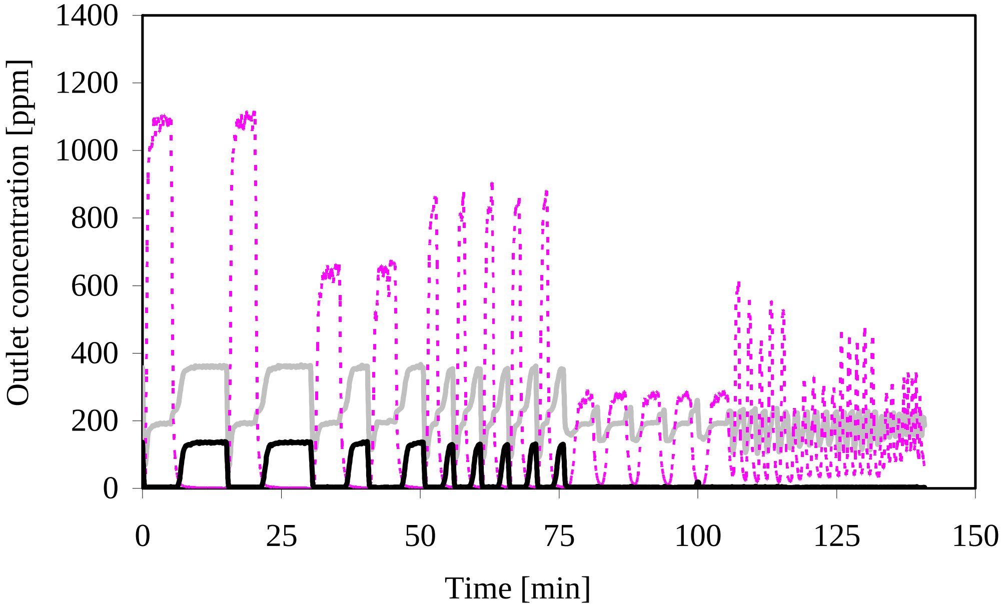

Figure 9.7 Outlet (—) NO, (━) NO$_2$ and (--) NH$_3$ concentrations vs. time at 250 °C.

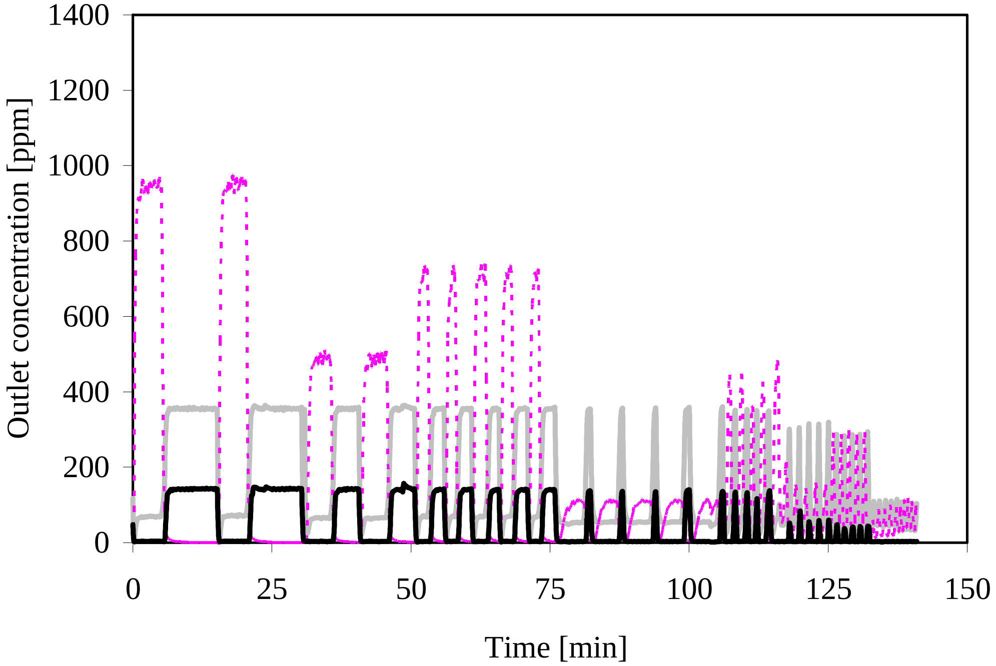

Figure 9.8 Outlet (—) NO, (━) NO$_2$ and (--) NH$_3$ concentrations vs. time at 350 °C.

Table 9.4 Average DeNOx (%) for 25% NO_2.

Pulse Type	150°C	250 °C	350 °C	450 °C
5/10	29	28	33	41
5/5	41	41	47	51
2/3	46	46	48	46
5/1	51	50	77	81
1/1	51	**63**	72	61
1/0.5	51	**64**	77	67
0.5/0.5	50	**64**	76	62
0.5/0.25	50	**64**	86	78
0.25/0.25	51	**63**	87	73
Continuous Supply	50	62	90	95

Table 9.5 Average NH_3 slip (ppm) for 25% NO_2.

Pulse Type	150°C	250 °C	350 °C	450 °C
5/10	335	330	309	318
5/5	276	271	210	202
2/3	250	262	262	248
5/1	170	163	67	53
1/1	192	192	161	166
1/0.5	196	**118**	63	88
0.5/0.5	185	175	99	157
0.5/0.25	241	141	40	83
0.25/0.25	249	161	61	118
Continuous Supply	150	120	22	13

At 250 °C, for pulse type 1/0.5, the NO_x conversion was slightly increased with less ammonia slip. Negligible amounts of NO_2 were detected at the catalyst outlet for pulses shorter than 5/1. N_2O was formed at all temperatures, but in negligible amounts (≈ average 5 ppm).

9.3.2.3 50 % NO_2 (NO_x = 250 ppm NO:250 ppm NO_2)

Figure 9.9 and Figure 9.10 show the pulse responses at 250 °C and 350 °C, when ammonia was dosed in the different pulse sequences as mentioned in table 9.1. Table 9.6, Table 9.7 and Table 9.8 summarize the average NO_x reduction, average NH_3 slip and average N_2O formation for different pulse sequences and for the continuous supply of ammonia.

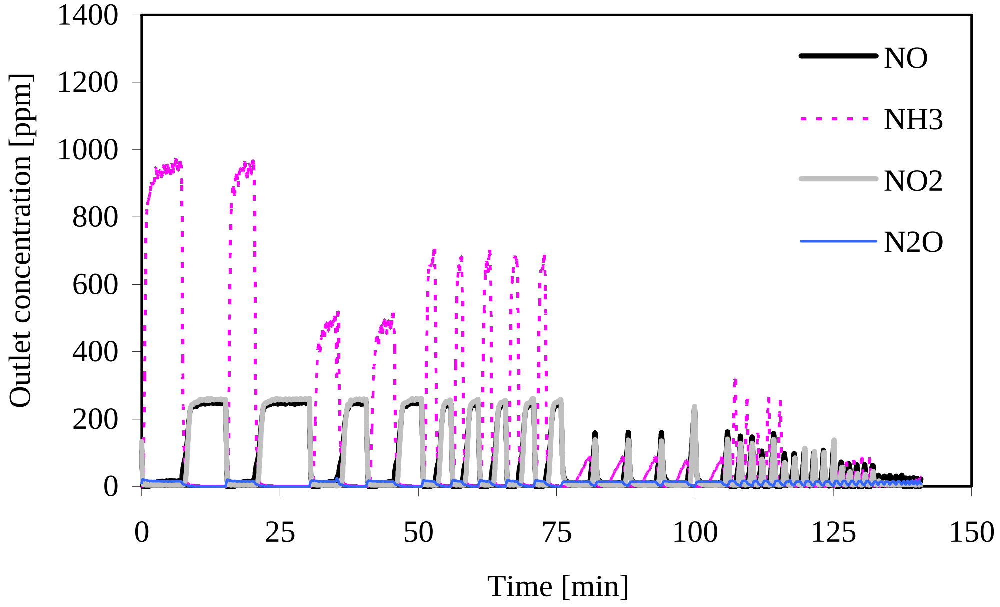

Figure 9.9 Outlet (—) NO_2, (▬) NO, (--) NH_3 and (—) N_2O concentrations vs. time at 250 °C.

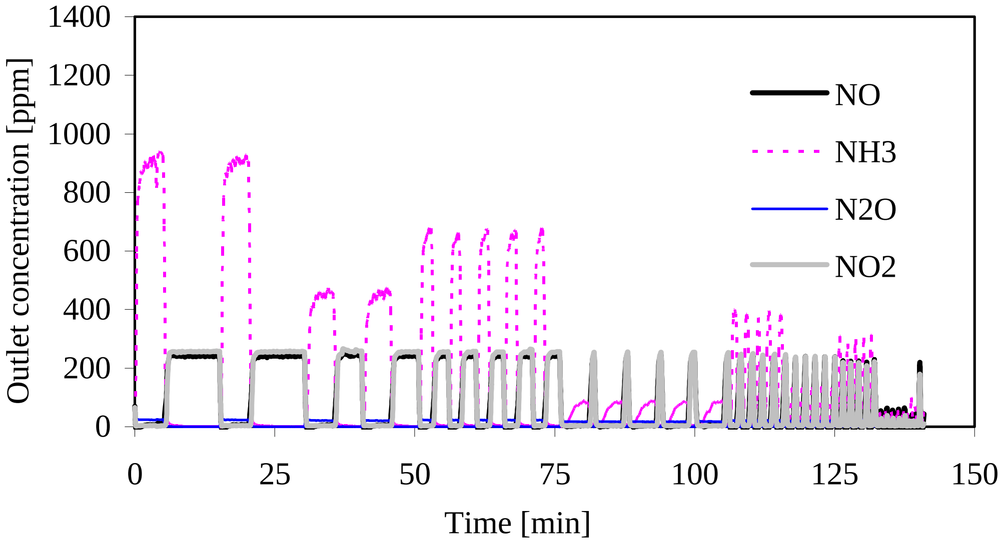

Figure 9.10 Outlet (—) NO$_2$, (▬) NO, (--) NH$_3$ and (—) N$_2$O concentrations vs. time at 350 °C.

Table 9.6 Average DeNOx (%) for 50% NO$_2$.

Pulse Type	150°C	250 °C	350 °C	450 °C
5/10	36	45	37	36
5/5	50	57	54	52
2/3	55	59	51	45
5/1	54	90	86	84
1/1	41	88	73	62
1/0.5	38	89	80	69
0.5/0.5	37	92	80	63
0.5/0.25	35	**96**	94	81
0.25/0.25	33	**97**	91	74
Continuous Supply	80	94	95	95

Table 9.7 Average NH_3 slip (ppm) for 50% NO_2.

Pulse Type	150°C	250 °C	350 °C	450 °C
5/10	304	350	294	227
5/5	227	196	204	197
2/3	218	204	236	236
5/1	201	26	44	48
1/1	300	65	138	180
1/0.5	234	4	43	85
0.5/0.5	302	21	97	63
0.5/0.25	312	**3**	20	81
0.25/0.25	331	11	26	74
Continuous Supply	13	1	1	1

Table 9.8 Average N_2O formation (ppm) for 50% NO_2.

Pulse Type	150°C	250 °C	350 °C	450 °C
5/10	2	7	9	3
5/5	2	8	11	3
2/3	2	8	10	3
5/1	2	12	14	6
1/1	2	10	13	4
1/0.5	2	10	13	5
0.5/0.5	1	10	13	5
0.5/0.25	1	**11**	15	7
0.25/0.25	1	**11**	13	7
Continuous Supply	5	16	16	9

In the case of 50 % NO_2 in the feed, for T = 250 °C, shorter pulses (e.g. 0.5/0.25) resulted in a better DeNOx activity with a reduction in NH_3 slip and N_2O formation. But at T = 150 °C, a continuous supply of ammonia yielded a better DeNOx at a very low ammonia slip. The production of N_2O was considerably reduced for both longer and shorter pulses at all temperatures. At 150 °C, only negligible amounts of N_2O were produced.

9.3.2.4 75 % NO_2 (NO_x = 125 ppm NO:375 ppm NO_2)

Figure 9.11 and Figure 9.12 show the pulse responses at 250 °C and 350 °C, when ammonia was dosed in the different pulse sequences as mentioned in table 9.1. Table 9.9, Table 9.10 and Table 9.11 summarize the average NO_x reduction, average NH_3 slip and average N_2O formation for different pulse sequences and for the continuous supply of ammonia.

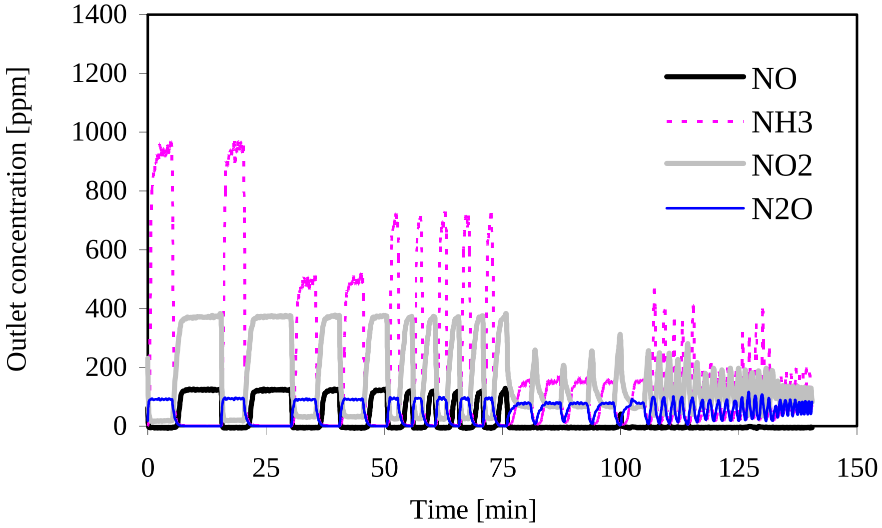

Figure 9.11 Outlet (▬) NO_2, (▬) NO, (--) NH_3 and (—) N_2O concentrations vs. time at 250 °C.

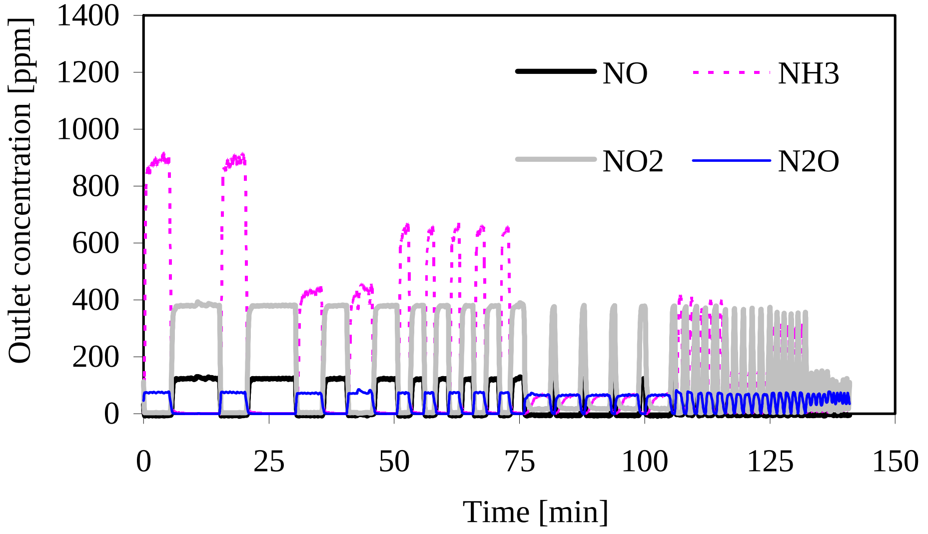

Figure 9.12 Outlet (▬) NO_2, (▬) NO, (--) NH_3 and (—) N_2O concentrations vs. time at 350 °C.

Table 9.9 Average DeNOx (%) for 75% NO_2.

Pulse Type	250 °C	350 °C	450 °C
5/10	39	37	35
5/5	55	54	51
2/3	57	50	46
5/1	79	82	83
1/1	76	70	60
1/0.5	77	76	67
0.5/0.5	79	76	62
0.5/0.25	80	88	78
0.25/0.25	**81**	**88**	71
Continuous Supply	80	90	90

Table 9.10 Average NH_3 slip (ppm) for 75% NO_2.

Pulse Type	250 °C	350 °C	450 °C
5/10	281	290	284
5/5	209	197	174
2/3	221	234	219
5/1	90	40	10
1/1	115	141	153
1/0.5	72	50	61
0.5/0.5	112	104	136
0.5/0.25	**84**	**29**	54
0.25/0.25	105	39	93
Continuous Supply	90	38	2

Table 9.11 Average N_2O formation (ppm) for 75% NO_2.

Pulse Type	250 °C	350 °C	450 °C
5/10	32	26	7
5/5	46	38	11
2/3	43	36	9
5/1	61	53	25
1/1	52	44	13
1/0.5	53	46	17
0.5/0.5	59	46	15
0.5/0.25	**60**	55	22
0.25/0.25	63	53	18
Continuous Supply	60	50	25

With 75 % of NO_2 in the feed, at temperatures 250 °C and 350 °C, shorter pulses yielded the same NO_x conversion as for the continuous supply but with less NH_3 slip and nearly the same N_2O formation. No N_2O was formed at 150 °C.

9.4 Discussion

The influence of ammonia pulsing on Fe-ZSM5 was investigated with pure NO and with different NO_x/NO_2 ratios in feed. The NO_x conversions over Fe-ZSM5 were considerably improved at intermediate temperatures by pulsing of ammonia, when pure NO was in the feed. From chapter 6, it is known that ammonia inhibition takes place at intermediate and lower temperatures. The inhibition effect might be due to competitive adsorption between and NO and NH_3 [4]. Due to this competitive adsorption, the ammonia might block the active sites needed for the oxidation of NO to NO_2 and thereby NO_x conversion is reduced. Thus stopping the ammonia dosage in regular intervals free the catalyst surface and enables higher NO oxidation as well as SCR rates. The optimum pulse frequencies depend on the temperature. The higher the temperature, the shorter the optimum dosing frequency, because the reactants on the surface are mush faster consumed than at lower temperatures. One important aspect of our observation is that no N_2O was produced during pulsing and continuous supply of ammonia, which is in opposite to H-ZSM5 as observed by Wallin et al. [3].

9.5 Conclusions

The influence of ammonia supply was studied by step response experiments between 200 and 450 °C. N_2O formation was not noticed at all temperatures. Pulsed ammonia supply yielded better NO_x conversions than continuous supply of ammonia. In general, with NO = 100 % in the feed short pulses of ammonia were advantageous for NO_x conversion at 300 °C and 350 °C. N_2O formation was not observed with pure NO in feed. For NO_2/NO_x ratio $\geq$ 50 %, the continuous supply of ammonia shows the best results. With increased NO_2 concentrations in the feed more N_2O was produced at intermediate and higher temperatures. For different $NO:NO_2$ ratios, short pulses i.e. where pulse time with ammonia and pulse time without ammonia are less, there is a considerable increase in DeNOx with more or less the same amount of NH_3 slip and N_2O formation.

9.6 References

[1] M. Koebel, M. Elsener, G. Madia, Ind. Eng. Chem. Res. 40 (2001) 52.

[2] M. Koebel, G. Madia, Catal. Today 73 (2002) 239.

[3] M. Wallin, C. J. Karlsson, M. Skoglundh, A. Palmqvist, J. Catal. 218 (2003) 354.

[4] S. A. Stevenson, J. C. Vartuli, C. F. Brooks, J. Catal. 190 (2000) 228.

10

Stability of Fe-ZSM5 catalyst

10.1 Introduction

Stability under real-world conditions is an important parameter for the assessment of the suitability of a catalyst. For Fe-ZSM5 to be considered as potential alternative catalyst for SCR, the stability towards thermal, hydrothermal and SO_2 treatment are a prerequisite. Therefore, Long et al. [1] investigated the durability of Fe-ZSM5 powder catalysts, aged in SO_2 and H_2O for 60 h at 350 °C. They observed a 20 % loss in NO conversion. Feng et al. [2] studied the durability of a Fe-ZSM5 powder catalyst for a period of 2500 h at 500 °C. They observed a minimal loss in NO activity in a simulated exhaust gas stream.

Since ZSM5 are stable at T > 600 °C, in our work, extreme ageing conditions were applied in order to determine the thermal and hydrothermal stability catalysts. Apart from this SO_2 resistance was also checked.

10.2 Experimental

The thermal and hydrothermal stability of the Fe-ZSM5 catalyst coated on cordierite was tested by ageing at 650 °C in the presence of 10 % oxygen in nitrogen for 50 h (denoted as “dry aged”) and by ageing at 650 °C in 10 % water and 10 % oxygen in nitrogen for 50 h (denoted as “wet aged”), respectively. The catalyst volume of both the dry aged and wet aged Fe-ZSM5 monolith was 7.7 cm^3. For SO_2 treatment, an Fe-ZSM5 monolith with a volume of 7.3 cm^3 was used and this catalyst was treated for 50 h at 500 °C with 100 ppm SO_2 in 5 % water and 10 % oxygen in nitrogen (denoted as “SO_2 treated”).

For tests of the standard SCR reaction, the composition of diesel exhaust gas was approximated by a model feed gas containing 10 % O_2, 5 % H_2O, 1000 ppm of NO and balance N_2. NH_3 was added in the range 100-2000 ppm. The catalysts were also tested with a mixture of NO and NO_2 in the feed: 10 % O_2, 5 % H_2O, 500 ppm of NO, 500 ppm NO_2 and balance N_2. In this case NH_3 was added in the range 100-2000 ppm. The gas hourly space velocity was 52,000 h^{-1}.

The catalysts were characterized by XRD, low temperature N_2 adsorption, H_2-TPR, NH_3-TPD and ^{27}Al MAS NMR. The catalytic testing and characterization results of the aged catalysts are compared to the results of a fresh catalyst (denoted as “fresh”).

10.3 Results

10.3.1 Catalytic Investigations

10.3.1.1 SCR with NO

Figure 10.1 compares the NO_x conversion at 10 ppm ammonia slip vs. reaction temperature of the aged catalysts with the results of the fresh catalyst. The coated Fe-ZSM5 catalyst was stable under dry ageing conditions. Only a small loss of NO_x conversion at 10 ppm NH_3 slip is discernible after dry aging over the entire temperature range. However, when the catalyst was aged in the presence of water a distinct loss in NO_x conversion was observed, which increases with temperature. At the same time, by treating the catalyst with SO_2, there was a small increase in DeNOx, which is more clearly seen at T > 450 °C.

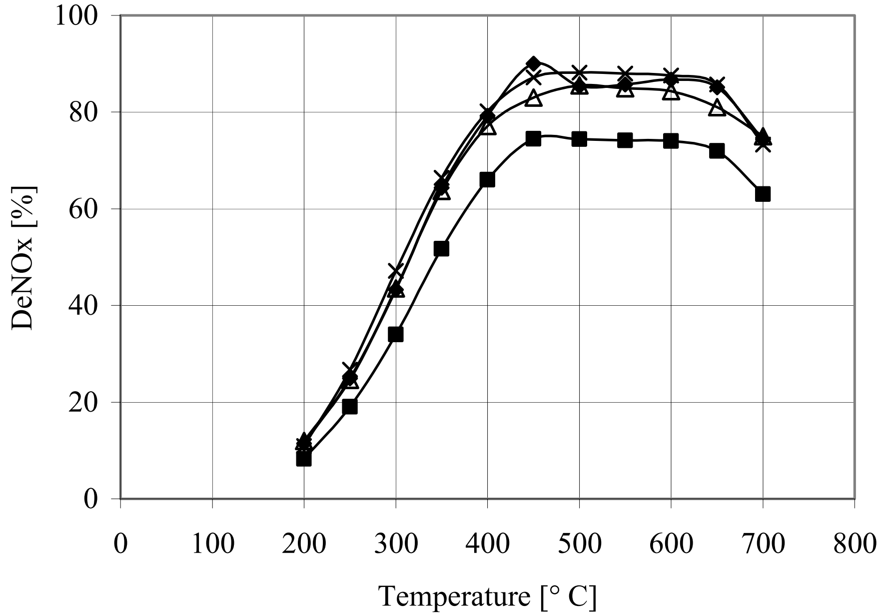

Figure 10.1 DeNOx at 10 ppm NH_3 slip for the (♦) fresh, (Δ) dry aged (■) wet aged and (x) SO_2 treated Fe-ZSM5 monolith catalysts vs. temperature.

Figure 10.2 shows the maximum DeNOx vs. temperature. The picture partly changes, where the DeNOx is virtually the same above 500 °C. Only at lower temperatures the wet aged Fe-ZSM5 exhibited a 5-15 % loss in DeNOx. The aged catalysts exhibited the same inhibition of the SCR reaction by ammonia as observed for the fresh catalyst and also no N_2O was formed at any temperature. The loss in NO_x conversion for the wet aged catalyst must be due to the influence of water during ageing. On the other hand, for the SO_2 treated catalyst, the small increase in DeNOx might be due to an increase in surface acidity of the catalyst sample by the sulphur treatment. Long et al. [3] also observed similar increase in DeNOx after sulphur treatment and attributed the increase in NO_x conversion to increase in surface acidity.

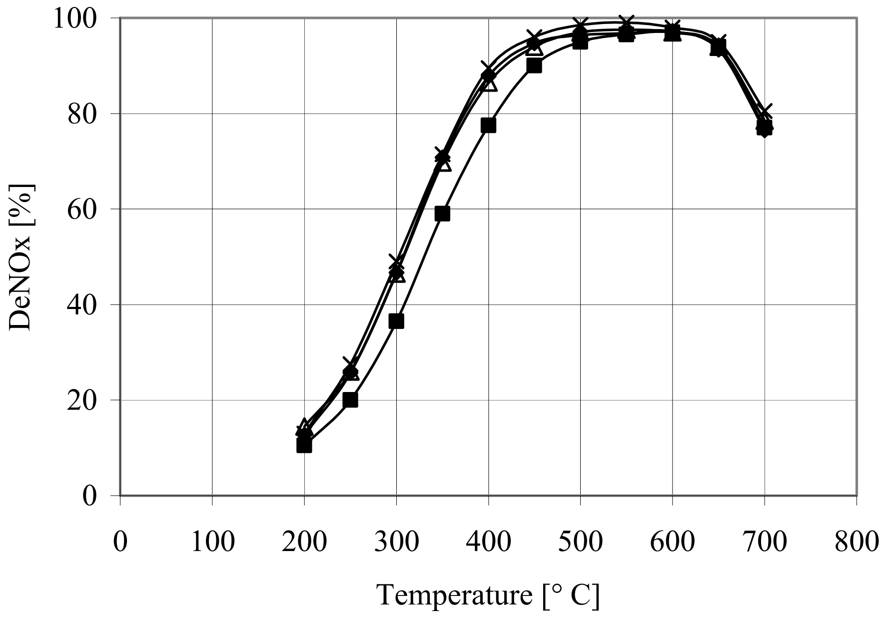

Figure 10.2 Maximum DeNOx for the (♦) fresh, (Δ) dry aged (■) wet aged and (x) SO_2 treated Fe-ZSM5 monolith catalysts vs. temperature.

10.3.1.2 SCR with NO-NO_2

Figure 10.3 shows the NO_x conversion at 10 ppm NH_3 slip for a feed containing 50 % NO_2 (500 ppm NO:500 ppm NO_2). As expected from chapter 7, DeNOx tremendously increased for both fresh and aged catalyst. The fresh and the dry aged Fe-ZSM5 catalyst had nearly the same conversion over the entire temperature range, but there was a loss in DeNOx for the wet aged catalyst. SO_2 treated Fe-ZSM5 had higher a DeNOx then the fresh catalyst till $T \leq 350$ °C.

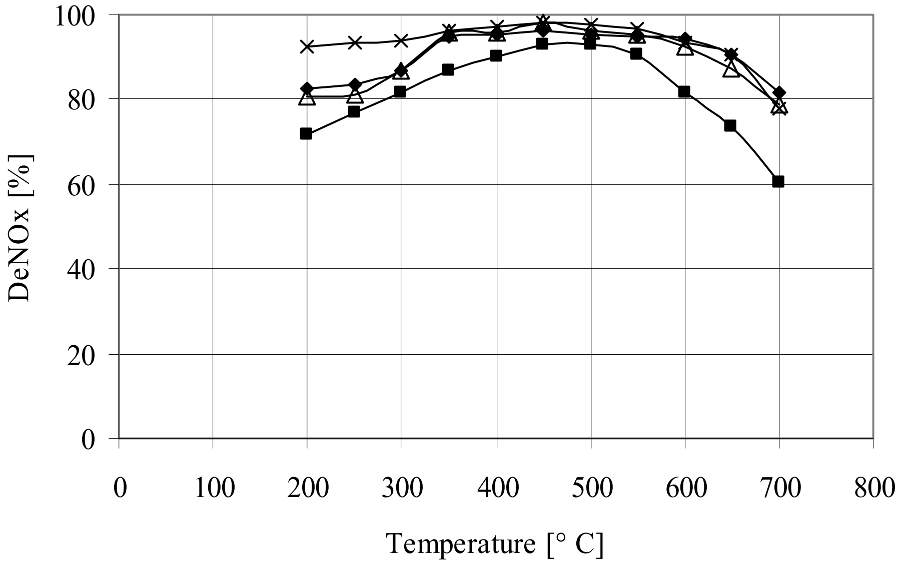

Figure 10.3 DeNOx at 10 ppm NH_3 slip for the (♦) fresh, (Δ) dry aged (■) wet aged and (x) SO_2 treated Fe-ZSM5 monolith catalysts vs. temperature (NO_x =50 % NO_2).

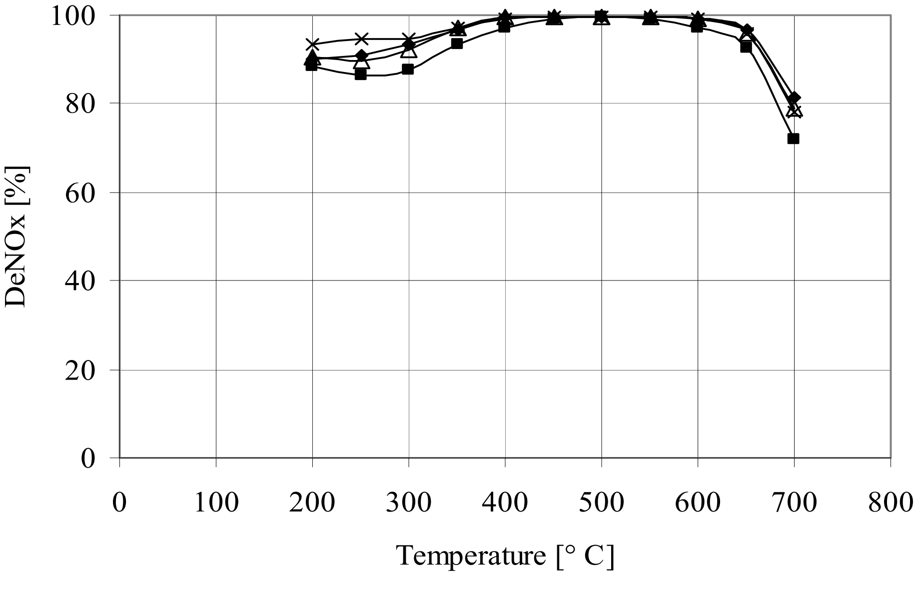

Figure 10.4 DeNOx for the (♦) fresh, (Δ) dry aged (■) wet aged and (x) SO_2 treated Fe-ZSM5 monolith catalysts vs. temperature (NO_x =50 % NO_2).

The scenario remained the same, when the maximum DeNOx is plotted against temperature (figure 10.4). The SO_2 treated catalyst exhibited the best performance for T ≤ 300 °C. The loss in DeNOx for the wet aged catalyst was small (≈4 %) for T ≤ 350 °C and beyond 350 °C all the catalysts exhibited nearly the same NO_x conversions.

In figure 10.5, the N_2O production at 10 ppm NH_3 slip is shown.

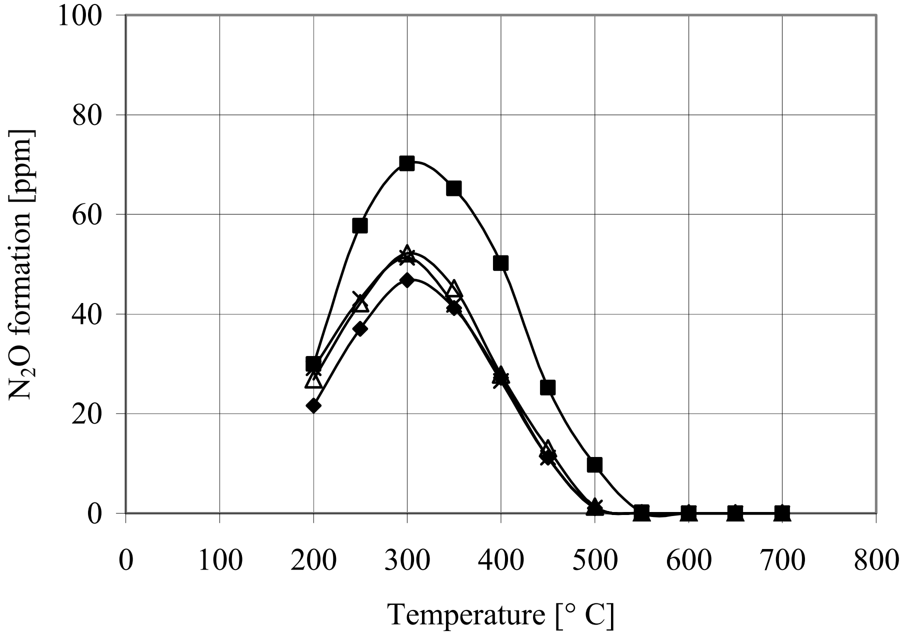

Figure 10.5 N_2O formation at 10 ppm NH_3 slip for the (♦) fresh, (Δ) dry aged (■) wet aged and (x) SO_2 treated Fe-ZSM5 monolith catalysts vs. temperature (NO_x =50 % NO_2).

All the catalysts exhibited the maximum N_2O formation at 300 °C and no N_2O at T ≥ 550 °C. The wet aged Fe-ZSM5 showed a much higher N_2O formation than the other catalysts. Around 70 ppm N_2O was formed at 300 °C. Another noticeable feature is that the dry aged and SO_2 treated catalyst exhibited nearly the same N_2O production over the entire temperature range, though the DeNOx was higher for SO_2 treated catalysts at T ≤ 350 °C (figures 10.3 & 10.4). The fresh catalyst had less N_2O production than the aged catalysts.

10.3.2 Characterization results

10.3.2.1 X-ray diffraction measurements

Figure 10.6 shows the XRD patterns of fresh and aged Fe-ZSM5 samples. X-ray diffractograms did not show any change in the diffraction peaks. The XRD patterns of the aged Fe-ZSM5 samples remained identical compared to the fresh Fe-ZSM5 sample. This indicates that the ZSM5 framework is not damaged by ageing, i.e. the zeolite structure was maintained even after relatively harsh conditions.

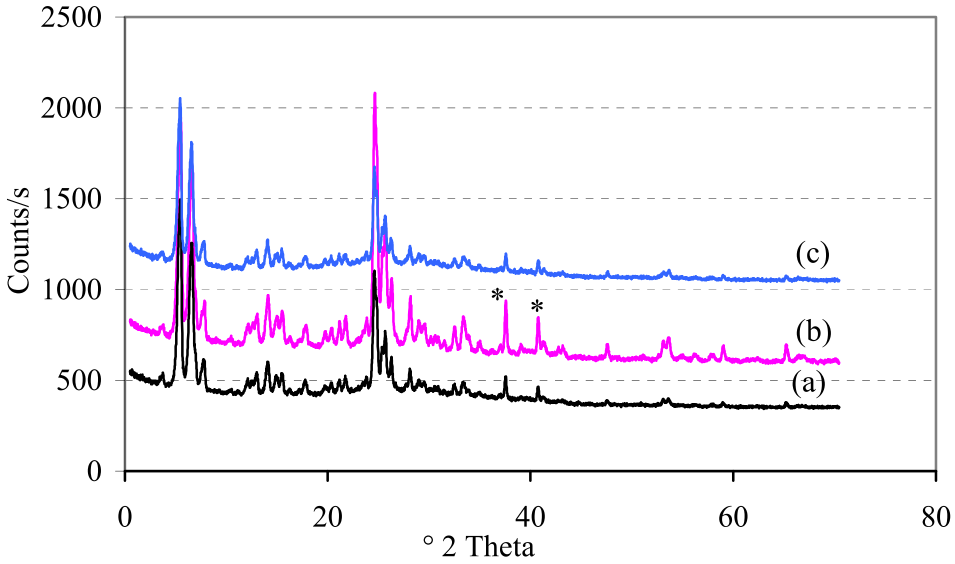

Figure 10.6 XRD patterns for (a) fresh Fe-ZSM5, (b) wet aged Fe-ZSM5 and (c) dry aged Fe-ZSM5 samples.

Low intensity diffraction lines at 37.65° and 40.85° (denoted by * in figure 10.6) were detected for the fresh and dry aged samples. These intensities were much higher for the wet aged samples. These peaks are attributed to traces of hematite (Fe_2O_3) particles.

10.3.2.2 Low temperature N_2 adsorption

The results are tabulated in table 10.1.

Table 10.1 N_2 Adsorption results

Sample	BET surface area (cm^3/g)	Micropore volume (m^2/g)
Fresh	301	0.089
Dry aged	297	0.088
Wet aged	297	0.079

From table 10.1, it is observed that the ageing procedure had a small influence on BET surface area and the micropore volume. There was small decrease in BET and micropore volume after ageing. But in general the catalyst structure is still intact.

10.3.2.3 H_2-TPR results

Figure 10.7 shows the H_2-TPR pattern of fresh and aged Fe-ZSM5 samples. For all the samples, reduction proceeded in two stages. The first reduction peak (peak 1) around 480 ° C corresponds to the reduction Fe^{3+} to Fe^{2+}. The second peak (peak 2) around 550 °C corresponds to the reduction of Fe^{2+} to Fe^0. Table 10.2 reports the H_2/Fe ratio of fresh and aged Fe-ZSM5 samples.

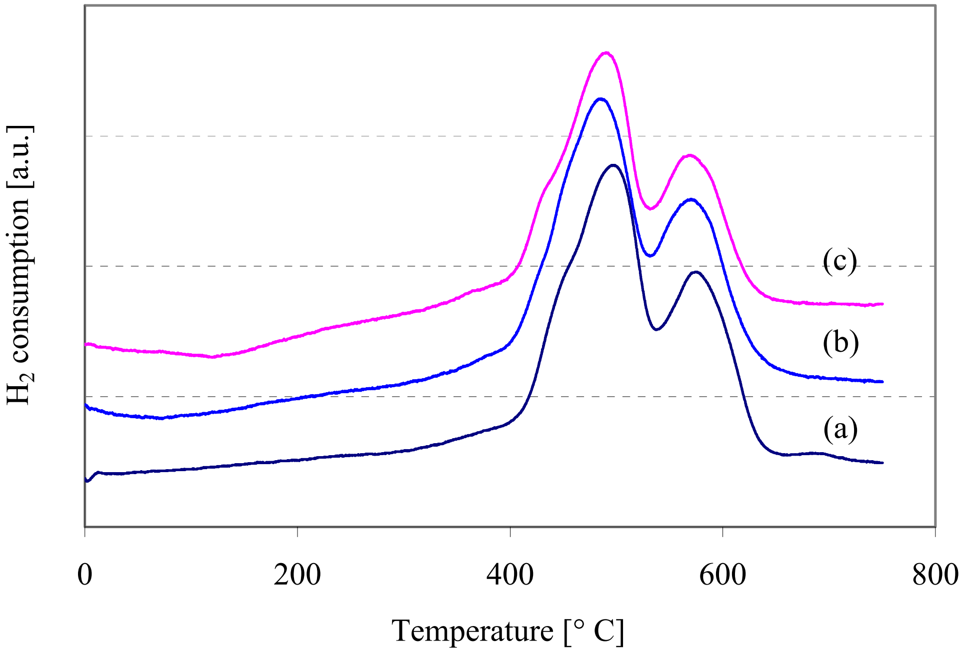

Figure 10.7 H_2-TPR profiles (a) fresh Fe-ZSM5, (b) wet aged Fe-ZSM5 and (c) dry aged Fe-ZSM5.

Table 10.2 H_2-TPR results

Sample	H_2/Fe ratio	
	Peak 1	Peak 2
Fresh	0.44	0.12
Dry aged	0.45	0.11
Wet aged	0.43	0.18

From figure 10.7 and from table 10.2, it can be seen that integration of peak 1 yielded an H_2/Fe molar ratio of ≈ 0.45, which is close to the theoretical value of 0.5, required for the reduction of Fe^{3+} to Fe^{2+}. Integration of peak 2 of the fresh and dry aged samples yielded an H_2/Fe molar ratio of ≈ 0.11 and this small consumption of H_2 indicates that most Fe^{2+} is hardly reducible in the Fe-ZSM5 [4], and that only a small fraction exists in a easily reducible form. It is also observed that the H_2/Fe ratio for peak 2 of the wet aged catalyst is considerably increased compared to the other samples, which means that the easily reducible Fe^{2+} fraction is increased.

10.3.2.4 NH_3-TPD results

Temperature programmed desorption experiments with ammonia were performed with the fresh and aged catalysts as shown in figure 10.8.

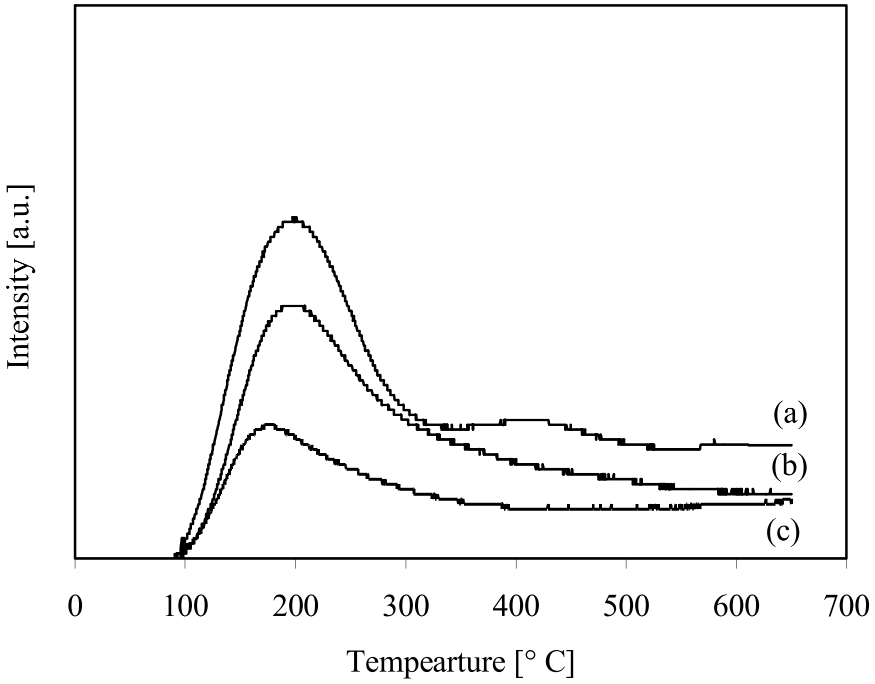

Figure 10.8 NH_3-TPD profiles of the (a) fresh (b) dry aged and (c) wet aged Fe-ZSM5.

For the fresh Fe-ZSM5 sample, two well resolved peaks are centered at about 220 °C and 425 °C. The low temperature peak shifted from about 220 °C to about 200 °C for the wet aged catalyst. The high temperature peak is always associated with ammonia adsorbed on acidic hydroxide groups (Brønsted acid sites) [5]. The low temperature peak might be due to physisorbed ammonia [6] or ammonia from a non-zeolitic impurity [7]. The decrease in the high temperature peak for the aged catalysts is attributed to the dealumination effect, whereby framework alumina moves out of the zeolite lattice, due to the extensive ageing procedure.

10.3.2.5 ^{27}Al MAS NMR results

A clearer picture of the coordination of the aluminium atoms in the structure of fresh and aged Fe-ZSM5 was obtained by ^{27}Al MAS NMR spectroscopy (figure 10.9).

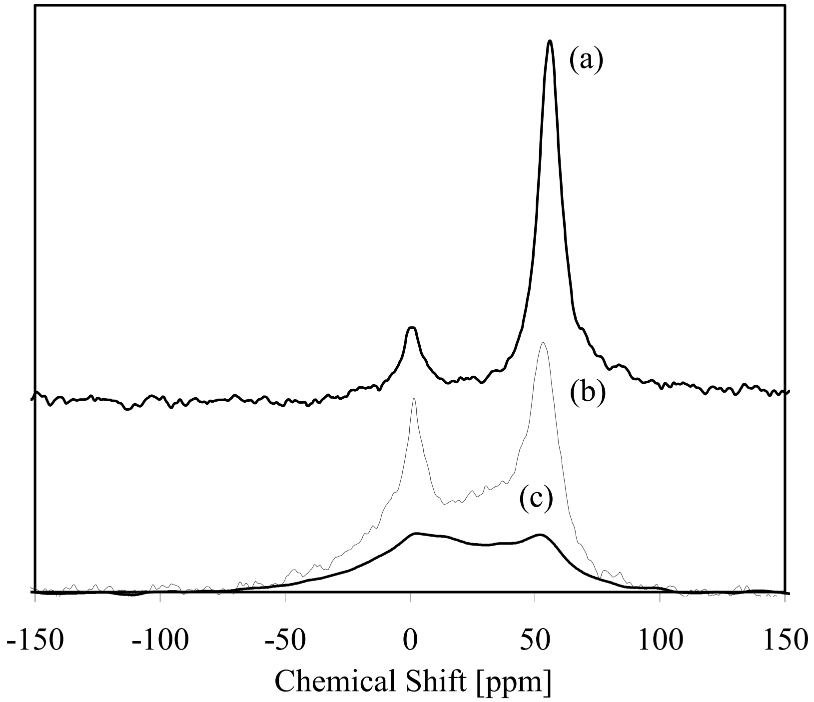

Figure 10.9 ^{27}Al MAS NMR spectra of the (a) fresh (b) dry aged and (c) wet aged Fe-ZSM5

As mentioned in chapter 5, the signals at 55-60 ppm in the spectrum correspond to tetrahedrally coordinated alumina $Al(OSiO)_4$ in the framework lattice [8]. The signal at 0 ppm is created by dealumination and it corresponds to the aluminium in octahedral AlO_6 groups [9]. A broad signal in the range of 30-50 ppm is also often observed. However, the assignment of this signal is still under debate: some authors attributed this resonance line to penta coordinated aluminium [10, 11], whereas others assigned it to tetrahedral extra-framework aluminium species [12]. It has to be noted that the signal at 55 ppm which is assigned to Brønsted acid sites is decreased after dry ageing and it became even broader if the catalyst was wet aged. This is in agreement with results of Marturano et al. [13] who suggested that dealumination of the zeolite occur under ageing conditions.

Apart from the dealumination the broadening of the resonance signals at 0 ppm might also be due to dislodgement of framework iron, which dampens the Al signal because of its paramagnetic effect [14].

10.4 Discussion

The thermal and hydrothermal stability of Fe-ZSM5 monolith catalyst was investigated. After harsh treatments, Fe-ZSM5 was thermally stable at all temperatures and nearly the same NO_x conversion was observed, whereas when the catalyst underwent ageing in the presence of water (hydrothermal), 5-15 % loss in DeNOx was observed. The absence of the N_2O formation under standard SCR conditions is a big advancement of Fe-ZSM5. However, by the addition of NO_2 to the feed, more N_2O was produced apart from the increase in DeNOx. The wet aged catalyst produced the maximum N_2O when compared to the other catalysts. The increase in DeNOx for sulphur treated catalyst is attributed to increase in surface acidity on the zeolite sample [3]. The catalyst structure remained intact even after ageing the catalyst under thermal and hydrothermal conditions. Ageing under water caused the formation Fe_2O_3 particles. The nitrogen adsorption experiments evidenced a decrease of the pore volume for the wet aged catalyst, indicating that some of the pores are blocked, probably by the iron oxide particles detected by XRD.

However, part of the particles might also be present on the outer surface of the zeolite crystals, not influencing the accessibility to the pores. The NH_3-TPD results clearly show the lowering of the Brønsted acidity by the ageing process. The decrease of the high temperature peak is likely due to the lowering of the amount of Brønsted sites by dealumination. The acidity is in the order fresh > dry aged > wet aged Fe-ZSM5. Further Al NMR results confirm the dealumination due to the thermal and hydrothermal treatment of the catalyst.

10.5 Conclusions

Fe-ZSM5 is a very thermally stable catalyst. No loss in DeNOx was observed. Under hydrothermal conditions a minimal loss (5-15 %) in DeNOx was observed, but since loss in DeNOx was not that drastic, it is reasonable to regard Fe-ZSM5 as both thermally and hydro thermally stable under stand SCR conditions. The same cannot be stated for fast SCR conditions, since the production of N_2O is relatively high (70 ppm at 350 °C) for wet aged catalysts. Fe-ZSM5 is also a very sulphur resistant - even increase in DeNOx was observed. The reduction of Brønsted acid sites due to ageing clearly causes a change of the surface acidity and also of the ammonia storage capacity.

10.7 References

[1] R. Q. Long, R. T. Yang, J. Am. Chem. Soc. 121 (1999) 5595.

[2] X. Feng, W. K. Hall, J. Catal. 166 (1995) 368.

[3] R. Q. Long, R. T. Yang, J. Catal. 186 (1999) 254.

[4] R. Q. Long, R. T. Yang, J. Catal. 194 (2000) 80.

[5] C. V. Hidalgo, H. Iton, T. Hattori, M. Niwa, Y. Murakami, J. Catal. 85 (1984) 362.

[6] N. Y. Topsøe, K. Pedersen, E. G. Derouane, J. Catal. 70 (1981) 41.

[7] K. Chao, B. Chiou, C. Cho, S. Jeng, Zeolites 4 (1984) 2.

[8] G. Engelhardt, D. Michel, High- Resolution Solid State NMR of Silicates and Zeolites, Wiley, New York, 1987.

[9] J. A. van Bokhoven, D. C. Koningsberger, P. Kunkeler, H. van Bekkum, A. P. M. Kentgens, J. AM. Chem. Soc. 122 (2000) 12842.

[10] P. B. Bodart, J. B. Nagy, G. Debras, Z. Gabelica, P.A. Jacobs, J. Phys. Chem. 90 (1986) 5183.

[11] J. L. Motz, H. Heinichen, W. F. Hölderich, J. Mol. Catal. A. Chem. 136 (1998) 175.

[12] J. Sanz, V. Fornés, A. Corma, J. Chem. Soc., Faraday Trans. 84 (1988) 3113.

[13] P. Marturano, L. Drozdová, A. Kogelbauer, R. Prins, J. Catal. 192 (2000) 368.

[14] J. P. Ramirez, J. C. Groen, A. Brückner, M. S. Kumar, U. Bentrup, M. N. Debbagh, L.A. Villaescusa, J. Catal. 232 (2005) 318.

11

Ammonia Storage Capacity on Fe-ZSM5

11.1 Introduction

Surface acidity is a vital property for SCR catalysts. The amount of ammonia which is adsorbed is determined by the surface acidity and the temperatures [1]. The higher the acidity and the lower the temperature, the higher the amount of ammonia stored on the catalyst. A variety of ammonia species are often observed on the catalyst surface [2]. Many researchers agree that strongly bound ammonia is active for the SCR reaction and the ammonia is adsorbed on both Lewis and Brønsted acid sites [3-5]. Apart from the investigation of Kleemann et al. [1], who studied in detail the storage of ammonia on vanadia based monolithic catalyst, not much has been reported on the ammonia storage capacity of Fe-ZSM5. In this work the ammonia adsorption capacity of the fresh and aged Fe-ZSM5 monolith catalysts was measured.

11.2 Experimental

The fresh and the aged catalyst (dry & wet) used for the determination of the ammonia storage capacity is the same which was used in the catalytic tests (details in chapter 6 and 10). The experimental set-up was the same as for the catalytic test. The ammonia adsorption capacities of the fresh, the dry aged and the wet aged monolith catalysts were measured at six different temperatures between 200 and 450 °C by two different methods. a) Thermal desorption: 1000 ppm ammonia was adsorbed on the fresh Fe-ZSM5 monolith catalyst at a fixed temperature in 10 % O_2, 5 % H_2O and balance N_2. The GHSV was maintained at 52,000 h^{-1}. In the desorption procedure, part of the ammonia was removed by purging the sample at the adsorption temperature with pure N_2, followed by increasing the temperature up to 450 °C in order to complete the ammonia desorption.

b) Combination of physical desorption and reaction of pre-adsorbed ammonia by NO according to the method of Kleemann et al. [1]: first, ammonia was adsorbed using a nitrogen gas flow containing 10 % O_2, 5 % H_2O, and 1000 ppm of NH_3, at a fixed temperature until this concentration was also reached at the catalyst outlet. Subsequently, the chemically accessible ammonia was removed by stopping the ammonia dosage and simultaneously dosing 10 % O_2, 5 % H_2O, and 1000 ppm of NO at the same temperature until the NO consumption ceased. The physically desorbed ammonia was measured in parallel. Oxygen and water were always added in order to obtain ammonia storage capacities, being representative for diesel exhaust gas conditions.

11.3 Results & Discussion

First, the ammonia storage capacity was measured in simple thermal desorption experiments. As expected, the ammonia storage capacity decreased with increasing temperature (figure 11.1). Since the maximum temperature of 450 °C is expected to be too low for the quantitative desoprtion of strongly bound ammonia, the total ammonia adsorption capacity of the catalysts was also determined by a combination of physical desoprtion and “chemical” desoprtion, i.e. the reaction of pre-adsorbed ammonia with NO according to the method of Kleemann et al. [1]. Figure 11.2, shows the typical adsorption experiment for Fe-ZSM5 catalyst at a temperature of 200 °C. The sum of the physically desorbed and reacted ammonia is depicted in figure 11.3, showing the same decreasing trend for the total amount of stored ammonia as figure 11.1. But, especially at $T \geq 250$, a higher ammonia storage capacity was found for the combined method, indicating that in fact part of the ammonia remains on the catalyst surface in the exclusive thermal desorption experiments even at T = 450 °C.

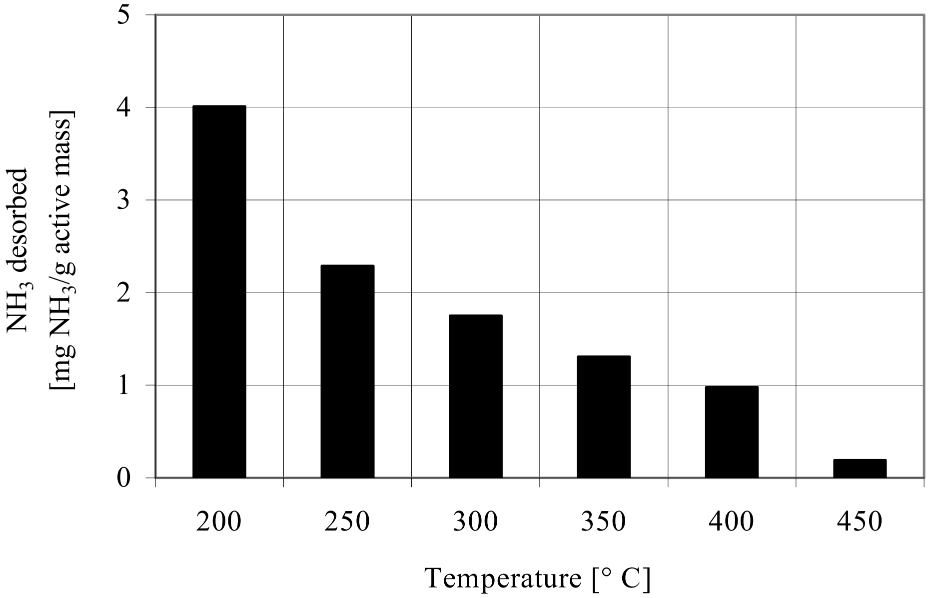

Figure 11.1 Ammonia storage capacity of the fresh Fe-ZSM5 monolith catalyst determined by thermal desorption of ammonia.

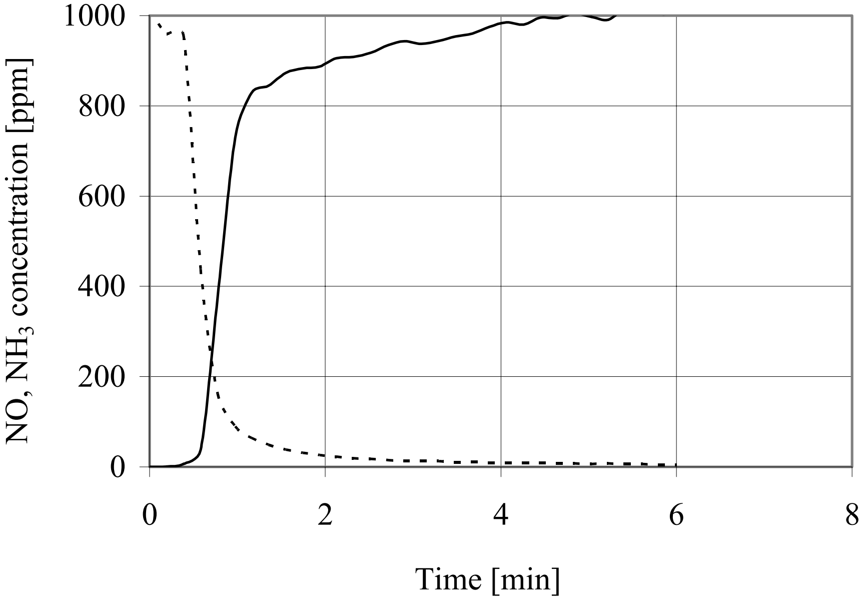

Figure 11.2 Transient evolution of (--) NH$_3$ and (-) NO during desorption/reaction of preadsorbed ammonia with 1000 ppm NO at T = 200 °C (Fresh Fe-ZSM5).

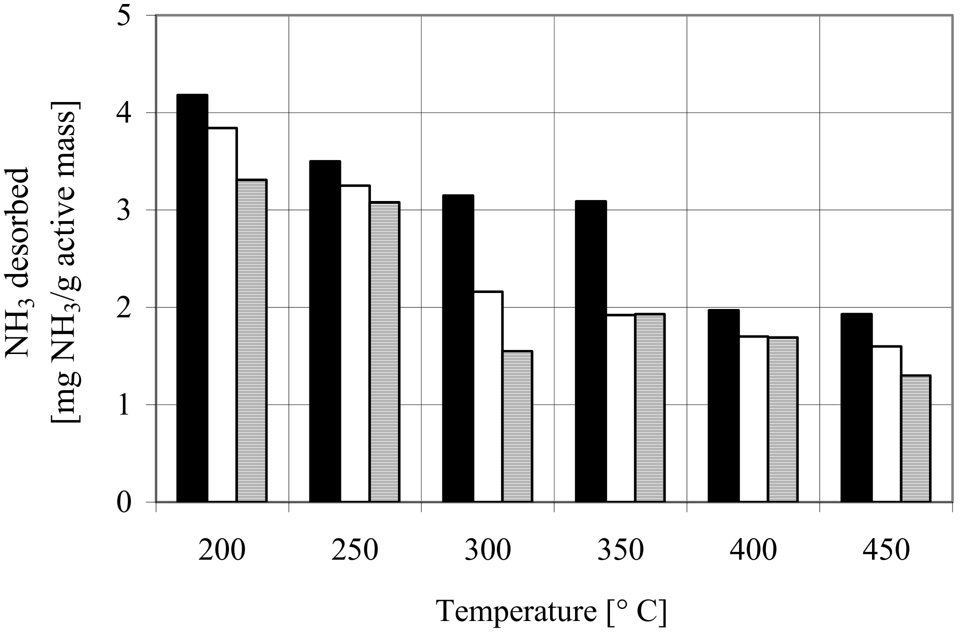

Figure 11.3 Total ammonia storage capacity of the (■) fresh, (□) dry aged and (≡) wet aged Fe-ZSM5 monolith catalysts determined by the combination of thermal and chemical desorption of ammonia.

The total amount of ammonia stored on the fresh catalyst is greater than on the aged catalysts (figure 11.3). The storage capacity in the catalysts decreases in the order fresh > dry aged > wet aged. As the ammonia storage capacity is a measure for the acidity of the samples, it is concluded that the acidity of Fe-ZSM5 is reduced by ageing, which supports the conclusions from the SCR results. According to the combined desorption method the total ammonia adsorption capacities depicted in figure 11.3 consist of two parts, which are plotted separately in figure 11.4, 11.5 and 11.6, i.e. the ammonia reacted with NO in the SCR reaction and the chemically non-accessible ammonia desorbed physically. In the case of the fresh catalyst (figure 11.4) there is a “step” in the amount of ammonia reacted above 350 °C and in the case of the aged catalysts (figures 11.5 and 11.6) this “step” is observed above 250 °C. For fresh Fe-ZSM5, up to 350 °C a constant amount of ammonia is reacting via SCR (figure 11.4), assigned to ammonia adsorbed on active SCR sites and mobile ammonia moving on the surface to the active sites. Beside this, a small amount of ammonia is desorbed unreacted before it gets in contact with NO.

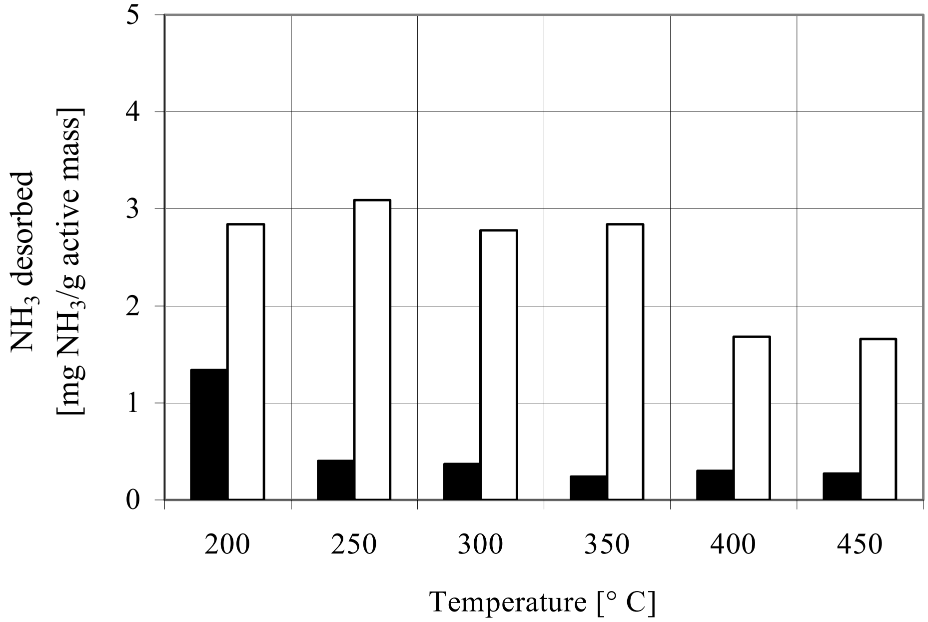

Figure 11.4 Ammonia storage capacity of the fresh Fe-ZSM5 monolith catalyst determined by the combination of thermal and chemical desorption of ammonia. (■) Thermally desorbed ammonia and (□) ammonia reacted with NO.

Above 350 °C the amount of reacting ammonia is considerably reduced. For the aged catalysts, up to 250 °C a constant amount of ammonia is reacting via SCR. If the acidity of an SCR catalyst is reduced, more ammonia is expected to be physically desorbed, which was found for the aged catalysts. The part of ammonia, which is physically desorbed, remains nearly constant over the whole temperature range for all three catalyst samples, except for T = 200 °C, where more ammonia is desorbed probably due to the very low SCR activity at this temperature. The observed “step” effect might be explained by two different acid sites on the surface, i.e. Brønsted and Lewis acid sites. Both types are covered at low temperature, but at high temperatures only the strong Brønsted acid sites are able to bind the ammonia.

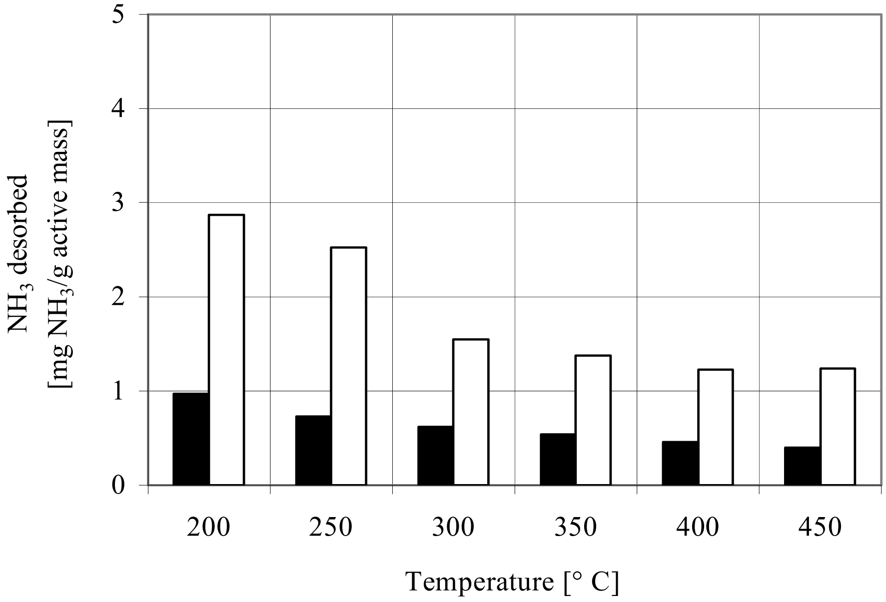

Figure 11.5 Ammonia storage capacity of the dry aged Fe-ZSM5 monolith catalyst determined by the combination of thermal and chemical desorption of ammonia. (■) Thermally desorbed ammonia and (□) ammonia reacted with NO.

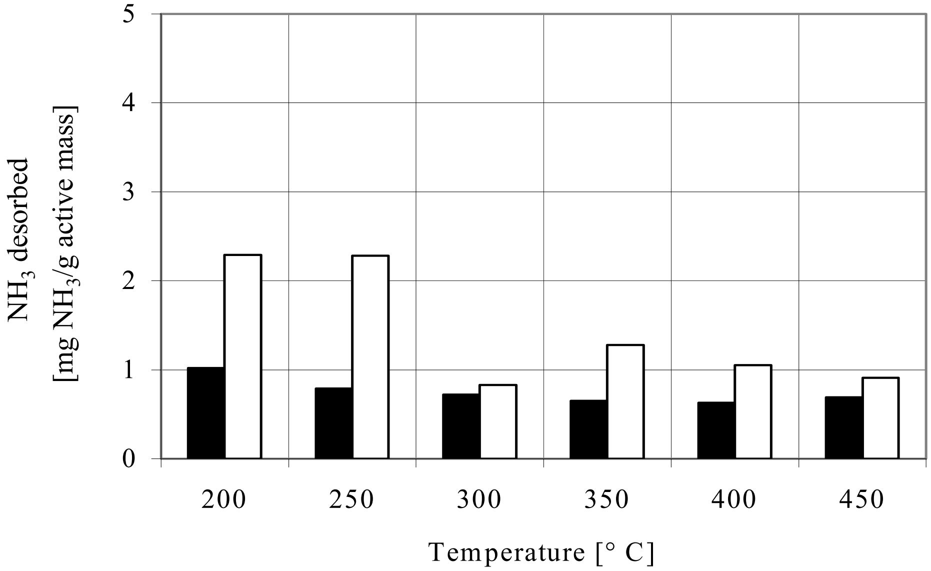

Figure 11.6 Ammonia storage capacity of the wet aged Fe-ZSM5 monolith catalyst determined by the combination of thermal and chemical desorption of ammonia. (■) Thermally desorbed ammonia and (□) ammonia reacted with NO.

From NH_3-TPD and Al NMR results (Chapter 10), a clear picture was observed regarding the loss of Brønsted acid sites for the aged catalyst. This decrease in the Brønsted acidity is in accordance with the conclusions from the measurement of the ammonia storage capacity of the catalyst.

11.4 Conclusions

The ammonia storage capacity of the fresh and aged catalysts was compared. The fresh catalyst had a much higher ammonia storage capacity than the aged catalyst. The distinct ammonia storage capacity could be attributed to the reduction of the number of Brønsted acid sites.

11.5 References

[1] M. Kleemann, M. Elsener, M. Koebel, A. Wokaun, Appl. Catal. B 27 (2000) 231.

[2] R. A. Radjadhyaksha, H. Knözinger, Appl. Catal. 51 (1989) 657.

[3] T. Z. Srnak, J. A. Dumesic, B. S. Clausen, E. Törnqvist, N. Y. Topsøe, J. Catal. 135 (1992) 246.

[4] N. Y. Topsøe, J. A. Dumesic, H. Topsøe, J. Catal. 151 (1995) 241.

[5] G. Ramis, L. Yi, G. Busca, Catal. Today 28 (1996) 373.

12

Catalytic Investigation of Cu-ZSM5

12.1 Introduction

Cu-exchanged pentasil zeolites (Cu-ZSM5) are among the most active catalyst for nitrogen oxide abatement [1-4]. Thus, this catalysts type was also investigated and compared to the performance of Fe-ZSM5.

12.2 Experimental

Cu-ZSM5 coated on a cordierite monolith was provided by Umicore automotive catalysts, Germany. Copper was loaded by a wet ion exchange method and the active mass which was loaded onto the monolith is 160 g/l. By ICP-AES analysis, the Si/Al ratio was determined to be 40 and the amount of copper which was loaded was 3.94 wt %.

For the catalytic investigation, a Cu-ZSM5 cordierite monolith with a volume of 8.1 cm^3 was fitted to the sample holder of the tube reactor. The catalyst was tested for standard SCR, fast SCR and oxidation of ammonia (SCO) reactions. The feed composition was the same as for the catalytic test of Fe-ZSM5 (chapters 6 & 7).

12.3 Results

12.3.1 Standard SCR

From figure 12.1, it is clearly observed that Cu-ZSM5 catalyst was active at $T \leq 600$ °C, in particular between 250 °C-500 °C, where a DeNOx of around 95 % was achieved. With increasing temperatures, the DeNOx gradually increased and beyond $T > 450$ °C, the DeNOx starts to level off. Though the catalyst was active, the formation of N_2O was observed up to 550 °C, with a maximum being at 450 °C.

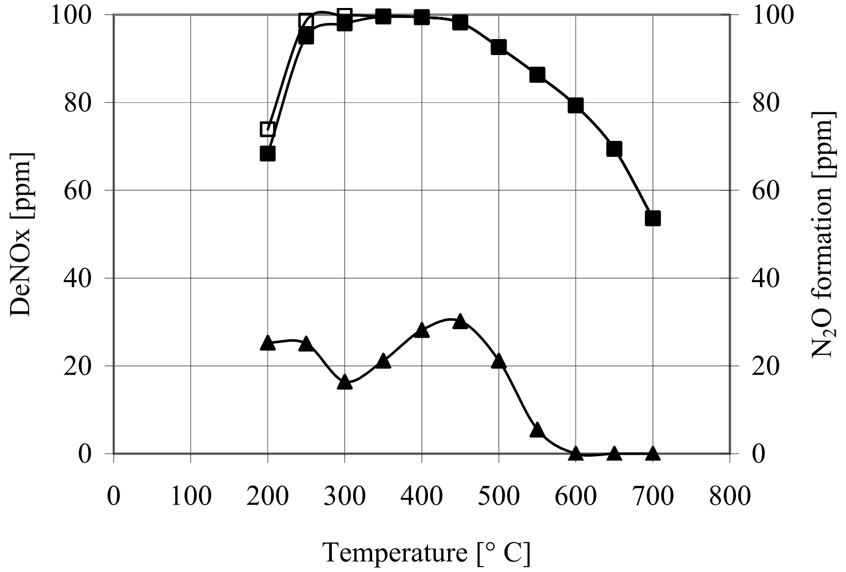

Figure 12.1 DeNOx vs. temperature for the fresh Cu-ZSM monolith (■) at 10 ppm NH_3 slip (□) at maximum conversion and (▲) N_2O formation at 10 ppm NH_3 slip.

12.3.2 SCR stoichiometry

The selectivity of the catalyst is checked by plotting the ratio of NH_3 consumed/NO_x reacted versus α (figure 12.2). A value of 1 indicates that all ammonia dosed goes into the SCR reaction. Deviations from the ideal stoichiometry are revealed by values > 1.

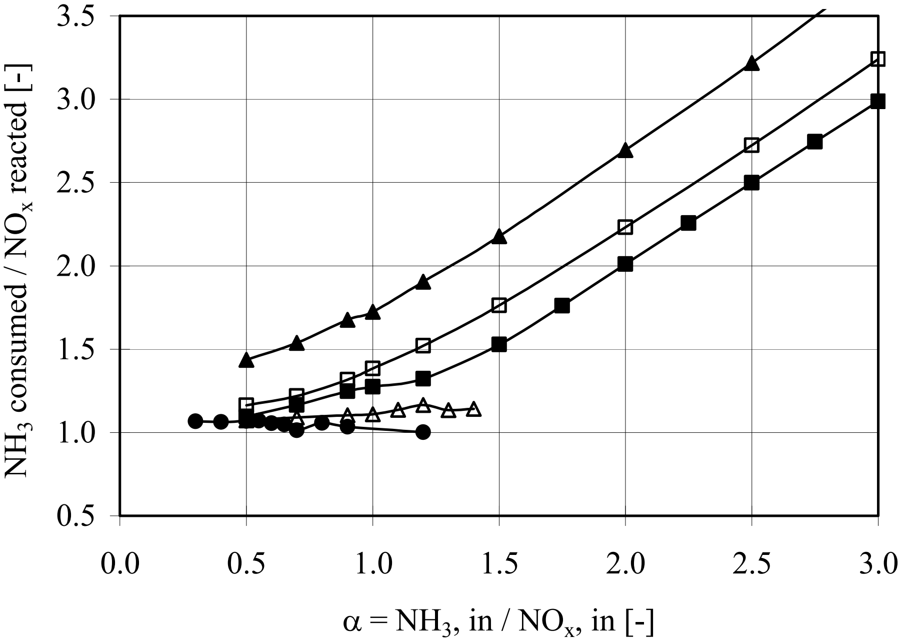

Figure. 12.2 Observed ammonia to NO_x stoichiometry vs. dosed ammonia to NO_x ratio at (●) 200 °C, (Δ) 300 °C, (■) 400 °C, (□) 500 °C and (▲) 600 °C.

The graph clearly demonstrates the high consumption of ammonia over Cu-ZSM5 in the SCR reaction. Cu-ZSM5 consumed an increasing excess of ammonia for higher temperatures, which can be attributed to the oxidation of ammonia to N_2 (SCO). This means, that large overdosing of ammonia is required.

12.3.3 Fast SCR

The catalytic activity was investigated with a feed containing 50% NO and 50% NO_2 (figure 12.3). Figure 12.3 reports the NO_x conversion (full symbols) and N_2O formation (open symbols) at 10 ppm ammonia slip.

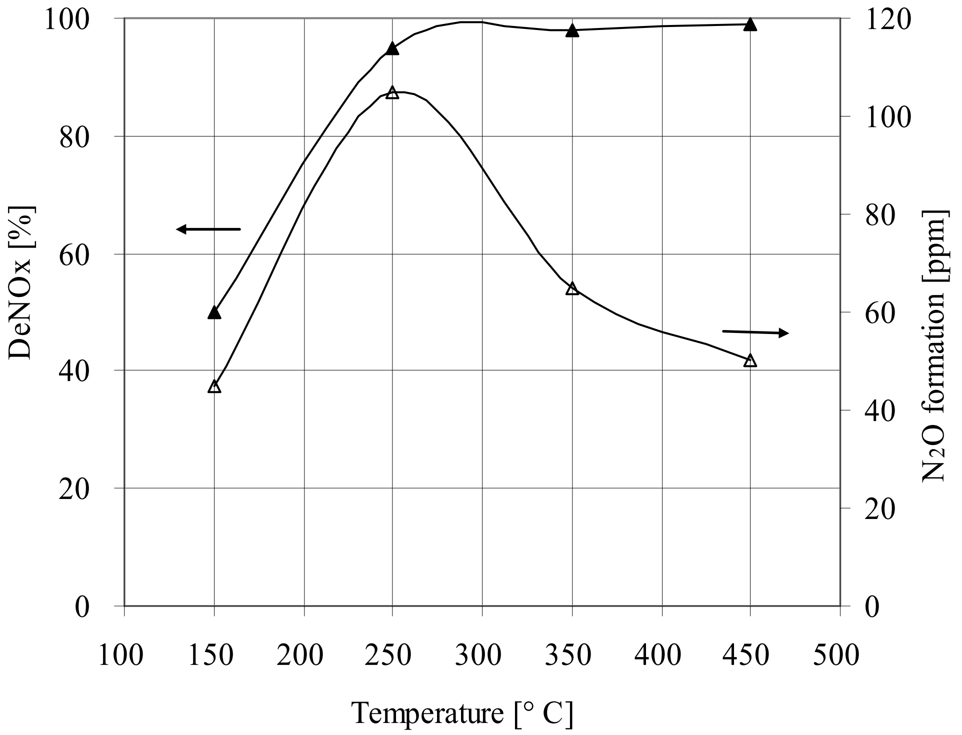

Figure 12.3 DeNOx at 10 ppm NH_3 slip and N_2O formation vs. temperature.

A DeNOx of around 50 % was achieved at T = 150 °C and beyond 250 °C around 95 % of NO_x conversion was achieved. The addition of NO_2 to the feed increased the N_2O production significantly, the maximum being at 250 °C (~ 105 ppm).

12.3.4 Ammonia oxidation

The oxidation of ammonia oxidation over Cu-ZSM5 is shown in figure 12.4. The catalyst exhibited a very high activity towards NH_3 oxidation and the ammonia conversion strongly increases with temperatures. Around 60 % of the ammonia was oxidized at T = 350 °C and 100 % conversion was achieved at $T \geq 400$ °C.

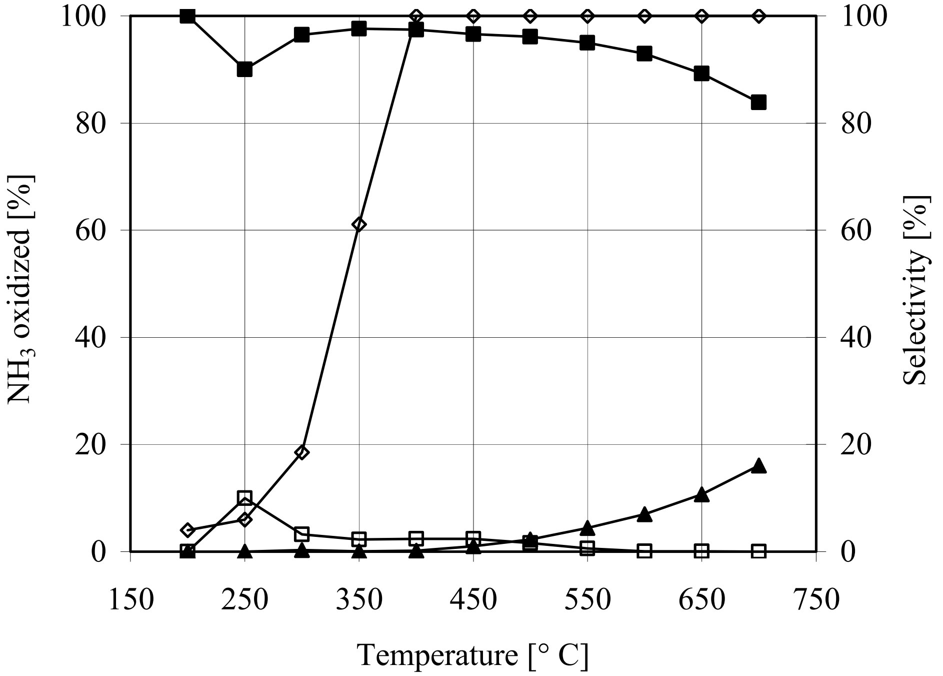

Figure 12.4 SCO properties of the fresh Cu-ZSM5 monolith vs. temperature (◊) NH_3 oxidized, (▲) selectivity towards NO and (■) selectivity towards N_2 and (□) selectivity towards N_2O.

The selectivity towards N_2 was around 95 % between 300 °C-550 °C, but beyond 550 °C the selectivity towards nitrogen decreased accompanied with an increase in NO formation.

12.3.5 Thermal and hydrothermal stability

In order to check the thermal and hydrothermal stability of the Cu-ZSM5 catalyst towards the SCR reaction, the Cu-ZSM5 monolith catalyst was aged under the same ageing conditions ("dry aged" & "wet aged") as Fe-ZSM5 (chapter 10). Figure 12.5 reports the DeNOx at 10 ppm ammonia slip for the aged Cu-ZSM5 catalysts and for the fresh Cu-ZSM5 under standard SCR conditions.

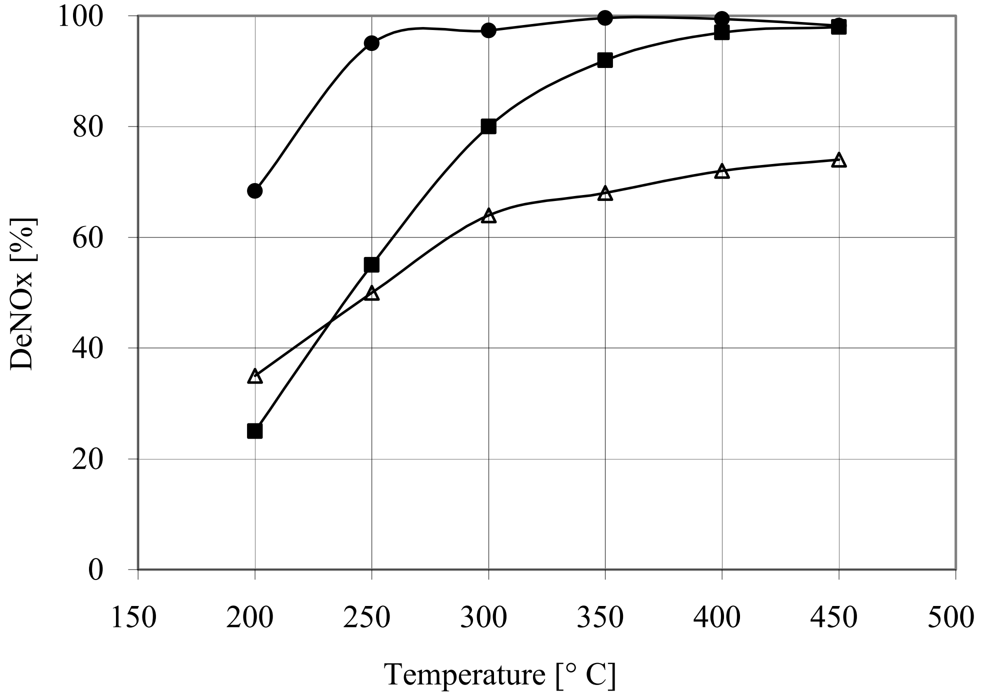

Figure 12.5 DeNOx at 10 ppm NH_3 slip for the (●) fresh, (Δ) dry aged and (■) wet aged Cu-ZSM5 monolith catalysts vs. temperature (standard SCR conditions).

From figure 12.5, it can be seen that the wet aged catalyst performed better than the dry aged catalyst. The NO_x conversions for the fresh and wet aged catalyst were nearly the same at $T \geq 400$ °C. Around 25 ppm of N_2O is produced at all temperatures. These results contradict to the behavior of Fe-ZSM5 (chapter 10), where the dry aged catalyst performed better than the wet aged catalyst. Figure 12.6 reports the NO_x conversion (full symbols) and N_2O formation (open symbols) at 10 ppm ammonia slip for the aged Cu-ZSM5 catalyst compared with the fresh Cu-ZSM5 catalyst under fast SCR conditions.

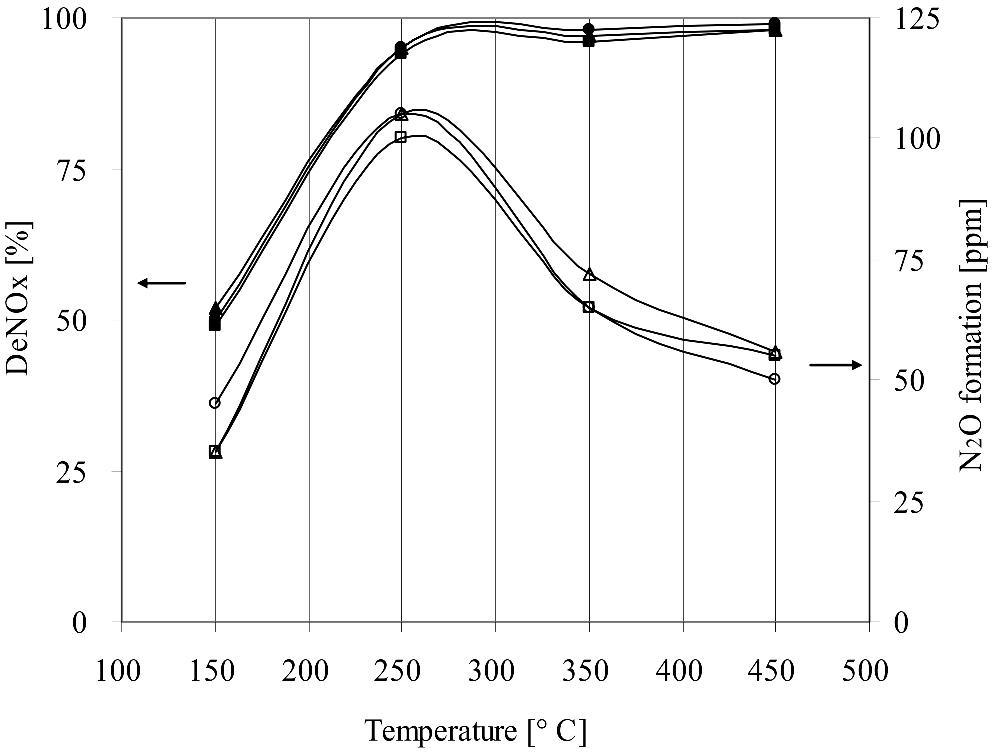

Figure 12.6 DeNOx & N_2O formation at 10 ppm NH_3 slip for the (●, o) fresh, (▲, Δ) dry aged and (■, □) wet aged Cu-ZSM5 monolith catalysts vs. temperature (fast SCR conditions).

The fresh as well as the aged Cu-ZSM5 catalysts exhibited a similar DeNOx and produced the same amount of N_2O when 50 % NO_2 was added to the feed mixture.

12.4 Discussion

The SCR activity of Cu-ZSM5 monolith catalyst was investigated. Under standard SCR conditions, the catalyst was highly active, which can be attributed to the high oxidation capability of NO to NO_2. As mentioned in [5], the presence of NO_2 either in the feed or produced by the catalyst from NO is pre-requisite for SCR activity. Cu-ZSM5 showed a high NO oxidation capability of around 5-20 % at T = 250-450 °C. Due to this, high DeNOx at low temperatures are achieved with this catalyst. The drawback of the high oxidation capability of Cu-ZSM5 is also high SCO activity (figure 12.4), resulting in high the amounts of ammonia needed for the SCR reaction. This is further showed in figure

12.2, showing that the selectivity over Cu-ZSM5 is not equal to the theoretical value of 1, but it was between 1.5 to 3.5. This means that a permanent over dosage of NH_3 is needed for the reaction to take place. With the high oxidation activity of the catalyst, the main drawback of the catalyst is that the production of N_2O is accompanied. The most obvious reason for the formation of N_2O under SCR would be the oxidation of NH_3 in agreement with [6]. Apart from NH_3 oxidation another possible reason for the N_2O formation in Cu-ZSM5 might be the presence of copper oxide species [7]. Under fast SCR conditions, the catalyst exhibited a very high DeNOx and at same time produced huge amount of N_2O as well.

The thermal and hydrothermal stability of the catalysts was investigated under harsh ageing conditions. Under standard SCR the wet aged catalyst performed better than the dry aged catalyst, in contrast to the Fe-ZSM5 catalyst (see chapter 10 for Fe-ZSM5 details). The possible reason for the loss in DeNOx for the aged catalyst might be the dealumination of the zeolite [8]. Nearly the same DeNOx and N_2O formation was observed when 50 % NO_2 was present in the feed.

In order to understand the functionality of Cu-ZSM5 in SCR completely, much more detailed experiments have to be performed.

12.5 Conclusions

Cu-ZSM5 is a highly active catalyst for the selective catalytic reduction of NO in simulated diesel exhaust gas in the temperature region 250-500 °C. Since much ammonia is oxidized to nitrogen over Cu-ZSM5, ammonia had to be permanently over dosed.

12.6 References

[1] M. Shelef, Chem. Rev. 95 (1995) 209.

[2] W. Held, A. Konig, T. Richter, L. Poppe, SAE Technical Paper Series 900496 (1990).

[3] J. A. Sullivan, J. Cunningham, M. A. Morris, K. Keneavey, Appl. Catal. B 7 (1995) 137.

[4] Y. Zhang, K. M. Leo, A. F. Sarohim, Z. Ho, M. F. Stephenopoulous, Catal. Lett. 31 (1995) 75.

[5] M. Devadas, O. Kröcher, M. Elsener, A. Wokaun, N. Söger, M. Pfeifer, Y. Demel, L. Mussmann, Appl. Catal. B, submitted.

[6] K. R. Tolonen, T. Maunula, M. Lomma, M. Huuhtanen, R. L. Keiske, Catal. Today 100 (2005) 217.

[7] S. Kieger, G. Delahay, B. Coq, B. Neveu, J. Catal. 183 (1999) 267.

[8] R. Mital, S. C. Huang, B. J. Storia, R. C. Yu, C. Z. Wan, SAE Technical Paper Series 010956 (2002) 119.

13

Outlook

In the present work, much emphasise is given for Fe-ZSM5 as SCR catalyst. However, the exploration of zeolite based SCR catalyst has just begun. In future other exchange metals, such as copper, palladium etc., should be investigated in order to improve the SCR performance. In catalyst preparation, the possibility of dual metal cation exchange could be an attractive option.

Apart from solid state ion exchange (used in this work), other ion exchange methods like wet ion exchange, sublimation, impregnation etc., have to be checked in order to find the optimum method which is needed to prepare highly active SCR catalyst. Fe-Beta zeolites were found to be active and stable up to very high temperatures (900 °C). Therefore, it is worth the check the performance of other zeolite materials like beta, mordenite etc.

Ammonia storage capacity as well as ion exchange capacity depends on the Si/Al ratio of the zeolite. Therefore, fine tuning of the catalyst properties should be possible by varying the module (Si/Al ratio).

Publications

The following list summarizes the papers, reports, talks and posters which resulted from this study.

Publications

- M. Devadas, O. Kröcher, A. Wokaun, “Catalytic Investigation of Fe-ZSM5 in the Selective Catalytic Reduction of NO_x with NH_3”, React. Kinet. Catal. Lett. 86 (2005) 347.
- O. Kröcher, M. Devadas, M. Elsener, A. Wokaun, N. Söger, M. Pfeifer, Y. Demel, L. Mussmann, “Investigation of the Selective Catalytic Reduction of NO by NH_3 on Fe-ZSM5 monolith catalysts”, Appl. Catal. B, submitted.
- M. Devadas, O. Kröcher, M. Elsener, A. Wokaun, G. Mitrikas, N. Söger, M. Pfeifer, Y. Demel, L. Mussmann, “Characterization and Catalytic Investigation of Fe-ZSM5 for urea-SCR” Catal. Today, submitted.
- M. Devadas, O. Kröcher, M. Elsener, A. Wokaun, N. Söger, M. Pfeifer, Y. Demel, L. Mussmann, “Influence of NO_2 on Urea-SCR over Fe-ZSM5”, Appl. Catal. B, submitted.

Reports

- M. Devadas, G. Piazzesi, O. Kröcher, A. Wokaun, “Characterization and Catalytic Activity of Fe-ZSM5 for Urea-SCR”, PSI Scientific Report 2004, V (2005) 85.
- M. Devadas, O. Kröcher, A. Wokaun, “Zeolite Catalysts-An Interesting Alternative to Vanadia-Titania Systems”, PSI Scientific Report 2003, V (2004) 73.

Talks

- M. Devadas, G. Piazzesi, O. Kröcher, M. Elsener, A. Wokaun, “Mechanistic and Catalytic Investigation of Fe-ZSM5 for Urea-SCR”, International Symposium on Air Pollution Abatement Catalysis, Sep. 21-24, 2005, Krakow, Poland.
- O. Kröcher, M. Devadas, M. Elsener, A. Wokaun, N. Söger, M. Pfeifer, Y. Demel, “Zeolite Catalysts for Urea-SCR”, Eighth DOE Crosscut Workshop on Lean Emissions Reduction Simulation, May 17-19, 2005, Dearborn, Michigan, USA.
- O. Kröcher, M. Devadas, G. Piazzesi, M. Elsener, “SCR Catalysts for Diesel Engines-Challenges for the Application of Urea-SCR in Vehicles”, International Workshop-Future Concepts in Energy Related Catalysis, March 13-17, 2005, Ascona, Switzerland.

Posters

- M. Devadas, G. Piazzesi, O. Kröcher, A. Wokaun, “Investigation of Fe-ZSM5 for Urea-SCR”, International Workshop-Future Concepts in Energy Related Catalysis, Ascona, Switzerland, 2005.
- M. Devadas, D. Poduval, O. Kröcher, A. Wokaun, C. Palivan, G. Mitrikas, A. Schweiger, “Investigation of Different Iron Exchanged Zeolite Catalysts for Urea-SCR”, New Developments in Catalysis, Saarbrucken, Germany, 2004.
- M. Devadas, D. Poduval, O. Kröcher, A. Wokaun, “Comparative Investigation of Metal Exchanged Zeolite Catalysts for Urea-SCR”, 13th International Congress on Catalysis, Paris, France, 2004.
- M. Devadas, O. Kröcher, A. Wokaun, M. Pfeifer, E. Lox, “New Iron Zeolite Catalysts for Urea-SCR”, Europa Cat VI, Innsbruck, Austria, 2003.

Curriculum Vitae

Name: Mukundan Devadas

Date of birth: 03-07-1976

Place of birth: Chennai (India)

Nationality: Indian

Education:

1982-1987	Primary School, Don Bosco Matriculation Higher Secondary School, Egmore, Chennai, India.
1987-1994	High School, Don Bosco Matriculation Higher Secondary School, Egmore, Chennai, India.
1995-1999	Bachelors in Chemical Engineering, Annamalai University, Chidambaram, India.
1999-2002	Masters in Chemical Engineering, Friedrich-Alexander Universität, Erlangen-Nürnberg, Germany.
2002-2006	Ph.D. Thesis under the supervision of Prof. Dr. Alexander Wokaun (Swiss Federal Institute of Technology - ETH Zurich) at the Paul Scherrer Institute in Villigen, Switzerland.